UNIVERSITE DE STRASBOURG-UNIVERSITÄT DES SAARLANDES

Discipline : Aspects moléculaires et cellulaires de la biologie- ED414 Science de la vie et de la santé

Présentée par: DACLEU SIEWE Vanessa

MOLECULAR AND STRUCTURAL BASES OF THE SELENOPROTEIN N DYSFUNCTION IN DIVERSE FORMS OF CONGENITAL MUSCULAR DYSTROPHIES

Thèse en cotutelle entre : Architecture et Réactivité de l'ARN UPR 9002 du CNRS

Lehrstuhl fur Strukturbiologie der Universitat des Saarlandes

Co-Directeur de Thèse : Dr. LESCURE Alain

Co-Directeur de Thèse : Prof. Dr. LANCASTER Roy

Localisation : Institut de Biologie Moléculaire et Cellulaire IBMC – 15 rue Rene Descartes, 67084 Strasbourg

Lehrstuhl fur Strukturbiologie der Universität des Saarlandes – Kirrbergerstrasse, Gebaude 60, 66421 Homburg

Soutenue publiquement le 29 novembre 2017 devant la commission d'examen :

RAPPORTEURS

Dr. Anne Catherine Dock-Bregeon	Chercheuse, Station Biologique Roscoff
Prof. Dr. Thorsten Friedrich	Enseignant-chercheur, Université de Freiburg

EXAMINATEURS

Dr. Bianca Schrul	Junior-professor, Université des Saarlandes
Dr. Marc Ruff	Chercheur, IGBMC-Strasbourg

Abstract

Selenoproteins are proteins containing a selenocysteine residue (U) in their amino acid sequence. Twenty-five proteins constitute the human selenoproteome. Among them is Selenoprotein N or SelenoN; mutations in the SELENON gene can lead to a group of congenital dystrophies now designated as SELENON-related myopathies. SelenoN is a 72 kDa membrane and glycosylated protein of the endoplasmic reticulum. It handles in its amino acid sequence a redox motif SCUG like the one of thioredoxin reductases, and an EF-hand domain which is a calcium binding site. Recent studies showed the implication of SelenoN in muscle development and maintenance, and position its function at the crossroad between oxidative stress control and calcium homeostasis. However, its catalytic function remains elusive. The research project presented in this thesis concerns the crystallization, characterization and comparison of one bacterial and the zebrafish SelenoNs. Bioinformatics analyses revealed that the two proteins share 37% degree of identity and a common domain which corresponds to a thioredoxin fold of unknown function which includes the redox motif SCUG. From the biophysical characterization, both recombinant proteins are found to be naturally well-folded and enriched in α-helical domains. The bacterial SelenoN which handles an additional C-terminal thioredoxin domain is an extended monomer whereas zebrafish SelenoN is a compact dimer. Biochemical characterization indicated that Ca^{2+} binding mediates zSelenoN oligomerization. Initial crystals of the zSelenoN in its deglycosylated form were obtained. Bacterial SelenoN crystallization yielded crystals belonging to two different space groups with different cell parameters. An initial partial model covering the C-terminal thioredoxin domain of the bacterial SelenoN was obtained at 2.3Å. Together, these results lay a foundation for the structure-function studies of SelenoN. Conditions for recombinant bacterial and zebrafish SelenoNs expression, purification and crystallization were optimized and strategies for solving the structure are being proposed.

Keywords : Selenoprotein, SelenoN, X-ray diffraction

Résume

Les Selenoprotéines sont des protéines contenant un résidu sélénocystéine (U) dans leur séquence en acide amines. Vingt-cinq sélénoprotéines constituent le sélénoprotéome humain. Parmi elles, la sélénoprotéine N ou SelenoN ; des mutations dans le gène SELENON donnent lieu à un groupe de dystrophies musculaires congénitales appelées myopathies liées à SELENON. SelenoN est une protéine membranaire glycosylée de 72 kDa localisée dans le réticulum endoplasmique. Sa séquence en acide aminés contient le motif redox SCUG, similaire à celui des thioredoxines réductases. Elle contient de même un domaine EF-hand qui est un domaine de liaison au calcium. Des études ont récemment démontré l'implication de cette protéine dans l'établissement et la maintenance du muscle squelettique. D'autres études ont montré qu'elle joue un rôle dans la protection contre le stress oxydatif et l'homéostasie du calcium. Cependant, le mécanisme catalytique de SelenoN reste inconnu à ce jour. Le projet décrit dans cette thèse s'intéresse à la caractérisation, la cristallisation et la comparaison des SelenoNs d'une bactérie, *Candidatus poribacteriae,* et du poisson zèbre. Les études bio-informatiques ont démontré que SelenoN bactérienne et du poisson zèbre partagent 37% d'identité et un domaine commun correspondant à un repliement de type thioredoxine de fonction inconnue, contenant le motif redox. Les caractérisations biophysiques ont démontré que les deux protéines sont naturellement bien repliées et riche en hélices α. La protéine bactérienne comportant en C-terminal de sa séquence en acide aminé un domaine thioredoxine additionnel, présente une forme étendue et est sous forme monomérique tandis que la protéine du poisson zèbre est un dimère compact. Des caractérisations biochimiques ont montré que le Ca^{2+} influence l'oligomérisation ou la conformation de SelenoN du poisson zèbre. Des cristaux initiaux de la protéine eucaryote sous sa forme déglycosylée ont pu être obtenus. La cristallisation de la protéine bactérienne a permis d'obtenir des cristaux appartenant à deux groupes d'espaces, avec des paramètres de cellule différents. Néanmoins, un model partiel à 2.3 Å couvrant le domaine C-terminal thioredoxine additionnel de SelenoN bactérienne a été obtenu. L'ensemble de ces résultats permettent de poser les bases de l'étude structure-fonction de SelenoN. L'expression, la purification et la cristallisation ont été optimisées et une stratégie pour résoudre la structure 3D de la protéine est proposée.

Mots cles : Selenoproteine, SelenoN, Crystallisation aux rayons-X

Abstrakt

Selenoproteine sind Proteine, die in ihrer Aminosäuresequenz einen Selenocystein Rest (U) enthalten. Fünfundzwanzig Proteine bilden das menschliche Selenoprotein. Unter denen ist Selenoprotein N oder SelenoN ; Mutationen im SELENON-Gen können zu einer Gruppe von kongenitalen Dystrophien führen, die jetzt als SELENON-verwandte Myopathien bezeichnet werden. SelenoN ist eine 72 kDa-Membran und ein glycosyliertes Protein des endoplasmatischen Retikulums. Es behandelt in seiner Aminosäuresequenz ein Redoxmotiv SCUG wie das von Thioredoxinreduktasen und eine EF-Handdomäne, die eine Calciumbindungsstelle ist. Jüngste Studien zeigten die Bedeutung von SelenoN bei der Muskelentwicklung und -erhaltung und positionieren seine Funktion an der Schnittstelle zwischen der Kontrolle des oxidativen Stresses und der Calciumhomöostase. Ihre katalytische Funktion bleibt jedoch schwer. Das in dieser Arbeit vorgestellte Forschungsprojekt befasst sich mit der Kristallisation, Charakterisierung und dem Vergleich von einem Bakterium und den SelenoNs des Zebrafisches. Bioinformatische Analysen zeigten, dass die beiden Proteine einen Identitätsgrad von 37% und eine gemeinsame Domäne teilen, die einer Thioredoxinfaltung unbekannter Funktion entspricht, die das Redoxmotiv SCUG umfasst. Aus der biophysikalischen Charakterisierung wurde herausgefunden, dass beide rekombinanten Proteine natürlich gut gefaltet und α -helikalen Domänen angereichert sind. Das bakterielle SelenoN, das eine zusätzliche C-terminale Thioredoxin-Domäne handhabt, ist ein verlängertes Monomer, während der Zebrafisch SelenoN ein kompaktes Dimer ist. Die biochemische Charakterisierung zeigte, dass die Ca^{2+} -Bindung die ZSelenoN-Oligomerisierung vermittelt. Es wurden anfängliche Kristalle des zSelenoN in seiner deglycosylierten Form erhalten. Die bakterielle SelenoN-Kristallisation ergab Kristalle, die zu zwei verschiedenen Raumgruppen mit unterschiedlichen Zellparametern gehörten. Ein anfängliches Teilmodell, das die C-terminale Thioredoxin-Domäne des bakteriellen SelenoN abdeckt, wurde bei 2,3 Å erhalten. Zusammen bilden diese Ergebnisse eine Grundlage für die Struktur-Funktions-Studien von SelenoN. Die Bedingungen für die Expression, Reinigung und Kristallisation von SelenoNs in rekombinanten Bakterien und Zebrafischen wurden optimiert und Strategien zur Lösung der Struktur vorgeschlagen.

Schlüsselwörter: Selenoprotein, SelenoN, Röntgenbeugung

Acknowlegments

My first thanks go to Dr. Alain Lescure for giving me the opportunity to work on this wonderful and so exciting project. He has been all along the project a wonderful supervisor by bringing me all the scientific and mental support that I needed. He always showed a real interest in all my experiments and a contagious enthusiasm during our communications.

I would also like to thank all the team working on Selenoprotein N in Strasbourg for their support: Melanie Thamy-Brayes (ma noisette!), Mireille Baltzinger (Madame Pichia pastoris), Luc Thomes (l'informaticien de la team).

I would like to thank Prof. Dr. C. Roy Lancaster for introducing me to Dr. Lescure and for the methodological and financial support of this work. The experiments which led to the results of this work were for the main part performed in the laboratory of Professor Lancaster.

Furthermore, I would like to thank Dr. Yvonne Carius for her intensive care. She always found the time for scientific discussion and to make me share her experience. Equally gratefull to Birgit Herrmann for the long discussion about life and her disponibility. Not forgetting the entire Structural Biology team for welcoming me as a full member, and for making my integration and working environment pleasant.

I would also like to thank all the people involved in organization of the French-German PhD Track program especially Dr Jöern Putz who gave me the opportunity to be a pioneer of this program.

Finally, I would like to thank the following persons who were always a support during my studies and in this thesis writing: my lovely mothers Ndengue Madeleine and Mboue Yvonne, my brothers Dacleu Antonin, Lowe Landry, my sisters Dr. Dacleu Ndengue Jessica and Dacleu Djiengue Lesly, my sweetheart Ekuh Jude for his comprehensive support during the writing, and of course all my lovely nephews.

Thanks for this!

Abbreviations

ATP	Adenosine Tri Phosphate
AU	Absorption Unit
Amp	Ampicillin
APS	Ammoniumperoxodisulfat
bSelenoN	Bacterial Selenoprotein N
BSA	Bovine serum albumine
Cam	Chloramphenicol
CD	Circular dichroism
CHAPS	3-[(3-Cholamidopropyl)-Diméthylammonio]-1-Propane Sulfonate
C-terminus	Protein carboxy-terminal end
DM	Decyl-β-maltoside
DDM	Dodecyl-β-maltoside
DMSO	Dimetyhlsulfoxide
DNA	Deoxyribose nucleic acid
EDTA	Ethylene diamine tetra acetic
EGTA	Ethylene glycol tetraacetic acid

ER	Endoplasmic reticulum
h	hour
Ig	Immunoglobulin
IPTG	Isopropyl ß-D-Thiogalactopyranoside
kDa	Kilodalton
LB	Lysogeny Broth
MES	2-(N-morpholino) ethanesulfonic acid
min	minute
MOPS	3-(N-morpholino) propanesulfonic acid
Ni-NTA	Nickel-Nitrilotriacetic acid
OD	Optical dansity
OG	Octyl glucoside
PDB	Protein data bank
RyR	Ryanodine receptor
SAXS	Small angle X-ray scattering
SelenoN	Selenoprotein N
TM	Transmembrane
zSelenoN	Zebrafish Selenoprotein N

Table of Contents

List of Figures

List of Tables

1 Introduction

1.1 Selenocysteine, the 21st amino acid of the genetic code

1.1.1 The trace element selenium and human health

Selenium (Se) is an essential trace element that is involved in many areas of vital importance to human and animal health. It is found in the activity center of several redox enzymes participating in numerous functions (reviewed in Labunskyy et al. 2014). Studies based on deficiency/supplementation of Se in area where the soil contains low level of the element highlighted its importance in various aspects of human and animal health.

A relationship between selenium and immune function was established as it is normally present in immune tissues and Se supplementation was found to have an immune stimulant effect on humans (Kiremidjian-Schumacher et al. 2017.). A relationship between Se and the virulence level of some viruses was established as it was demonstrated that in Se-deficient hosts, harmless viruses can turn virulent. In fact, a benign strain of coxsachie virus when inoculated in Se-deficient mice becames virulent due to mutations in the genome, causing the Keshan Disease (Beck 1999). A relation was also established between HIV and Selenium. Studies showed that Se-deficient HIV patients are twenty times more likely to die from HIV-related causes (Baum et al. 1997).

Concerning the reproduction function, administration of Se supplement to livestock prevented early pregnancy loss (Hidiroglou 1979). In male fertility both in humans and animals, Se was required for testosterone synthesis and the formation and development of reproduction cells (Behne, Weiler, and Kyriakopoulos 1996).

There are also evidence for the importance of Se for brain function, as In Alzheimer's patient, Se level in the brain was measured to be 60% less than in a control panel (Hawkes and Hornbostel 1996). Also, Se deficiency correlates with an altered turnover rate of some neurotransmitters. On the other hand, it was found that Se supplementation helped to decrease anxiety, depression and tiredness (Benton and Cook 1990).

Thyroid hormones metabolism was also related to Se as the enzymes that drive the pathway are

Se containing proteins. Their activity is directly related to Se level and availability (Bianco et al. 2002).

There is evidence of a protective effect of Se against cardiovascular diseases as well as pancreatitis and cancer. A study made in China where Hepatocellular Carcinoma (HCC) is the highest cause of cancer mortality, revealed that supplementation with Se led to a decrease of 35% of HCC in comparison to a control panel (Yu, Zhu, and Li 1997).

1.1.2 Biological forms of selenium

1.1.2.1 Chemical forms of selenium used in biomolecules

There are several biological forms of Se (**Figure 1**). Some forms are bacterial specific such as the 5-methylaminomethyl-2-selenouridine, an analogue of uridine where Sulfur atoms are replaced by Se atoms by the enzyme 2-selenouridine synthase which uses selenophosphate as Se donor. The molecule is found in the anticodon of some bacterial tRNA including tRNAGlu, tRNAGln, tRNALys (A J Wittwer et al. 1984; A J Wittwer 1983; A J Wittwer and Ching 1989) and is believed to improve the fidelity of the translation (Caton-williams and Huang 2008).

Selenoneine is analogue of ergothioneine, a naturally occurring amino acid derivative of histidine. Selenoneine is mostly found in fish. Notably, it is the major form of organic selenium in tuna (Yamashita and Yamashita 2010). This specific form of selenium binds to heme-protein such as hemoglobin and has an antioxidant ability. It was also found to be involved in mercury detoxication in fish (Yamashita et al. 2011).

Selenomethionine is a naturally occurring amino acid. It is the major form of selenium found in plants. It is a very important dietary form of selenium which is accessible to animals via protein plants. Ingested SeMet is either convert into active forms of selenium via the transulfurase pathway or stored as selenium stock in place of methionine in body proteins (reviewed in Weekley and Harris 2013).

Monoselenophosphate is synthesized from ATP and selenide by the selenophosphate synthetase (Lacourciere 1999). It is an intermediate for selenoenzymes (**Figure 1**) and tRNAs synthesis and act as Se donor (Caton-williams and Huang 2008).

1.1.2.2 Selenocysteine

Selenocysteine is an analogue of cysteine in which sulfur atom of the thiol group is replaced by selenium atom to form a selenol group (**Figure 2**). Due to the value of its pKa (pKa=5.24), this group presents the advantage of been ionized at physiologic pH. Thus, this amino acid is a better nucleophilic group than Cysteine (pKa 8.25) and enables the selenoproteines to have a higher reactivity (Cunniff et al. 2014). It has been demonstrated that many selenoproteins are involved in reduction oxidation (redox) reactions (Fomenko and Gladyshev 2003) that drive a wide range of functions in animal and humans.

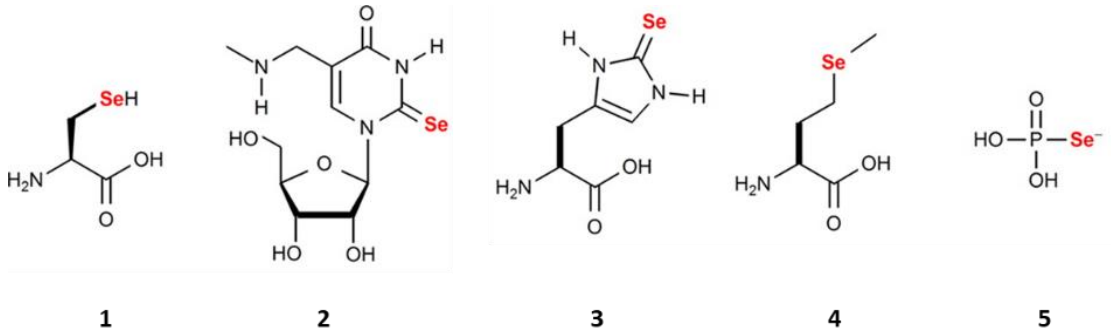

Figure 1: Different chemical forms of selenium used in biomolecules.

Selenocysteine (Sec, U). (2) 5-Methylaminomethyl-2-selenouridine. (3) Selenoneine. (4) Selenomethionine (SeMet). (5) Monoselenophosphate (Reich and Hondal 2016).

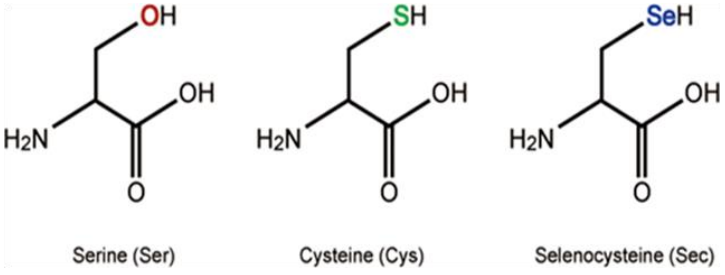

Figure 2: Comparison of Selenocysteine to similar amino acids Serine and Cysteine

(www.riken.jp/en/pr/press/2010/20100813/)

1.1.3 Incorporation of selenocysteine during the translation process

Selenocysteine is known as the 21st amino acid of the genetic code. Its incorporation is a dedicated process as it is directed by the UGA codon, which is normally the stop codon „opal“. The reprogramming of an opal codon requires several specific factors, particularly the presence on the mRNA of a specific secondary structure, named selenocysteine insertion sequence (SECIS). There is no Sec tRNA Synthetase, the synthesis of the SelenyltRNASec (SectRNASec) occurs as a tRNA-dependant modification of the SeryltRNASec (SertRNASec).

In eukaryotes, the first step of this synthesis is the aminoacylation of the tRNASec with serine (Ser) to produce SertRNASec. This first reaction is catalysed by the serine synthase. Following this step, the SertRNASec is phosphorylated by the O phosphoseryl kinase (PTSK) and gives an intermediate: the O-phosphoseryltRNASec. Then, the selenocysteine synthase (SecS), also known as SecA in archea and SelA in bacteria, converts the phosphoseryltRNASec into an activated intermediate and uses the active selenium (monoselenophosphate) as donor to give the selenocysteyltRNASec. This monoselenophosphate is a product of the reaction which uses selenite (HSe-) and ATP as substrates, and is catalyzed by the SPS2 enzyme (**Figure 3**) (Labunskyy et al. 2014).

The SECIS element, is a RNA secondary structure localized on 3’UTR of selenoproteins mRNA. This *cis*-element is essential for the reprogramming of the stop codon into selenocysteine. It consists in a stem loop which is highly conserved at the structural level. The apical loop is very important during the process of incorporation of the selenocysteine as it enables the binding of the specific elongation factors, eEFSec together with the SectRNAsec. The SECIS binding protein 2 (SBP2) binds to a kink-turn motif localized at the bottom of the SECIS stem loop (**Figure 4**). The conservation of the SECIS element allowed the identification of many selenoproteins by bioinformatics approaches, particularly the identification of selenoprotein N (SelenoN) in 1999 by Lescure and co-workers in Strasbourg.

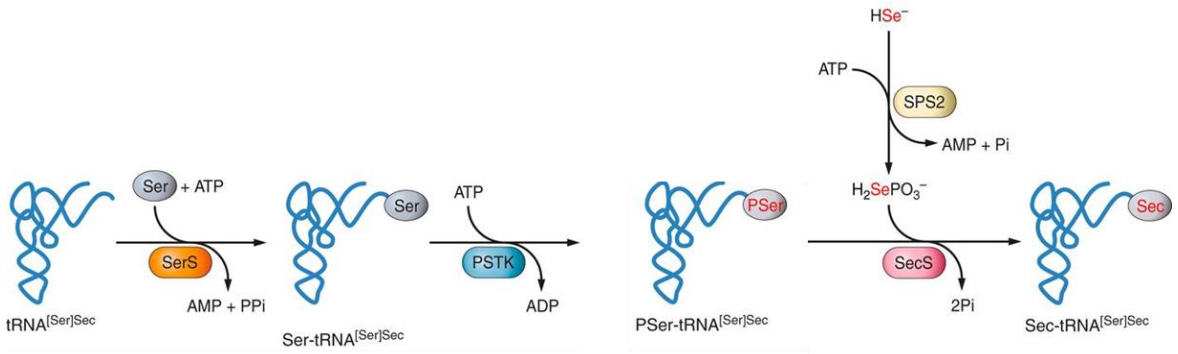

Figure 3 Synthesis of Sec-tRNA SerSec in Eukaryotes

phosphoseryl-tRNASec kinase (PSTK) phosphorylates aminoacylated serine to form O-phosphoseryl-tRNA. Sep (O-phosphoserine) tRNA: SectRNA synthase, abbreviated as SepSecS, then converts O-phosphoseryl-tRNA to Sec-tRNA, using selenophosphate as the nucleophile to displace the phosphate group. Selenophosphate is produced by selenophosphate synthetase (SPS2) (Labunskyy et al. 2014).

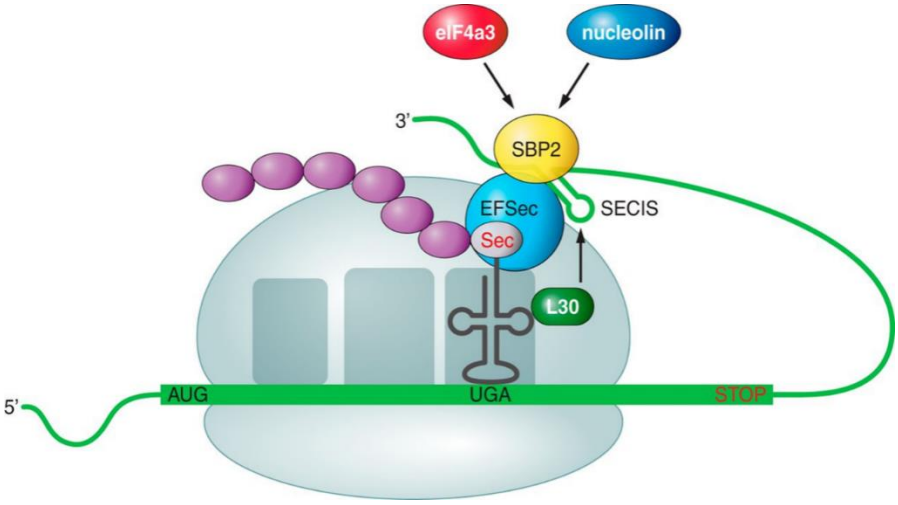

Figure 4: Eukaryotic Sec-insertion machinery.

The Sec-tRNA is bound by a specialized eukaryotic elongation factor (EFSec), and recruited to the ribosome at a UGA codon by the use of a special stem-loop structure in the 3'-untranslated region of the mRNA (SECIS element) and a SECIS binding protein (SBP2) (Labunskyy et al. 2014).

1.2 Selenoproteins – a structural perspective

1.2.1 The Selenoproteome

Selenoproteins are characterized by at least one Sec residue in their amino acid sequence. There are twenty-five genes coding for selenoproteins that where identified by different methods in the human genome (**Table 1**). These proteins constitute the so-called selenoproteome. Knockout experiments of the Trsp gene from which tRNASec is synthesized yielded to early embryonic lethality in mouse and an increased sensitivity of cells to reactive oxygen species (Bösl et al. 1997) which suggested the essentiality of selenoproteins and their involvement in protection against reactive oxygen species.

Proteins of this family exhibit diverse tissue distribution from ubiquitous to tissue specific, subcellular localization as well as functions. Most of these proteins exhibit one single Sec residue (**Table 1**), generally localized within the catalytic site and therefore contributing as a major actor to redox reactions. The protein SelenoP is the only one with ten Sec residues. The function of this protein is directly related to Se transport in the organism. However, the function of many selenoproteins is still poorly characterized. The most characterized are the thioredoxin reductases and glutathione peroxidases, deiodinases and the methionine-R-sulfoxyreductase that are known to be involved in redox -related reactions.

Table 1 :List of proteins constituting the human selenoproteome and their related functions
(Modified from Labunskyy et al. 2014)

Selenoprotein	Abbreviation	Sec location (Protein size)	Function
Glutathione peroxidase 1	GPx1	47(201)	Cytosolic Glutathione peroxidase
Glutathione peroxidase 2	GPx2	40(190)	Gastrointestinal glutathione peroxidase
Glutathione peroxidase 3	GPx3	73(226)	Plasma Glutathione peroxidase
Glutathione peroxidase 4	GPx4	73(197)	Phospholipid hydroperoxide, glutathione peroxidase,
Glutathione peroxidase 6	GPx6	73(221)	olfactory glutathione peroxidase
Iodothyronine deiodinase 1	DIO1	126(249)	Thyroid hormone-activating iodothyronine deiodinase
Iodothyronine deiodinase 2	DIO2	133,266(273)	Tissue-specific thyroid hormone-activating iodothyronine deiodinase
Iodothyronine deiodinase 3	DIO3	144(278)	Tissue-specific thyroid hormone-deactivating iodothyronine deiodinase
Thioredoxin reductase 1	TR1	498(499)	Reduction of cytosolic thioredoxin
Thioredoxin/glutathione reductase	TGR	655(656)	Testis-specific thioredoxin reductase
Thioredoxin reductase 3	TR3	522(523)	Reduction of mitochondrial thioredoxin and glutaredoxin
Methionine-R-sulfoxide reductase	MSRB1	95(116)	Reduction of oxidized methionine residues
Selenophosphate synhetase 2	SPS2	60(448)	Involved in synthesis of selenoproteins
Selenoprotein W	SelenoW	13(87)	Unknown
Selenoprotein T	SelenoT	36(182)	Unknown
Selenoprotein H	SelenoH	38(116)	Unknown
Selenoprotein V	SelenoV	273(346)	Unknown
Selenoprotein I	SelenoI	387(397)	Unknown
Selenoprotein F	SelenoF	93(162)	Putative role in quality control of protein folding in the ER
Selenoprotein M	SelenoM	48(145)	Unknown
Selenoprotein K	SelenoK	92(94)	Putative role in ER associated degradation
Selenoprotein S	SelenoS	188(189)	Putative role in ER associated degradation
Selenoprotein O	SelenoN	667(669)	Unknown
Selenoprotein N	SelenoN	428(556)	Putative role during muscle development and maintenance
Selenoprotein P	SelenoP	59, 300, 318, 330, 345, 352, 367, 369, 376, 378(381)	Se transport

1.2.2 Structural motif conserved over the selenoproteome -The thioredoxin fold

When having a close look at the structural organization of well-described proteins of the selenoproteome, one prominent feature is the presence of a conserved fold in most selenoproteins: the thioredoxin-fold. Interestingly, the Sec residu is replacing one of the two main cysteines usually located in a specific motif C-X-X-C which is part of this fold and is important for the catalytic mechanisms (**Figure 5**). Thioredoxins belongs to a family of proteins that is involved in numerous redox reactions as electron donors. The founding member of this family, the thioredoxin is involved in the maintenance of reduced forms of cysteines in many cytoplasmic proteins or the formation of disulfide bounds of membrane-surface or secreted proteins within the endoplasmic reticulum. Oxidized thioredoxin is a substrate of the enzyme thioredoxin reductase. Structurally, the thioredoxin-fold is organized as a core of beta sheet surrounded by alpha helices (Figure 10B). The cysteines motif located at positions 32 and 35 between the first alpha helix and the first beta sheet is essential for the binding with protein partners as well as the electron transfer from the reduced thioredoxin to the protein partner (Figure 10C). There are several thioredoxine-like folds presenting different structural organization and characteristic of each subgroup of the family (Pan and Bardwell 2006).

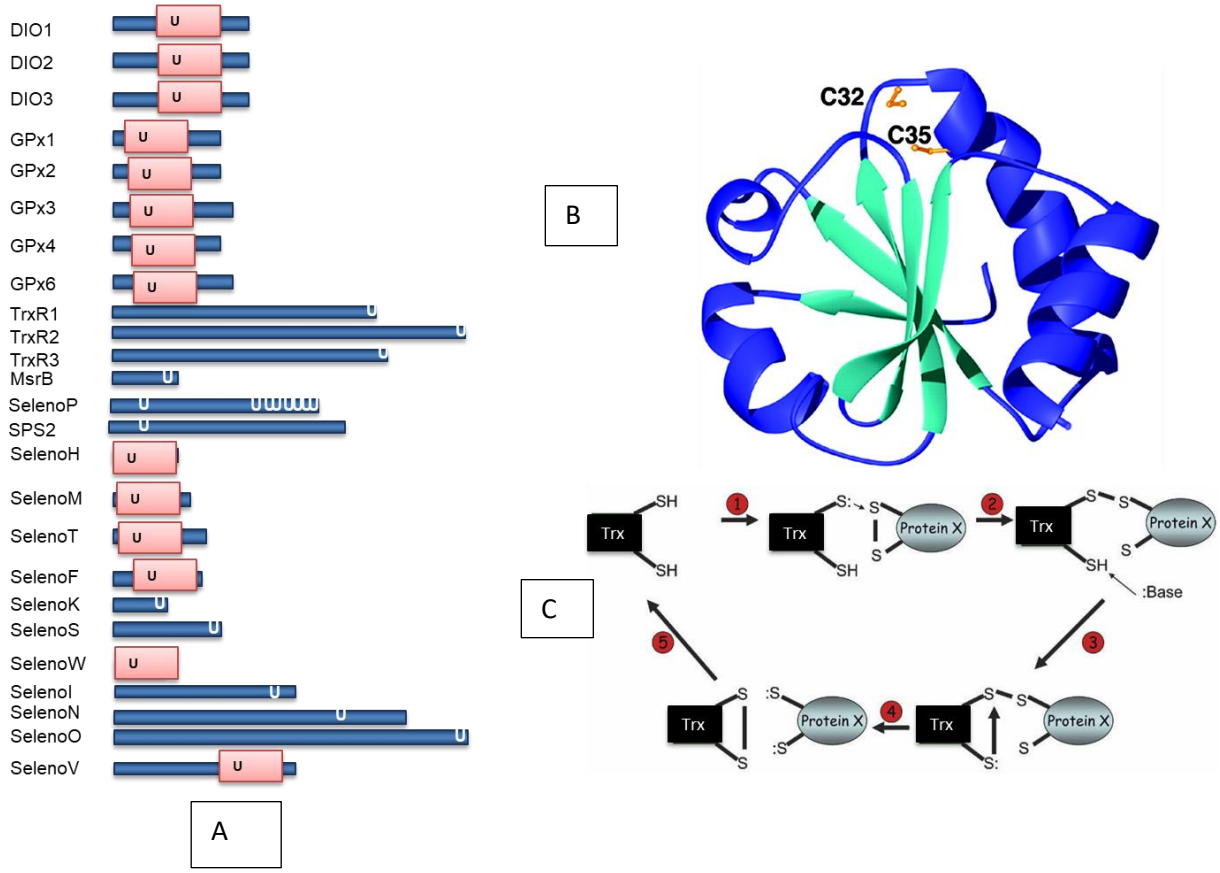

Figure 5: The thioredoxin-fold is well represented among the selenoproteome

(A) Distridution of the thioredoxin-fold in selenoproteome. The pink box represents the thioredoxin-fold which includes the sec (U) residu. (B) Structural organization of the thioredoxin-fold displaying the two important cysteines. (C)Schematic representation of the reaction involving the reduced thioredoxin and showing the importance of the two catalytic cysteines 32 and 35 (Pan and Bardwell 2006).

1.2.3 Structural Organization and Function of Sec containing oxidoreductases

1.2.3.1 Thioredoxin reductase

Thioredoxin reductases (TR) are enzymes that use NADPH to reduce oxidized thioredoxin. The so reduced thioredoxin is then used as electron donor in reactions involving dithiol-disulfide couples to regulate the cell redox environment at different levels (**Figure 6**). There are three TR homologues in mammals Thioredoxin Reductase 1 or TR1, Thioredoxin Reductase 2 or TR2 and the Thioredoxin/Glutathione Reductase or TGR. All three isozymes have different cellular locations and are all selenoproteins (reviewed in Reeves and Hoffmann 2009).

TR1 is the major protein disulfide reductase of the cell and is found in the cytoplasm and the nucleus. It reduces the thioredoxin 1 via an NADPH dependent reaction (**Figure 6)** (Arnér and Holmgren 2000). Studies enable to identity the implication of this enzyme in a wide range of functions notably DNA repair, regulation of cell signaling, redox homeostasis, as well as cancer prevention (Arnér and Holmgren 2000).

TR2 is a mitochondrial isoform involved in the reduction of the mitochondrial thioredoxin 2 and glutaredoxine2 but is also capable of binding thioredoxin 1 (Turanov, Su, and Gladyshev 2006).

TGR is specifically expressed in testis and differs from the two firsts by an additional N-terminal glutaredoxine domain. By this feature, this isozyme is believed to be involved in the reduction of both thioredoxin and glutathione systems (Sun et al. 2001).

All three TRs share common features. They are organized in homodimer. Each subunit of the dimer is organized in four domains: the FAD binding domain, and NADPH binding domain, the interface domain and the conserved C-terminal domain including the conserved redox motif Gly-Cys-Sec-Gly or GCUG. The later domain is in an extended sequence that is structurally flexible (**Figure 7**). This flexibility enables the electron transfer from the active site to the protein surface (Fritz-Wolf, Urig, and Becker 2007; Fritz-Wolf et al. 2011).

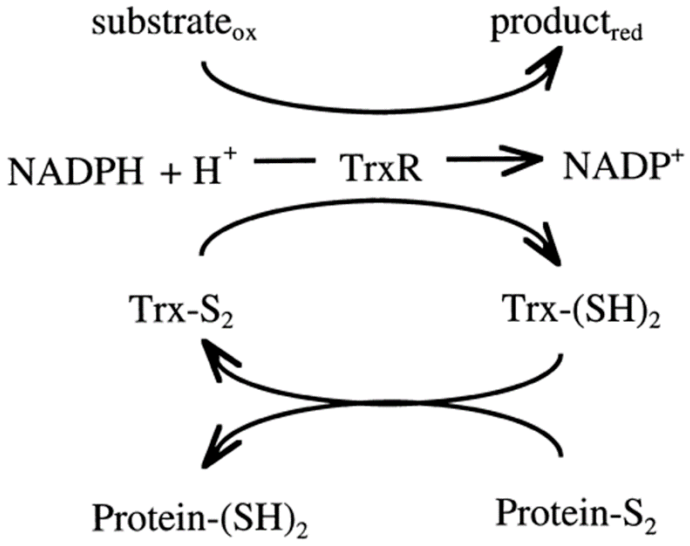

Figure 6: NADPH dependant reduction reaction of Thioredoxine by thioredoxine reductase

The figure schematically depicts the reduction of the active site disulfide in oxidized thioredoxin, Trx-S_2, to a dithiol in reduced thioredoxin, Trx-$(SH)_2$, by thioredoxin reductase (TrxR) and NADPH. Trx-$(SH)_2$ reduces protein disulfides by its general oxidoreductase activity, generating Trx-S_2. (Arnér and Holmgren 2000).

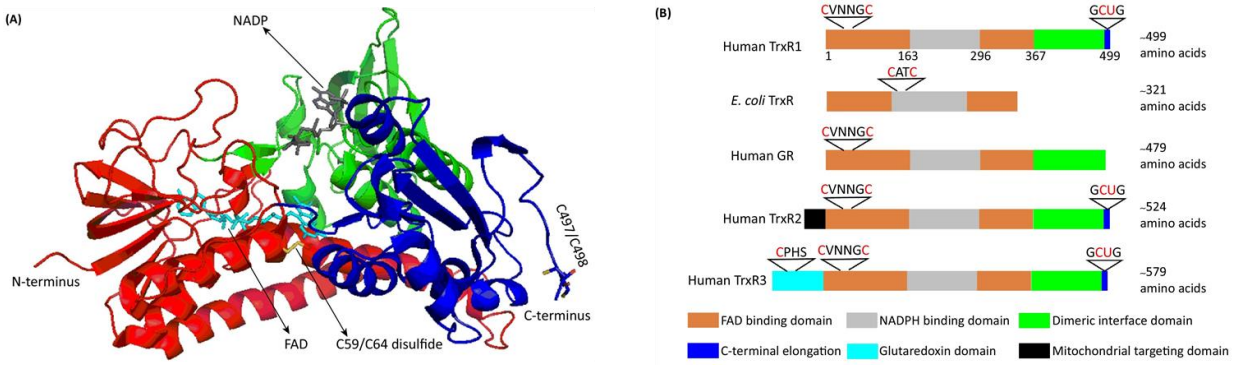

Figure 7: Structure (A) and Domain organization (B) of mammalian Thioredoxine Reductases.

(A) Structure of a monomer of the rat Thioredoxine reductase (PDB accession number 1H6V). The FAD and NADPH are depicted in their respective binding domains, the N-terminal redox center C59-C64 and the C-terminal redox center C497-C498 are localized in flexible extensions. The FAD binding domain, the NADPH binding domain and the interface domain are indicated in red, green and blue respectively.

(B) Domain organization of thioredoxine reductase. The different binding domains as well as the interface domain and the C-terminal extension containing the selenocysteine (U) and its neighbouring cysteine residues (C) are represented. (Zhang J et al, 2017).

1.2.3.2 Glutathione peroxidase

Human Glutathione Peroxide family has height members. Six of them, GPx1 to 6 are selenoproteins (reviewed in Reeves and Hoffmann 2009). The Sec residue is highly conserved and is located in the enzyme active site. It plays an essential role in the reactions and in the interaction with substrates. Proteins of this family use glutathione as an electron donor to catalyze the reduction of peroxides notably hydrogen peroxide and phospholipid peroxides and thus have a central function in oxidative stress protection.

Glutathione peroxidase 1 or GPx1 was the first selenoprotein identified (Flohe, Günzler, and Schock 1973) and is one of the most abundant (Lei, Cheng, and McClung 2007). It is an ubiquitously expressed protein of 22 kDa which active form is a homotetramer. As other enzymes of this family, it uses two glutathione molecules GSH as substrate to catalyze the reduction of peroxides and produces oxidized glutathione GSSG, which is later reconverted into GSH by the enzyme glutathione reductase (Lubos, Loscalzo, and Handy 2011).

Structurally, GPx1 is characterized by a thioredoxin-fold organized in seven β-sheets, with five of them forming the core of the enzyme surrounded by four α-helices (Structure by Kavanagh et al 2005 PDB accession number 2F8A). The unique Sec residue is located at position 46 and forms with two other amino acids Gln81 and Trp136 the catalytic center.

Reactions catalyzed by GPx1 are implicated in a wide range of physiological processes (reviewed in Reeves and Hoffmann 2009). Overexpression of the enzyme in mice was reported to lead to several effects including hyperglycemia, resistance to insulin and obesity (McClung et al. 2004).

1.2.3.3 Methionine-R-sulfoxide reductase1

Methionine (Met) is with cysteine (Cys) the second sulfur containing amino acid of proteins. Oxidation of this residue can lead to important functional and structural protein alterations, therefore, the importance of Methionine-R-sulfoxide reductases to maintain enzymatic cellular activities. This family of proteins is composed of four enzymes: MsrA, MsrB1, MsrB2 and MsrB3. The function of this family of enzymes is to reduce S- and R- enantiomers of methionine sulfoxide that are produced during Met oxidation by reactive oxygen species. The MsrB1 is the only

selenoprotein of the family that contains a Sec residue in its catalytic site. This enzyme reduces the R- enantiomer only. It is localized in the cytosol and in the nucleus and shows a maximum activity in liver and kidney (Fomenko et al. 2009).

1.2.4 Structural organization of mammalian ER resident selenoproteins

Seven proteins of the selenoproteome reside in the Endoplasmic Reticulum (ER) (Shchedrina et al. 2010). Those proteins are found to be involved in a wide range of functions, notably the regulation of thyroid hormone synthesis, calcium homeostasis, protein folding and ER associated degradation (reviewed in Pitts and Hoffmann 2017) but for many of them, as it is the case for selenoproteins in general, their function is still unclear. Among ER resident selenoproteins, five of them are membrane proteins (**Figure 8**), notably, the Iodothyronine Diodinase type 2 (DIO2), SelenoproteinK (SelenoK), SelenoproteinS (SelenoS), SelenoproteinT (SelenoT) and SelenoproteinN (SelenoN) (**Figure 8**). Four of the ER selenoproteins handle a thioredoxin-like motif that contains the single Sec residue and for only three of them, the thioredoxin motif is oriented inside the ER Lumen. SelenoN is the only one with a calcium binding EF-hand domain. However, SelenoK was also found to be involved in the calcium homeostasis control.

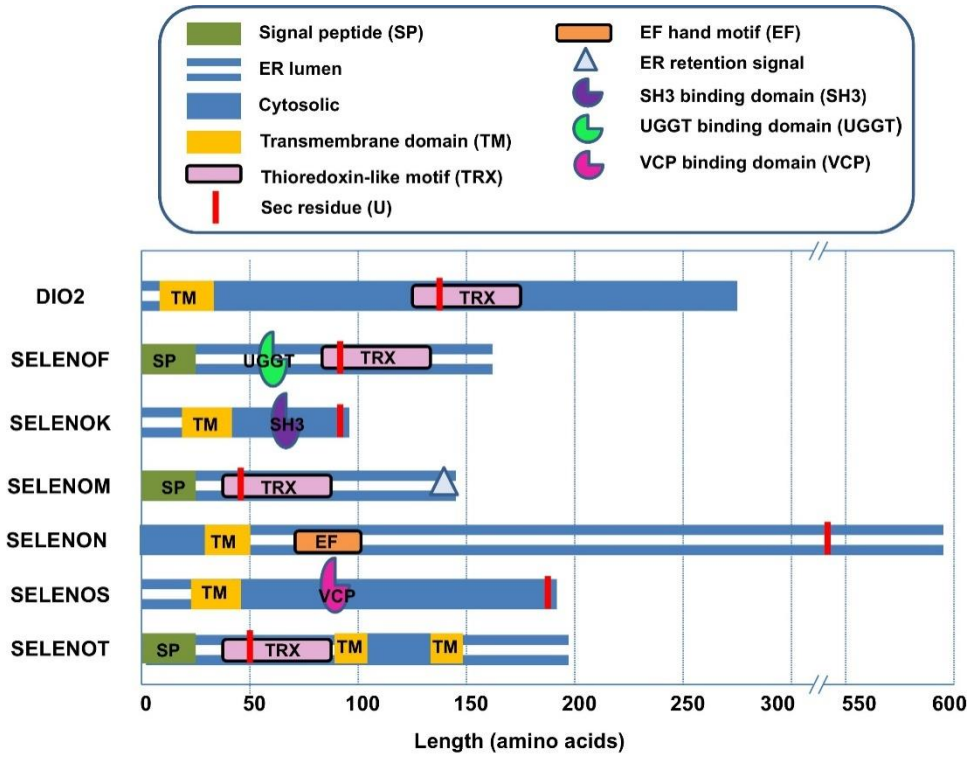

Figure 8: Domain organization of ER selenoproteins

This diagram illustrates the relative position of Sec residues (red), signal peptides (green), transmembrane domains (yellow), thioredoxin-like motifs (pink), EF hand motifs (orange), and ER retention signals (white triangles). Established binding/interaction sites are denoted by three-quarter circle symbols (Pitts and Hoffmann 2017).

1.2.4.1 Selenoprotein K (SelenoK)

SelenoK is a small 16 kDa protein from the SelS/SelK family (Shchedrina et al. 2011a; Liu, Zhang, and Rozovsky 2014) localized at the endoplasmic reticulum (ER) membrane (Lu et al. 2006). Topologic prediction revealed that the small N-terminal domain is oriented toward the cytosol whereas the intrinsically disordered C-terminus is oriented in the ER lumen. This C-terminal domain handles the Sec residue at position 92 (Shchedrina et al. 2010) and an SH3 binding domain (Li 2005). It is inserted in ER membrane by one single transmembrane domain matching amino acids 20 to 42.

SelenoK is organized as a homodimer through a diselenide intermolecular bound that can be reduced by thioredoxin reductase (Liu, Zhang, and Rozovsky 2014).

SelenoK was proved to be involved in many processes. It is used as cofactor by the acyl transferase DHHC6 for the inositol 1-4-5 triphosphate receptor (IP3R) palmitoylation. This post-translationnal modification stabilize the calcium channel IP3R (Hoffman 2015). Increased expression level of SelenoK was correlated to an increase of misfolded proteins in the endoplasmic reticulum and it was proved that SelenoK is involved in the degradation of glycosylated substrates by the endoplasmic reticulum associated protein degradation pathway (ERAD) (Shchedrina et al. 2011a).

1.2.4.2 Selenoprotein S (SelenoS)

SelenoS or VCP interacting membrane protein (VIMP) is another ER membrane protein. It is also a member of the SelS/SelK family which has thirty-three members in human. This family shares common characteristics. Notably, they are proteins of maximum 300 amino acids, with a unique transmembrane domain. Among the last five residues of the intrinsically disordered C-terminus is usually found a Sec or a Cys residue (Shchedrina et al. 2010, 2011b).

SelenoS has two isoforms. The longer isoform contains a Sec residue and is constituted by a coil-coiled domain organized in two helices followed by a disordered domain where the Sec residue is located at the position 188. The coil-coiled domain is important for the dimerization and for the binding of the p97 ATPase (Christensen et al. 2012).

Functional studies revealed that SelenoS has a disulfide reductase activity similar to that of the

thioredoxin reductases (Liu, Zhang, and Rozovsky 2014) as well as a peroxidase activity (Liu, Zhang, and Rozovsky 2014). As SelenoK, it is a member of the ERAD machinery and it is responsible of misfolded protein retro-transport from the ER to the cytoplasm where they will be addressed to the proteasome for degradation (Ye et al. 2004).

1.2.4.3 Type 2 Iodothyronine Deiodinase 2 (DIO2)

Iodothyronine deiodinase is a family of proteins involved in the regulation of thyroid hormone. In human, this family is composed of three members, Iodothyronine Deiodinase type 1, 2 and 3 or DIO1, DIO2, DIO3. DIO 1 and 3 are localized within the plasma membrane whereas DIO2 is an ER membrane protein.

DIO2 has a single transmembrane domain. Its small N-terminus is in the ER lumen whereas the main part of the protein resides in the cytosol. It contains one thioredoxin-fold domain that handles the Sec residue. (**Figure 9**). The enzyme is responsible for the conversion of the prohormone thyroxine to active thyroid hormone 3,3',5- triiodothyronine (T3). Studies addressing its expression demonstrated its implication in muscle regeneration and development, as its maximum expression level was observed in muscle after birth or following an injury (Mullur, Liu, and Brent 2014).

Structure of the DIO3 catalytic domain was solved and enable to confirm the presence of the predicted thioredoxin-fold motif and a peroxiredoxin-like catalytic domain that suggested a mechanistic relationship with peroxiredoxine (Schweizer and Steegborn 2015) (**Figure 9**). It revealed also the structural arrangement of the deiodinase-specific insertion site (Dio-insertion) as well as the structural location of the Sec residue that appears to act as a substrate binding residue (Schweizer and Steegborn 2015).

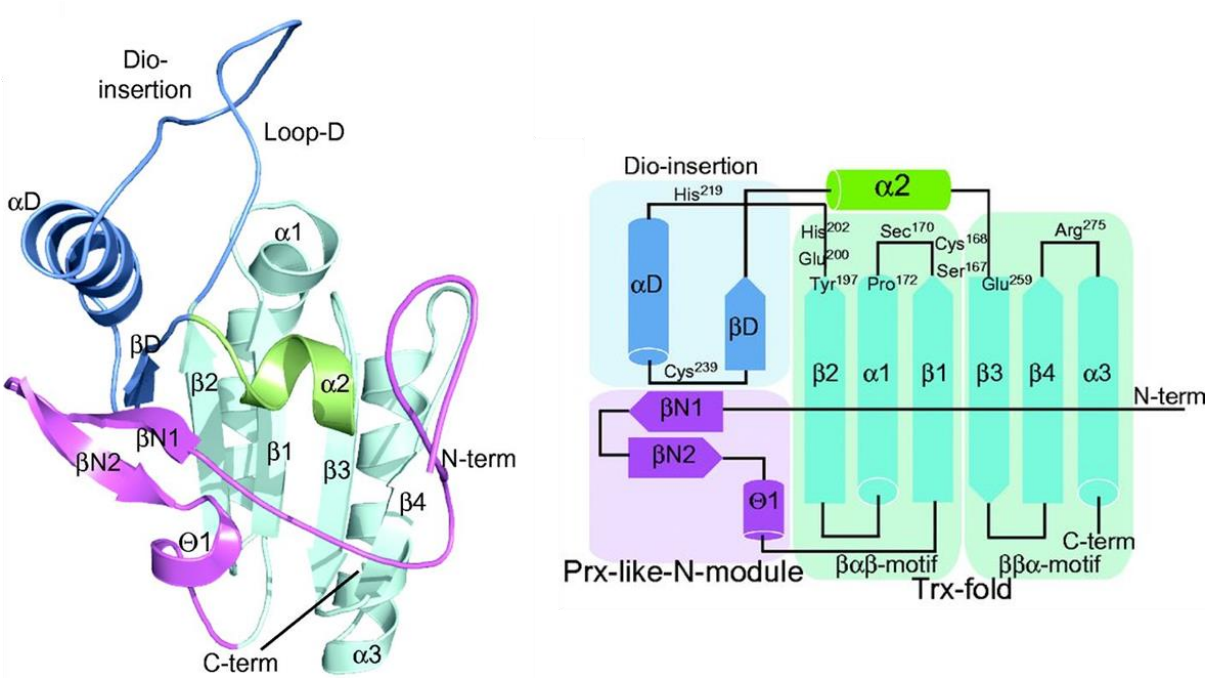

Figure 9: 3D Structure and Topology of DIO3 catalytic domain.

The catalytic site is composed of three main domains. A peroxiredoxine-like domain (purple), a thioredoxine fold (light green) and a deiodinase-insertion site (blue). (Schweizer and Steegborn 2015).

1.2.4.4 Selenoprotein T (SelenoT)

Selenoprotein T or SelenoT is a member of a family of proteins identified as Redox or Rdx family. Other members in the selenoproteome are SelenoW, SelenoH and SelenoV. Members of Rdx family are present in numerous organs and tissues, but SelenoT expression is very high during development, also confined to endocrine tissues in adulthood. One characteristic of this family is the presence of a thioredoxin-fold (Dikiy et al. 2007).

SelenoT is a small membrane protein of 19 kDa that is inserted in the ER membrane through two transmembrane domains (**Figure 8**). Studies showed that it is also localized in the Golgi and possibly in the cytosol (Dikiy et al. 2007).

The thioredoxin-fold structurally organized as described in chapter 1.2.2 is oriented toward the ER lumen and contains the single Sec residue at position 17 in the conserved redox motif CxxU. In another protein of the same family, Selenoprotein W, the redox motif was found to be located on

a loop between β_1 and α_1 adjacent to the β-sheet (Aachmann et al. 2007). Homology-based modelling of SelenoT revealed a thioredoxin-like secondary structure β_1-α_1- β_2- β_3- β_4-linker- α_2 (Aachmann et al. 2007).

Several studies demonstrated that SelenoT exhibits a thioredoxin reductase-like activity (Boukhzar et al. 2016) and that it is implicated in calcium homeostasis. Its overexpression was correlated to increased cytosolic calcium mobilization (Grumolato et al. 2008). Recently, SelenoT was found to be a novel subunit of the A-type OST complex, necessary for ER homeostasis and exerting a pivotal adaptative function that allows endocrine cells to properly achieve the maturation and secretion of hormones (Hamieh et al. 2017).

1.2.4.5 Selenoprotein M (SelenoM) and Selenoprotein F (SelenoF or Sep 15)

Selenoprotein M or SelenoM is a small 15 kDa selenoprotein of the endoplasmic reticulum which is expressed predominantly in the brain (Y. Zhang et al. 2008). Functional studies revealed that, SelenoM is implicated in body weight regulation as well as calcium homeostasis, but its molecular mechanism is still unclear.

NMR structure of SelenoM disclosed a thioredoxin-fold domain, which incudes the Sec residue. Its secondary structure is organized as followed, β_1-α_1-α_2-β_2-β_3-β_4-α_3 with the redox motif CxxU localized between β_1 and α_1 (**Figure 10**).

Selenoprotein F or SelenoF shares 37% sequence identity with SelenoM and it is also localized within the ER. Studies revealed that SelenoF binds the UDP-glucose:glycoprotein glucosyltransferase (UGGT) through its UGGT binding domain (**Figure 8**). Therefore, ti was thought to mediate disulfide bond of glycoproteins that are modified by UGGT (reviewed in Pitts and Hoffmann 2017).

NMR structure of SelenoF showed a thioredoxin-fold with secondary structures organized as SelenoM with CxU redox motif between the first β sheet and α helix (**Figure 10**). Analysis of this structure revealed a local conformational modification of the redox center of both SelenoM and SelenoF after thiol-disulfide exchange. This observation suggested a thiol-disulfide isomerase activity (Ferguson et al. 2006).

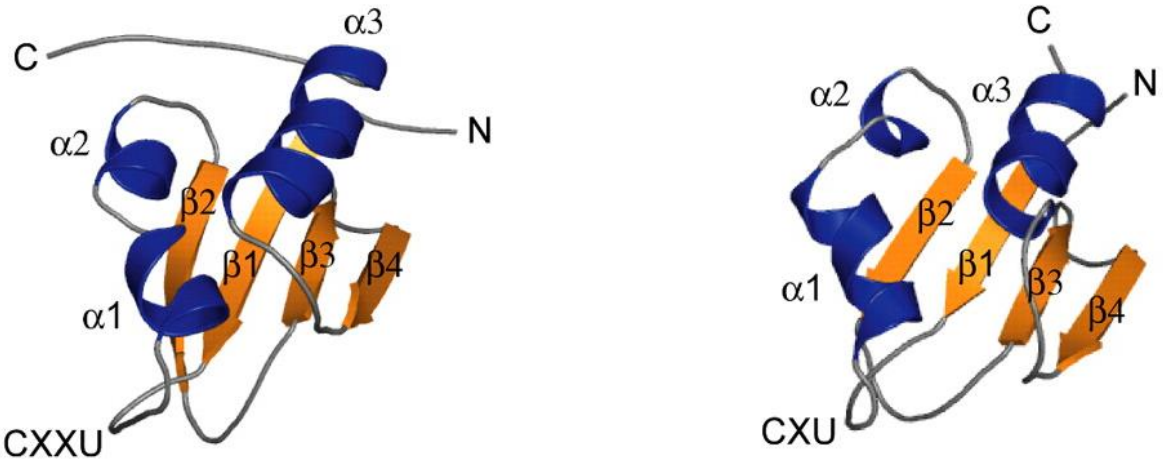

Figure 10: NMR structure of Selenoprotein M (with CxxU motif) and Selenoprotein F (with CxU motif)(Ferguson et al. 2006)***. Both proteins are formed by a canonical thioredoxin-fold domain.***

1.3 Selenoprotein N

1.3.1 SELENON gene and diseases

1.3.1.1 SELENON Related Myopathies

Selenoprotein N gene, SELENON, is the first gene coding for a selenoprotein which mutation was directly linked to a human genetic disease. Mutations in SELENON can lead to a group of four different muscular disorders: the rigid-spine congenital muscular dystrophy, the multiminicore disease, the Mallory body-like desmin related myopathy and the congenital fiber-type disproportion myopathy. These different clinical syndromes are now classified as SELENON-related myopathies (SELENON-RM) (Castets et al. 2012). Despite different clinical descriptions, SELENON-RM patients present common symptoms such as weakness of the neck, spine rigidity leading to scoliosis (***Figure 11***) and respiratory insufficiency (Lescure et al. 2016; Castets et al. 2012). Recent reports suggested that the respiratory insufficiency syndrome that was traditionally attributed to respiratory muscles weakness could also be attributed to abnormal lung development, as demonstrated in *Selenon-/-* mice as a model for SELENON-RM (Moghadaszadeh et al. 2013).

Many mutations in the SELENON gene were characterized, including the coding region, and the SECIS element located in the 3'UTR region(Allamand et al. 2006). This last mutation inhibits thebinding of SBP2 tp the SECIS RNA structure. As this interaction is essential for Sec incorporation, the SECIS mutation inhibits SelenoN expression. Surprisingly and despite the specific muscular phenotype in SELENON-RM patients, SelenoN is ubiquitously expressed. However, analyses of SelenoN expression pattern in both zebrafish and mouse embryos demonstrated a strong expression of this mRNA in fetal tissues, specifically in somites and notochord that are precursors of muscle and spine structures (Deniziak 2007; Castets 2011), and in proliferative muscle progenitors (Petit et al. 2003).

1.3.1.2 SELENON and breast cancer

SELENON gene expression has been reported to be post-transcriptionaly regulated by the microRNA miR-193-3p, one microRNA that suppresses breast cancer cell growth (Tsai et al. 2016).

Microarray experiments combined to bioinformatics approaches identified SELENON among five genes as regulated by the miR-193-3p. Real time PCR experiments confirmed the downregulation of the expression of the SELENON gene and two other genes CCDN1 and PLAU in miR-193-3p mimic transfected cells. In addition, knockdown of SELENON and the other target genes suppressed cell growth similar to miR-193-3p overexpression in breast cancer cells. This suggested that the miR-193-3p suppresses cancer cell growth by silencing those genes (Tsai et al. 2016) and it indicated a putative oncogenic function for the SELENON gene which remains to be investigated.

Figure 11 : Clinical effect of SELENON mutations on children affect by muscular congenital disorders (Flanigan et al, 2000)

1.3.2 Selenoprotein N associated functions

1.3.2.1 Function in muscle establishment and maintenance

In order to study the role and impact of SelenoN deficiency, two knock out models in mice and zebrafish were established. On one hand, SelenoN depletion in zebrafish led to a somite disorganization and a strong alteration of the global muscle architecture (Jurynec et al. 2008; Deniziak et al. 2007). This model also presented a defect in the slow fiber development (Jurynec et al. 2008). On the other hand, loss of function of SelenoN in mice induced no obvious phenotype compared to wild-type in normal breeding situation but. However, when exposed to a forced swimming test, a situation mimicking global stress and situation combining physic, environmental, thermal and respiratory stresses, the *selenon-/-* mice developed symptoms similar to SELENON-RM patients such as a spinal rigidity, development of a kyphosis accompanied by a reduced mobility, and small change in proportion of slow fibers in the paraspinal muscles (Castets et al. 2011). Altogether, this information raised the hypothesis that SelenoN is essential for the establishment of muscle during embryogenesis, and for its maintenance under stress condition. Another study showed that SelenoN depleted muscles of knock-out mice are defective in regeneration, due to decrease in number of muscle stem cells or satellite cells. This last phenotype was also observed in SELENON-RM patients. Muscle biopsies from patients showed a reduction of satellite cells that worsened with age, probably due to degeneration. Tacken together, these results suggested that SelenoN could be essential for the proliferation and/or the maintenance of muscle progenitors in adult muscle.

1.3.2.2 Calcium concentration regulation: Ryanodine receptor and SERCA1 activities control

The link of SelenoN and to ryanodine receptors (RyR) was demonstrated *in vivo*. RyRs are a family of calcium channels implicated in the ion transport from the sarcoplasmic reticulum (SR) to the cytoplasm and are essential for muscle contraction. It was reported that SelenoN is essential for RyR activity, since SelenoN deficiency caused RyR dysregulation, impairing calcium influx into the cytoplasm (Jurynec et al. 2008). These data suggest that SelenoN could play a role in RyR regulation by controlling its oxidative status or by acting as a chaperone. Indeed, it was proved that RyR activity is controlled by the oxidation/reduction of several cysteine residues (Castets et

al. 2012).

SarcoEndoplasmic Reticulum Ca^{2+}ATPase (SERCA) is anoter family of proteins involved in calcium homeostasis by transporting the bivalent ion from the cytoplasm to the endopasmic reticulum (ER). This calcium pump family counts many members and among them, Serca2b which is an ubiquituously expressed variant (Baba-Aïssa et al. 1998). Serca2b activity is regulated by the redox status of two cysteines at position 875 and 887 that are localized within the ER lumen (Li Y et al, 2014). Trapping-mutant experiments by modification of SelenoN active site combined to mass spectrometry analysis enlighted the binding of SelenoN to Serca2b. In addition, it was shown that the two Serca2b regulating cysteines are important for this binding. Moreover, comparison of calcium concentration in ER ($[Ca^{2+}]_{ER}$) and of accumulation rate indicated that both are significantly increased in cells expressing SELENON, compared to knock-out cells. In this later situation, concentration level is restored either by introducing SELENON or by providing a catalase-peroxidase, which induced a peroxidase dependent reduction of Serca2b cysteines. Taking together, this study suggested that SELENON plays a role in intra-ER calcium concentration regulation through activation of the calcium pump Serca2b, consecutive to the reduction of its two cysteines in the ER Lumen (Marino et al, 2015).

Taking together, studies of SelenoN regulation activity on both ryanodine receptors RyRs and the calcium pump Serca2b indicated that SelenoN might play an essential role in calcium cellular homeostasis by controlling its transport between cytoplasm and ER. The question that arises is what is the signal or the condition that will trigger the action of SelenoN on calcium cellular transport in one direction compared to the other?

1.3.2.3 Cell redox homeostasis and cell defense against oxidative damages

SelenoN is ubiquitously expressed with a higher expression level in proliferative muscle cells, such as the fibroblasts and the myoblasts (Petit et al. 2003). A measurement of oxidant activity level in cells from SELENON-RM patients revealed an increased basal oxidant activity in myoblasts compared to controls. Moreover, blot-assays revealed an increase in oxidized proteins content in fibroblasts and myoblasts of SELENON-RM patients. In addition, both type of cells treated with peroxide showed a reduced cell survival, suggesting an increased sensitivity to oxidative stress in cells lacking SelenoN. Taken together, the results of this study suggested increased sensitivity to oxidative stress is associated to the lack of SelenoN in SELENON-RM patient cells, as a consequence of an increase in basal oxidant activity level. Therefore, it was proposed that SelenoN protect cells from oxidative damage by reducing or by keeping the basal level of oxidative activity (Arbogast et al. 2009).

1.3.3 Description of SelenoN associated domains

1.3.3.1 The eukaryotic SelenoproteinN

In humans, the third exon which is an Alu sequence is alternatively spliced out leading to two isoforms. The longer isoform contains two Sec codons, whereas the shorter without exon three contains only one. This second isoform is predominantly expressed and abundantly found in skeletal muscle, brain, lungs, and placenta. Only the shorter isoform is translated into a 70 kDa protein with one single Sec residue (Petit et al. 2003). SelenoN is an integral ER membrane protein with an N-terminal hydrophobic region that represents the transmembrane (TM) domain. This domain was found to present an addressing and retention signal in the ER (Petit et al. 2003). Topologic analysis locates the protein N-terminal end in the cytosol, whereas the main protein, including its predicted active site, is located in the ER lumen (**Figure 12**). Moreover, inspection of the amino acid sequence revealed the presence of an EF-hand calcium binding domain. Bioinformatics analyses predicted, three glycosylated asparagines, and a redox motif SCUG containing the Sec or U residue (Error! Reference source not found.). This redox motif possesses s equence similarities with the thioredoxin reductases conserved catalytic motif GCUG (Castets et al. 2009). In the mammalian thioredoxin reductases, the selenolthiol formed by the Cys and Sec

residues of the motif represents the active site (Sandalova et al, 2001). As proposed by Sandalova et al, the couple Cys497-Sec498 represents a second redox center in the reaction of electron transfer to the substrate Thioredoxin (***Figure 13***).

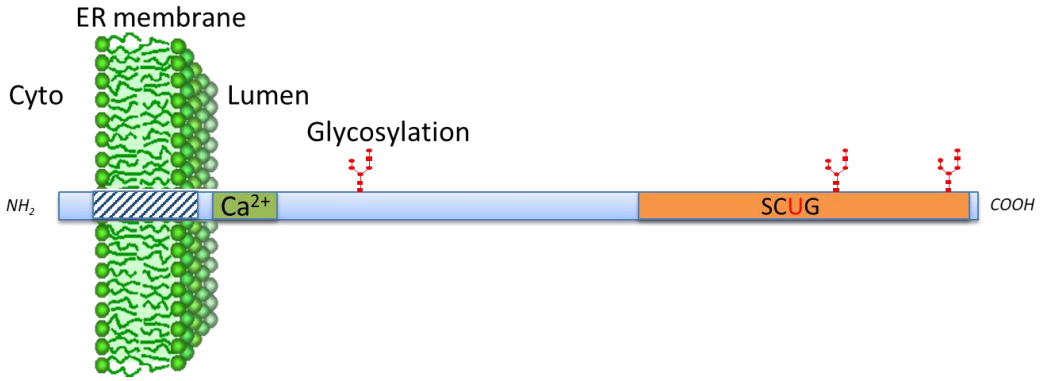

Figure 12: Schematic representation of the topology of the human SelenoN in the endoplasmic reticulum lumen and of its bioinformatics predicted domains.

SCUG= Putative catalytic site. Bioinformatics searches using SelenoN sequence revealed no significant homology to any other known protein. In SelenoN, aside from the N-terminal transmembrane domain (blue dashed box), motif prediction searches identified a typical EF-hand motif (green box), corresponding to a Ca2+ binding domain. Selenoprotein activity may also be deduced from the sequence context of the Sec residue, which constitutes a landmark of the catalytic center. SelenoN harbors a SCUG predicted catalytic site, reminiscent of the thioredoxin reductase GCUG motif. This similarity suggests a reductase activity. This redox motif is included within an UAS conserved domain, a domain of unknown function (orange box). It was shown that the protein is glycosylated and the positions of the three Asn modified residues were identified (depicted as red Y shapes). (adapted from Castets et al, 2012)

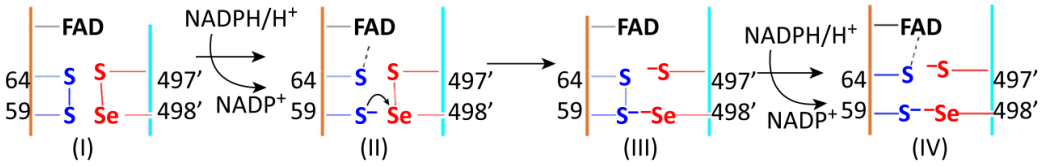

Figure 13 : Reaction mechanism for mammalian TrxR

The fully oxidized enzyme-bound FAD picks up two electrons from one NADPH (I) and reduces the disulfide to a dithiol pair (redox center C59/C64) to form the N-terminal reduced intermediate (II), which further passes the electrons to generate the N-terminal oxidized (C59/C64) and C-terminal selenylsulfide reduced intermediate (C497/U498) (III). Finally, another NADPH further donates two electrons to the partially reduced enzyme (III) to generate the fully reduced enzyme (IV) (Zhang et al. 2017)

As described previously, zSelenoN is located within the endoplasmic reticulum membrane with its N-terminus oriented in the cytosol, whereas the C-terminus with the main part of the protein is localized within the lumen of the organelle. The endoplasmic reticulum is known to be the primary storage site for cellular calcium with concentration reaching micromolar levels (Treiman M. et al, 2002). Eukaryotic SelenoN contains an EF-Hand domain, a predicted calcium binding domain. Structurally, EF-Hand domains are organized as α-helix-β-sheet-α-helix motifs (**Figure 14**). Binding of the calcium to the domain can have several effects ranging from a scaffold or structural organization role to a conformational induce-change that can lead to an inactive/active protein transition. The affinity of the calcium depends on the structure of the domain.

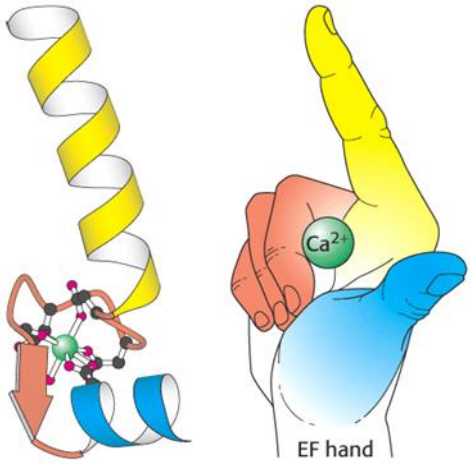

Figure 14: Structural organization of an EF hand domain

(https://www.quora.com/What-is-the-difference-between-EF-Hand-and-helix-turn-helix-protein-motifs)

1.3.3.2 Bacterial Selenoprotein N

Phylogenetic analyses identified one single bacterial SelenoN homolog among all bacteria genome sequenced so far, in *Candidatus poribacteria*. This bacterium is a sponge obligatory symbiot (Siegl et al, 2011) and genomic examination suggested that the presence of SelenoN in this only bacterial organism might have originated from a horizontal gene transfer. The bacterial SelenoN displays two main features: absence of an N-terminal transmembrane domain, and a thioredoxin-like sequence naturally fused to its C-terminal end (**Figure 15**). The presence of this thioredoxin-like domain was identified by bioinformatical approaches comparing the bacterial SelenoN with proteins of known function. Interestingly this domain is well conserved including two cysteines that are important in the function of thioredoxin, but in the bacterial SelenoN, there is only one cysteine whereas the first one is mutated into Asparagine (Figure 15). This particularity suggests

that this domain might correspond to either a one cys-peroxiredonin or to a monothiol glutaredoxin. The exact characterization of this domain can be assessed by the structure.

As found in the human SelenoN, the bacterial SelenoN sequence handles the conserved SCUG motif which, as mentioned above might be the catalytic site comparable to that of thioredoxin reductases. Hence, one can hypothesize on a possible functional interaction between the bacterial SelenoN and its C-terminal thioredoxin-like extension. This could be achieved either by a structural conformation of a monomer to enable the contact between both domains, or by a dimerization of the protein in a way that the C-terminal thioredoxin domain of one monomer contacts the SCUG redox center of the second monomer. This latest situation is reminiscent to the conformation and functional organization of the thioredoxin reductases.

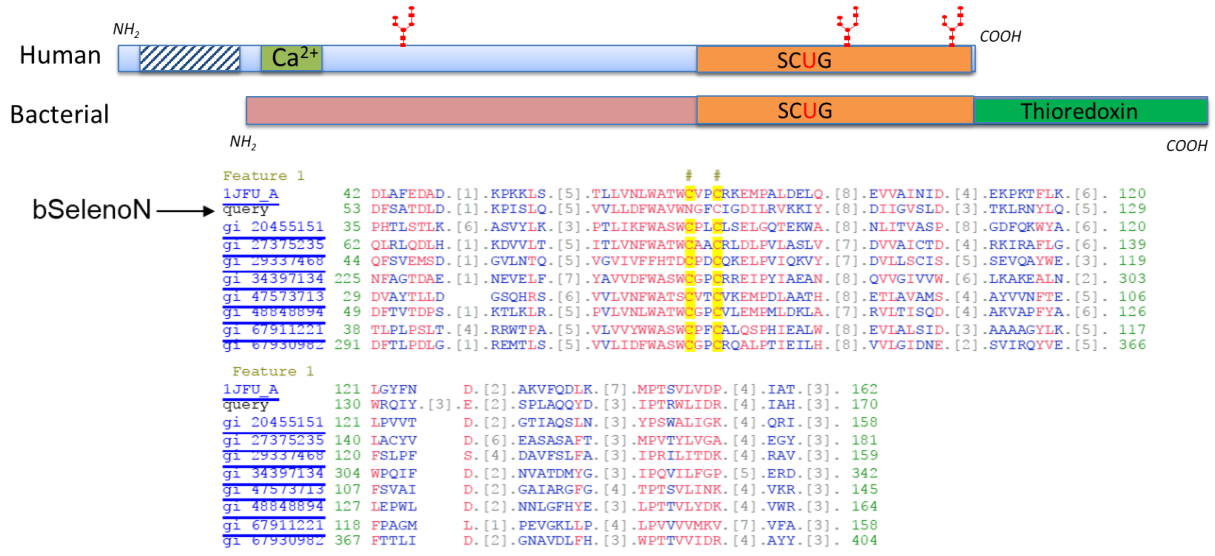

Figure 15: Schematic representation of the bacterial SelenoN and comparison to its human ortholog

The upper panel showed a schematic comparison of the bacterial and the human SelenoN. SCUG= putative catalytic site. The lower panel is an alignement of the bacterial C-terminal domain with known thioredoxin-folds. The conserved Cysteines of the motif are highlighted in yellow.

1.4 Aim of the thesis and theoretical methodology

From the evidence presented above, one can conclude that SelenoN function resides at the crossroad between diverse pathways covering the calcium signalling and oxidative stress, controlling the redox status of different cellular partners. However, as for many other selenoproteins, its exact molecular function and catalytic mechanism remains elusive.

The research program on selenoprotein N initiated by Dr. Lescure in the department of RNA architecture and reactivity of the IBMC (Strasbourg), combines two approaches to elucidate its mechanism: a biochemical enzymatic approach and in parallel a structural approach. The structural approach of the project will be conducted in collaboration with the departement of structural biology in Homburg leaded by Prof. Dr. Roy Lancaster. The advantage of a structural approach resides in the fact that it can disclose an unsuspected function based on the identification of possible characteristic conserved folds that are not necessarily directly accessible from the protein sequence, but that are informative about potential catalytic core binding activities. Such a situation was previously presented for the mouse deiodinase DIO3, as identification of a peroxiredoxine-like fold provided valuable hints concerning its catalytic mechanism. Additionally, investigations on the folding and structural rearrangement unveiled the functional mechanism for SelenoM and SelenoF.

The aim of my PhD project is to lay the foundations for SelenoN structure-function studies. For this purpose, the structure of purified Selenoprotein N should be determined by crystallization and X-ray analyses following the strategy detailed in **Figure 16**. Preliminary expression assays in human cells showed that the human protein is less stable and that it is expressed at a very low level compared to the zebrafish protein. The reason for this difference in protein stability and accumulation is unknown, however and because of this property, the zebrafish instead of the human protein will be used in this study. In addition, the bacterial protein will be also studied in parallel. This bacterial protein presents interesting features corresponding to common domains with the eukaryotic protein, but also a specific domain that suggests an evolution of the function.

Expression assays made in bacterial system leads to a protein of quality high enough for structural studies.

Importantly, analysis of the SelenoN structure might be an essential contribution to a better understanding of its function, as well as its dysfunction in the diverse forms of SELENON-related myopathies. In order to identify possible characteristic conserved folds, determination of the SelenoN 3D-structure is a prerequisite. This 3D-structure will be interpreted within the framework of SelenoN phylogenic residues conservation and positions of pathogenic mutations characterized in patients with SELENON-related myopathy.

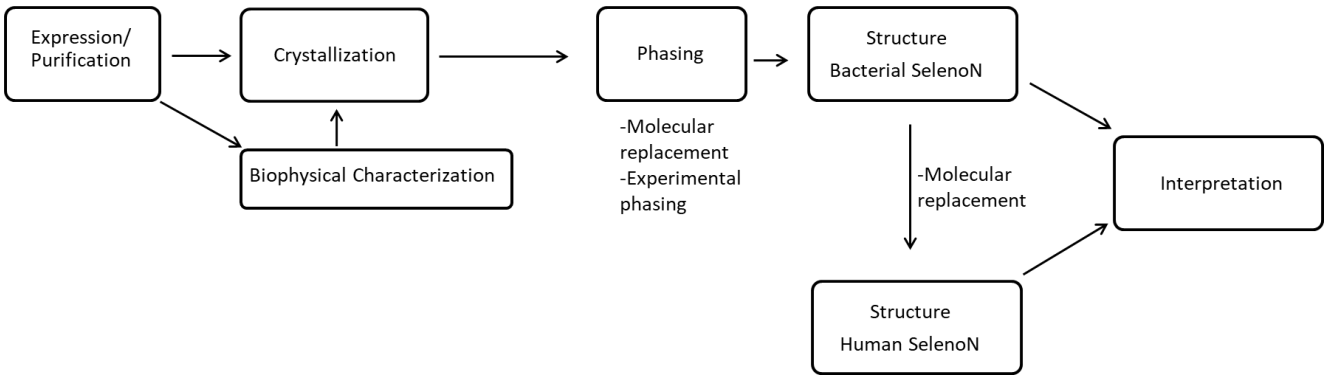

***Figure 16**: Flowchart of the methodology to be used for SelenoN structural studies*

The comparison of the bacterial and human SelenoN structures, together with the interpretation of the overall protein architecture, will be conducted based on SelenoN phylogenic conservation and the positions of pathogenic mutations characterized in patients with SELENON-related myopathies.

2 Materials and Methods

2.1 Materials

2.1.1 Chemicals

Table 2: Chemicals

Chemicals	Supplier
Acetone	VWR, Darmstadt
Agar: Bacto Agar	BD, Sparks USA
Agarose: SeaKem LE Agarose	Cambrex, Rockland, USA
Ammoniumperoxodisulfat (APS)	Roth, Karlsruhe
Ampicillin	Roth, Karlsruhe
Antifoam 204	SIGMA-Aldrich, Steinheim
Benzamidine Hydrochloride Hydrate	AppliChem, Darmstadt
Bromchlorindolylphosphate (BCIP)	SIGMA-Aldrich, Steinheim
Bromphenol blue	SIGMA-Aldrich, Steinheim
Calciumchloride	VWR, Darmstadt
Chloramphenicol	Roth, Karsruhe
Coomassie Brilliant Blue G250	Roth, Karlsruhe
dNTP-Mix (100 mM)	Bioline, Luckenwalde
Acetic acid	Zentrales Chemikalienlager, Universität des Saarlandes
Dimethylformamide (DMF)	Sigma-Aldrich, Hannover
Ethanol, absolut (99%)	VWR, Löwen, Belgien
Ethidium bromide	Roth, Karlsruhe
Ethylene diamine tetraacid (EDTA)	SIGMA-Aldrich, Steinheim
Dextrose	Zentrales Chemikalienlager, Universität des Saarlandes
Glycerol (99%)	Zentrales Chemikalienlager, Universität des Saarlandes

Bacto Yeast Extract	BD, Sparks USA
Imidazole	Zentrales Chemikalienlager, Universität des Saarlandes
Isopropanol	VWR, Darmstadt
Isopropyl ß-D1-Thiogalactopyranosid (IPTG)	SIGMA-Aldrich, Steinheim
HEPES	Roth, Karlsruhe
Lyzozyme	Sigma-Aldrich, Hannover
ß-Mercaptoethanol (ß-ME)	MERCK, Darmstadt Roth, Karlsruhe
Magnesium chlorid Hexahydrat (MgCl)	VWR, Löwen, Belgien
Methanol	VWR, Darmstadt
Milk powder	Roth, Karlsruhe
Sodium cacodylate	Sigma-Aldrich, Hannover
Sodium chloride	VWR, Löwen, Belgien
Sodium dodecylsulfate (SDS)	Roth, Karlsruhe
Sodium hydroxyde	AppliChem, Darmstadt
Nickel(II)-Sulfat-Hexahydrat	VWR, Darmstadt
Polyethylene glycole (PEG) 3350	Sigma-Aldrich, Hannover
Polyethylene glycole (PEG) 6000	Sigma-Aldrich, Hannover
Peptone	BD, Sparks USA
Phenylmethylsulfonylfluorid (PMSF)	SIGMA-Aldrich, Steinheim
Rothiophorese Gel30 (37,5:1)	Roth, Karlsruhe
Chloridric acid (37%)	VWR, Löwen, Belgien
Tetramethylethylendiamine (TEMED)	Roth, Karlsruhe
Tween 20	Roth, Karlsruhe
Tryptone	BD, Sparks USA

2.1.2 Standards, enzymes, antibodies

Table 3: Standards

Standard	Supplier
Protein-Standard: SeeBlue Plus2 Pre-Stained	Invitrogen, Karlsruhe
NativeMark™ Unstained	Invitrogen, Karlsruhe

Table 4: Enzymes

Enzymes	Supplier
NDegly Kit	SIGMA-Aldrich, Steinheim
Alcaline Phosphatase and Buffer: FastAP^{TM} Thermosensitive Alcaline Phosphatase	Fermentas, St. Leon-Rot
PNGaseF	SIGMA-Aldrich, Steinheim

Table 5 : Primary and secondary antibodies

Antibodies	Supplier
Monoclonal Anti-polyHistidin antibodies produced in mouse	SIGMA-Aldrich, Steinheim
Anti-Mouse-IgG-Alcaline Phosphatase, produced in rabbit	SIGMA-Aldrich, Steinheim
Monoclonal Anti SelN antibodies produced in mouse	Dr Alain Lescure- Strasbourg

2.1.3 Commercial kits

***Table 6**: Crystallisation screens*

Screen	Supplier
Crystal Screen	Hampton Research, Aliso Viejo, CA, USA
Crystal Screen 2	Hampton Research, Aliso Viejo, CA, USA
PEG/Ion Screen	Hampton Research, Aliso Viejo, CA, USA
Cryo Screen	Hampton Research, Aliso Viejo, CA, USA
JSCG Core I suite	Qiagen, Hilden
HT Memgold	Molecular Dimension, Suffolk, UK
HT Memgold II	Molecular Dimension, Suffolk, UK
Wizard	Jena Bioscience
Morpheus I	Molecular Dimension, Suffolk, UK
Morpheus II	Molecular Dimension, Suffolk, UK

2.1.4 Purification material

The protein purification was carried out using a ÄKTA Purifier system (GE Healthcare)

***Table 7**: Column and matrix used for Chromatography*

Column/Matrix	Supplier
His 60 Ni Superflow resin	Clontech Takara
HiTrap, 1ml-column	GE Healthcare, München
HiLoad 16/60 Superdex 200 column	GE Healthcare, München
HiPrep 10/300 Superdex 200	GE Healthcare, München

2.1.5 Equipment and accessories

***Table 8**: Equipment*

	Device	Supplier
Analytical balance	CPA225D	Sartorius, Göttingen
Growing shaker	Minitron	Infors-HT, Bottmingen, Schweiz
	Unitron	Infors-HT, Bottmingen, Schweiz
Agarose and Gel electrophorese Apparatus	MINI-SUB CELL-GT“	BioRad, München
Blot-Apparatus	Mini Trans-Blot Electrophoretic Transfer Cell	BioRad, München
Incubator (37°C)		Binder, Tuttlingen
Chromatography-System	ÄKTApurifier FPLC	GE Helthcare, München
Ice machine		Manitowoc, Herborn
Freezer (-20°C)		Liebherr, Ochsenhausen
Freezer (-80°C)		Liebherr, Ochsenhausen
High-pressure cell disruption apparatus	EmulsiFlex	Avestin, Ottawa, Kanada
Inkubator for crystallisation plates (18°C)	VinoThek Crystal Mation	Liebherr, Ochsenhausen Rigatu, Kent, England
Crystallisation robot	Phoenix	Art Robbins, Sunnyvale USA
Fridge (4 °C)		Liebherr, Ochsenhausen
Lab balance	Extend	Sartorius, Göttingen
Magnetic	MSH20A	IDL, Nidderau

Stirer	Variomag mobil	Thermo Scientific, Waltham (MA), USA
Microscope „CX31“		Olympus, Hamburg
Microscope „SZX9“		Olympus, Hamburg
Microwave		Severin, Sundern
Orbital-Shaker (Blots und Gele)	DOS-10l	NeoLab, Heidelberg
	DOS-20S	NeoLab, Heidelberg
pH-Meter	Seven Easy	Mettler Toledo, Giessen
Photometer	Ultrospec 2100 pro	GE Healthcare, München
	WPA BiowaveCOa 8000 cell density meter (Zur Messung der optischen Dichte OD_{600})	Biochrom Ltd. Cambrige UK
Pipettes ((2/10/20/100/200/1000 µL)		Gilson, VilliersLeBel, France
SDS-Gel electrophorese Apparatus	Xcell SureLock Mini Protean3	Invitrogen, Karlsruhe BioRad, München
Voltage sensor	PowerPac BASIC	BioRad, München
Sterilbanch	MSC-Advantage	Thermo Scientific, Waltham (MA), USA
Thermomixer	Comfort	Eppendorf, Hamburg
Thermocycler	MyCycler	BioRad, München
Drying incubator (60°C)		Binder, Tuttlingen
Rotator	Intelli-Mixer	NeoLab, Heidelberg
UV-Table		Bender, Wiesloch
Water system	*Ultra Pure,* Milli-Q Integral 15	Millipore, Schwalbach/Ts

Vortexer	Vortex-Genie 2	Scientific Industries, Bohemia (NY), USA
Centrifuge	Avanti J-26XP	Beckman Coulter, Krefeld
	Eppendorf 5424	Eppendorf, Hamburg
	Eppendorf 5810R	Eppendorf, Hamburg
	Microfuge 18	Beckman Coulter, Krefeld

2.1.6 Supplie and other material

Table 9: Supplies

Material	Supplier
96 deep well Block, 2 mL Crystallization-Assay	Costar, Amsterdam, Niederlande
96 well Cristallisation plate „MD 11-00-100“	Molecular Dimensions, Suffolk, UK
24 well Plate „Comboplate”	Greiner Bio-One, Frickenhausen
Aluminum foil 30u-quality	Roth, Karlsruhe
Beakers, various sizes	VWR, Darmstadt
Blotmembrane: Immobilon-Transfer Membrane (PVDF)	Millipore, Schwalbach/Ts
Dialysis-tube: MWCO 30 kDa, 43 mm	Millipore, Schwalbach
Disposable Scalpels	Braun, Melsungen
UV cuvette	Sarstedt, Nümbrecht
Erlenmeyer various sizes	VWR, Darmstadt
EasySeal DWB Sheets for cristallisations plates	Molecular Dimensions, Suffolk, UK
SureSeal DWB Sheets for deep well Blocks	Molecular Dimensions, Suffolk, UK
Falcon-tubes 15 ml, 50 ml	Greiner Bio-one, Nürtingen

Glass bottles, various sizes	VWR, Darmstadt
Concentrator: Centriprep Centrifugal Filter Devices, MWCO 30 kDa, 50 mL	Millipore, Schwalbach/Ts
Parafilm	Pechiney, Menasha, USA
Pasteur pipettes (plastic)	Sarstedt, Nümbrecht
Pipettes (plastic), sterile (5, 10 and 25 ml)	Greiner Bio-One, Frickenhausen
PCR tubes 200 µl	Biozym, Hessisch Oldendorf
Petri dishes (plastic)	Sarstedt, Nümbrecht
Tubes of 1.5 ml / 2 ml	Sarstedt, Nümbrecht
Tubes (plastic), sterile (13 ml)	Sarstedt, Nümbrecht
Tips 10 / 200 / 1000 µl	Gilson, VilliersLeBel, Frankreich
Syringes 1 ml	Becton Dickinson, Madrid, Spanien
Syringes 5/10/20/50 ml	Braun, Melsungen
Sterilfilter (0,2 und 0,45 µm)	Millipore, Schwalbach/Ts
Glass cylinder, various sizes	Vitlab, Seeheim-Jugenheim
Sterilfilter (0,2 und 0,45 µm)	Sarstedt, Nümbrecht
Whatman-Paper: Mini Trans Blot Filter paper	BioRad, Münschen
Centrifuge tube (70 ml, 1 l)	Beckman Coulter, Krefeld

2.1.7 Computer program

***Table 10**: Computer program*

Program	**Supplier**
Adobe Acrobat	Adobe
Crystal Trak	Rigaku, Kent, UK
ExPASy	http://web.expasy.org
Kappa Camera Control	Kapp optronics, Gleichen
Microsoft Word 2007	Microsoft
NanoDrop 2000	Thermo Scientific, Bonn
OmniSEC	Malvern Instruments, Herrenberg
Origin Pro 9G	Originlab, Northhampton, USA
Unicorn Workstation 5.11	GE-Healthcare, München, Germany
ATSAS 2.8.0	EMBL, Hamburg, Germany
CCP4 Program suite	STFC Rutherford Appleton Laboratory, Oxon, UK (Winn MD 2011)
Phenix Program suite	Berkely, USA (Kapral 2010)
WinCOOT	UK
PyMOL	DeLano Scientific LLC, San Carlos, USA

DICROWEB	http://dichroweb.cryst.bbk.ac.uk
Phyre2	http://www.sbg.bio.ic.ac.uk/~phyre2

2.1.8 ESRF Beamlines

Table 11: ESRF beamlines used and their characteristics

Beamline	Wavelength	Characteristics	References
BM29	7-15 keV	-for experiment small angle x-ray scattering of proteins in solution	(Pernot et al. 2010)
ID29	6-20 keV	-tunable wavelength for single or multi wavelength anomalous dispersion -10-50 µm beam diameter	(de Sanctis et al. 2012)
ID23-1	5-20 keV	-tunable wavelength for single or multi wavelength anomalous dispersion -10-45 µm beam diameter	(Nurizzo et al. 2006)
ID23-2	14.2 keV	-10 µm beam diameter	(Flot et al. 2010)
ID30B	6-20 keV	-tunable wavelength for single or multi wavelength anomalous dispersion -20-200 µm beam diameter	(Mueller-Dieckmann et al. 2015)

The access of ESRF beamlines was provided through the Frankfurt-Homburg Block Allocation Group (BAG)>

2.1.9 Buffers and stock solutions

Table 12: Buffers, Stock solutions and their composition

Buffer and solution	Composition
Ampicillin stock solution (100x)	100 mg Ampicillin/mL in H_2O (sterile filtered, stored at -20°C)
5-Brom-4-chlor-3-indolylphosphat(BCIP) solution	50 mg BCIP/mL DMF (stored at –20°C)
Chloramphenicol (stock solution)	31 mg Chloramphenicol/ml in ethanol, stored at -20°C
Coomassie solution	1.25 g Coomassie Brilliant Blue R250, 200 mL H2O, 50 mL Acetic acid, 250 mL Methanol
Destaining solution Coomassie gels	10% Acetic Acid
Kanamycin stock solution	30 mg/mL in water, stored at –20°C
Penicilline-Streptomycine	
Hygromycine	
Doxicyclyne	

Table 13: Buffers, Stock solutions and their composition

Buffer/Stock solution	Composition
Loading buffer 6x (SDS-PAGE)	0.25 mM Tris-HCl pH 6.8, 40% (w/v) Glycerol, 20% (v/v) ßmercaptoethanol, 8% (w/v) SDS, 0.004% (w/v) Bromophenol Blue
Nitro-blue tetrazolium (NBT) solution	50 mg NBT/mL in 70% Dimethylformamid (DMF), stored at 4°C
Phenylmethylsulfonylfluoride **(**PMSF) stock	100 mM PMSF in 100% isopropanol
Running buffer 10x (SDS PAGE)	500 mM Tris-HCl, 1.92 M Glycine, 1% (w/v) SDS
Sodium dodecyl sulfate**(**SDS) 10%	10 g SDS in 100 mL water
PBS buffer 10X	160 g NaCl, 4 g KCl, 4 g KH_2PO_4, 23.2 g Na_2HPO_4 in 2 L water; pH 7.45
PBST buffer	100 mL 10X PBS, 0.5 mL Tween 20, in 1L water
Blot buffer (Western blot)	38 mM Glycine, 10 mM Tris-HCl, 20% (v/v) Methanol
Blocking solution (Western Blot)	5 g/L milk dissolved into TBST

2.1.10 Gels

2.1.10.1 SDS-PAGE gels

8 % Separating gel:

Component	4 Gels
H_20	9.3 mL
Rothiphorese 30	5.3 mL
1 M Tris-HCl pH 8.8	5 mL
SDS 10%	200 µL
Temed	10 µL
10 % APS	200 µL

10 % Separating gel:

Component	4 Gels
H_20	7.9 mL
Rothiphorese 30	6.7 mL
1 M Tris-HCl pH 8.8	5 mL
SDS 10%	200 µL
Temed	10 µL
10 % APS	200 µL

5 % Stacking gel:

Component	4 Gels
H_20	4.1 mL
Rothiphorese 30	1 mL
1 M Tris pH 6.5	750 µL
SDS 10%	60 µL
Temed	10 µL
10 % APS	60 µL

2.1.10.2 Clear Native PAGE

8% Separating gel

Component	4 Gels
H_20	9.3 mL
Rothiphorese 30	5.3 mL
1 M Tris-HCl pH 8.8	5 mL
Temed	10 µL
10 % APS	200 µL

5% Stacking gel

Component	4 Gels
H_20	4.1 mL
Rothiphorese 30	1 mL
1 M Tris pH 8.8	750 µL
Temed	10 µL
10 % APS	60 µL

2.1.11 Media for cell culture

Table 14**: **Media for** Escherichia coli **culture

Medium	Composition
LB medium	10 g/L Bacto Tryptone, 5 g/L Bacto Yeast Extract, 5 g/L NaCl
LB plate	10 g/L Bacto Tryptone, 5 g/L Bacto Yeast Extract, 5 g/L NaCl, 15 g/L Bacto Agar

Table 15: Media for** HEK 293 Trex cells **culture

Medium and stock solution	Composition and preparation
DMEM	Commercial
Foetal Bovine Serum	Commercial
CD293	Commercial

2.1.12 Buffers for purification

Table 16: Buffers used for bacterial SelenoN purification

Purification step		Composition
Lysis	Lysis and loading on the Ni-NTA matrix	30 mM Tris-HCl pH 8.0, 300 mM NaCl, 2 mM $MgCl_2$, 10% glycerol, 0,5 mM TCEP, 1 mM PMSF, 2 mM Benzamidine, 130 µg/mL of denaturated lysozyme
Affinity chromatography	Chaperone removal or ATP wash	30 mM Tris-HCl pH 8.0, 300 mM NaCl, 2 mM $MgCl_2$, 0,5 mM TCEP, 30% glycerol, and 5 mM ATP
	Elution	30 mM Tris-HCl pH 8.0, 300 mM NaCl, 2 mM $MgCl_2$, 10% glycerol, 0,5 mM TCEP, 750 mM Imidazole
Size exclusion chromatography		30 mM Tris-HCl pH 8.0, 300 mM NaCl, 10% Glycerol, 2 mM $MgCl_2$, and 0.5 mM TCEP.

Table 17 : Buffers used for zebrafish SelenoN purification

Purification step		Composition
Lysis		100mM Tris HCl pH 7.5
Solubilization		30 mM Tris-HCl Ph 7.5, 5 mM $MgCl_2$, 1.25 CaCl2, 10% glycerol, 0.5 mM TCEP, 150 mM NaCl, 0.5 β DM
Afinity chromatography	Loading on matrix	30 mM Tris-HCl pH 7.5, 5 mM $MgCl_2$, 1.25 CaCl2, 10% glycerol, 0.5 mM TCEP, 150 mM NaCl, 0.05 β DM
	Elution	30 mM Tris-HCl pH 7.5, 5 mM $MgCl_2$, 1.25 CaCl2, 10% glycerol, 0.5 mM TCEP, 150 mM NaCl, 0.05 β DM, 400mM Imidazole
Size exclusion chromatography		30 mM Tris-HCl pH7.5, 2mM EGTA, 2mM EDTA, 10% glycerol, 0.5 mM TCEP, 150 mM NaCl, 0.05 β DDM

2.1.13 Biological material

2.1.13.1 Vectors

Table 18 : Vectors and their specifications

Plasmid	Specification	Promoter	Resistance marker	Inducer	Supplier
pGRO7	GroES- GroEL	AraB	Cm	Arabinose	Qiagen
pQE70	Cter $(His)_6$ tag	T5	Amp	IPTG	Qiagen
pcDNA5	Cter$(His)_6$ tag	CMV	Hygromicine	Doxycycline or tetracycline	Thermofisher

pGRO7 vector: Expression of recombinant proteins in *Escherichia coli* (*E. coli)* often results in various problems, such as the formation of insoluble proteins accumulating in inclusion bodies and protease degradation of the protein. These issues often are result of the improper folding of the expressed proteins. Molecular chaperones have been demonstrated to be involved in the proper protein folding process (Nishihara et al. 1998). Thus, coexpression of a chaperone with the protein of interest has been shown to stimulate well folded protein production in high quantity. The pGRO7 vector presents these following features: Chloramphenicol resistance as marker, Arabinose-dependent induction of GroES and GroEL chaperones expression (**Figure 17**).

pQE70 is a vector suitable for expression in *E. coli* that enables the introduction of the $(His)_6$ tag at the C terminus of the recombinant protein, and also ensures that only the full length of the recombinant protein will be purified. Protein expression is induced by addition of IPTG (**Figure 17**).

pcDNA5 is a vector for high level expression in mammalian cells designed for use with the Flp-In™ System (Thermofisher). The protein expression in under control of thehuman CMV promoter and induced by tetracycline or doxycycline. The FLP Recombination Target (FRT) site enable the Flp

recombinase-mediated integration of the vector into the Flp-In™ host cell line. Selection of a stable cell line is made by the resistance to hygromycin (**Figure 18**).

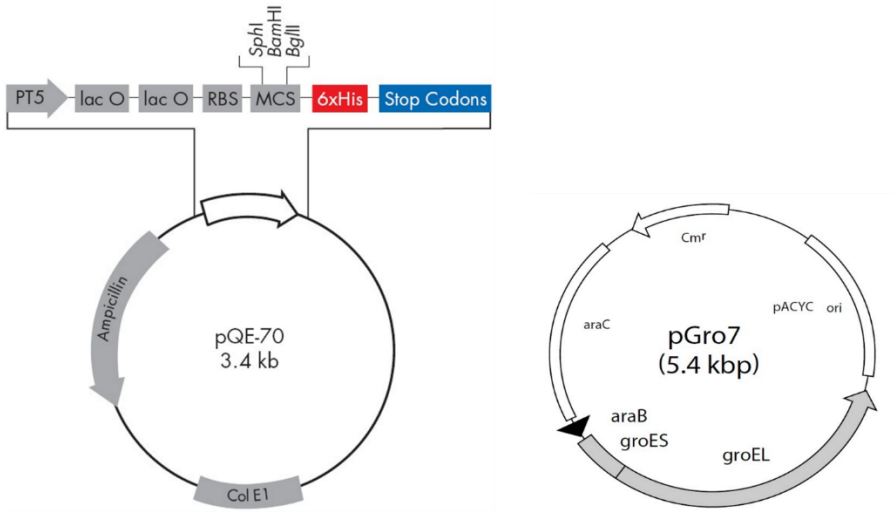

Figure 17: Vectors used for bacterial SelenoN expression in E coli (http://www.biofeng.com)

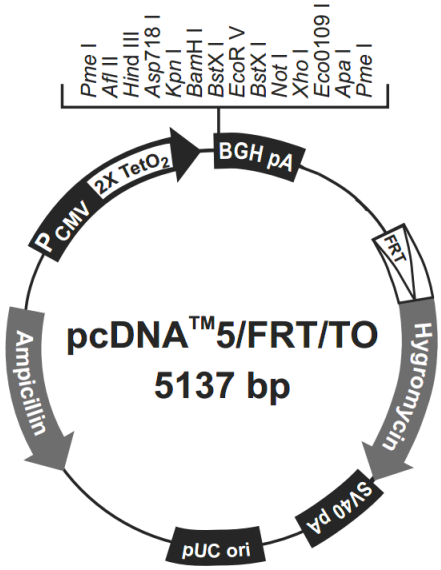

Figure 18: pcDNA5 vector used for zebrafish SelenoN expression in HEK 293 Trex cells (http://www.biofeng.com)

2.1.13.2 *Escherichia coli* and HEK cells strains

Structural studies by x-ray crystallography requires not only soluble, but also well folded and conformationally homogenous material.

Escherichia coli is a bacterial host system that is often used for the protein expression in structural biology. Besides the high quantity of protein that it is possible to yield, it presents advantages that it is easy to handle. The strain used here to express recombinant bacterial SelenoN is XL1-Blue.

Besides all benefits cited above, bacterial expression system has some limitation e.g. lacking post translational modifications when used to express eukaryotic. Those modifications are required for a proper protein folding and tentative to express this kind of proteins in bacterial system usually lead to unfolded protein resulting to insoluble material. In such case, mammalian expression systems are used. Human Embryonic Kidney (HEK) cells is one of the two most used mammalian expression system. The strain used to express is HEK 239Trex ™ is a strain specifically designed for stable cell line generation.

2.2 Methods

2.2.1 Biochemical Methods

2.2.1.1 Heterologeous expression in different systems

2.2.1.1.1 Bacterial SelenoN (bSelenoN) heterologeous expression in *E. coli* system

2.2.1.1.1.1 Transformation by electroporation of electrocompetent Ecoli cells

An aliquot of 100µL of electrocompetent cells was mixed with 10 ng of pQE70(bSelenoN) vector and incubated on ice during 5 min. The mix was then transferred in a cold electroporation cuvette and the electroporation was conducted according to BioRAD instructions for *E. coli* cells. Right after the electropulse, 1 mL LB was added to the mix and then incubated at 37 °C. After 1 h, the mixture was centrifuged 4200 rpm for 15 min, 1 mL was removed from the mixture without disturbing the cell pellet, and the rest is plated on selective plates of LB (Cam 30 µg/mL, Amp 100 µg/mL) + 2% dextrose and incubated overnight at 37 °C.

2.2.1.1.1.2 Expression of Candidatus poribacteriae SelenoN in E coli

2 expressing clones were grew overnight at 37°C in LB containing Amp 100 µg/mL + Cam 30 µg/ml + 2% glucose to generate a seed culture. The following morning, the seed was used to inoculate a culture medium with the same composition supplemented with arabinose 5 mg/ml at final OD_{600} 0.1. The culture was incubated at 30°C with constant shaking till OD_{600} reaches 0.6, and then incubated on ice for 15 min (cold chock). Cells were then collected through a centrifugation step during 15 min at 4200 rpm to change the growth medium. The purpose of this step was to remove the Arabinose which induces chaperones expression and Glucose which inhibits SelenoN expression. The pellet was resuspended into the same volume of LB (Amp 100 µg/mL + Cam 30 µg/mL) + 0,5 mM IPTG. After an overnight incubation in the shaker (around 170 rpm) at 18°C, cells were harvested by centrifugation at 4200 rpm for 15 min at 4°C.

2.2.1.1.1.3 Expression of Selenomethionine labelled bSelenoN (Semet-bSelenoN)

Expression of Selenomethionine labelled bSelenoN was made following the same protocol as previously described. After growing the seed culture, the culture medium (see composition above) was inoculated at final concentration OD_{600} 0.1. Cells were grown at 30°C until OD_{600} reaches 0.7-0.8 then after a cold chock, cells were washed in sterile deionized water before being resuspended at the same density in minimum medium containing 50 µg/mL L-Selenomethionine.

After 30 min of shaking at 30°C, IPTG was added at final concentration 0,5 mM and temperature was decreased to 18°C for the overnight induction.

2.2.1.1.2 Zebrafish SelenoN heterologous expression in HEK 293 Trex cells

2.2.1.1.2.1 Transfection of pcDNA5(zSelenoN) in HEK 293 Trex cells and selection of an expressing clone (Made by Melanie Thamy-Braye in Strasbourg)

Flp-In ™ T-Rex™ system was used to generate a stable inducible cell line following the manufacturer instructions. The system has three main components: pcDNA5™/FRT/TO vector containing already the gene of interest zSelenoN, pOG44 vector for transient expression of Flp recombinase (Broach and Hicks 1980; Broach, Guarascio, and Jayaram 1982) and mammalian HEK 293 Trex cells. The DreamFect™ Gold (Oz Bioscience) was used as the transfection agent. It is a Lipid-mediated reagent that form complex with the DNA (plasmids) and will be internalized inside mammalian cell by endocytosis (Felgner and Ringold 1989).

Co-transfection with pO44 and pcDNA5 vector was made with a cell concentration of $6*10^5$ and 10^6 cells/mL and consists on adding to HEK 293 Trex cell culture (in DMEM+ 10%FCS, +1% Penicillin and Streptomycin), the mixture of DNA and Dreamfect™ gold according to the manufacturer instructions.

Selection was made in three steps. First cells were selected for integration of the gene, secondly integrants were tested for the integration of the gene of interest at the right position, and finally integrant are tested for their expression level.

48h after the transfection, cells were trypsinized and resuspended in fresh medium. 24h after medium exchange, clone selection based on antibiotic resistance was started. Integration of pcDNA5 in the host confers hygromycin resistance. Medium was then exchanged with DMEM supplemented with 250 µg/mL hygromycin (selection medium). The selection medium was renewed five times every two days. After the last exchange, resistant clones were isolated at a concentration one clone per well in a 96 well plate. Selection was continued over 8 days. After this first step of selection, integrants were expanded and prepared for the second step of selection.

The second step of the selection consisted on testing for integrants lack of β-galactosidase activity. Flp-In T-Rex Cells are designed so that they express galactosidase under the control of SV40 early promoter. These properties aim at controlling the gene insertion. The integration of the gene via the Flp recombinase-mediated DNA recombination at the FRT site (Gorman, Fox, and Wahl 1991) leads to the inactivation of LacZ gene transcription therefore a lack of galactosidase activity. The galactosidase activity is translated by a blue coloration of cells in reaction to the lacZ reaction buffer ($K_4Fe(CN)_6$, $3H_2O$, 5 mM $K_3Fe(CN)_6$, 1 mM $MgCl_2$, 1.25mg/mL X-gal). Integrants with blue color were discarded and colorless integrants were prepared for the last selection step.

The last selection consisted on testing the expression level. Protein expression was induced during 24h by adding doxycycline which is a stable analogue of tetracycline at final concentration 0.01 µg/mL. Cells were lysed by sonication and the protein loading buffer was directly added to the crude extract. The mixture was charged on a SDS-PAGE gel and after the run, total proteins were transferred on a PVDF membrane for a western blot. The membrane was later incubated with anti zSelenoN primary antibodies and anti mouse-IGg secondary antibodies.

2.2.1.1.2.2 Expression of recombinant zSelenoN in HEK 293 Trex cells

2.2.1.1.2.2.1 Expression in suspension

Initially, the biomass was generated in adherent culture using either 75 or 175 cm2 flasks. After reaching confluence, the adherent cells were trypsinized and resuspended into 60mL/flask to enable the transportation from the IBMC to the platform instruct of the CBI. The suspension culture was then started using 2*60mL at 10^6cells/mL concentration. The used medium was DMEM supplemented with 10% fetal bovine serum and 1% penicillin-streptomycine to limit bacterial contamination. The generation time of the HEK 293 Trex cells is about 24hours in the DMEM. Therefore, the dilution in increasing volume was made so that the initial cell concentration was maintained. After reaching the expected volume, doxycycline was added to a final concentration of 0.5µg/mL to induce protein expression during 24 to 48 hours (**Figure 19**). The expression was carried out at 37°C in an atmosphere with 5% CO2 and 70% humidity, with an agitation speed of 90rpm.

5.2 g of expressing cell pellet was collected per liter DMEM medium.

2.2.1.1.2.2.2 Cell adaptability to CD293 medium

Cells adaptation to medium designed for expression in suspension such as CD293 medium without FBS was assayed. The adaptation consisted on gradually switch from the DMEM to the CD293 medium. Cells were cultured at 37°C in an atmosphere with 5% CO2 and 70% humidity, with an agitation speed of 90rpm. Initially, cells were in a medium composed of 95% DMEM and 5% CD293. After each two weeks, the amount of DMEM was reduced and CD293 increased. During each medium modification step, viability of cells was counted, and cells resuspended in a medium volume to keep a density of $1*10^6$ cells /mL. During this adaptation, the viability curve was supposed to decrease until it reached a point where it increased to the normal level were cells are considered adapted.

2.2.1.1.2.2.3 Adherent culture in plate

Overexpression of zSelenoN was also made in adherent HEK cells culture. The expression was carried out at 37°C in an atmosphere with 5% CO2 and 70% humidity. Initially, the biomass was generated in adherent culture using 75 cm^2 flasks. After reaching confluence, cells were

trypsinized, resuspended to a dilution ¼ and dispensed in 4 *75cm^2 flasks. Culture reached confluence after 2 days. Each flask was treated with trypsin before being resuspended in 6*37.5 ml and dispensed in 6*225 cm^2 plates. The last passing step was made from 225 cm^2 flasks to 500cm^2 plates (**Figure 20**). After cells reached confluence, medium was removed by aspiration and replaced with the DMEM medium containing 0.5µg/mL doxycycline to induce protein expression. After 48hours, medium was aspired, and cells were rinsed with PBS and collected by scratching them from plate surfaces.

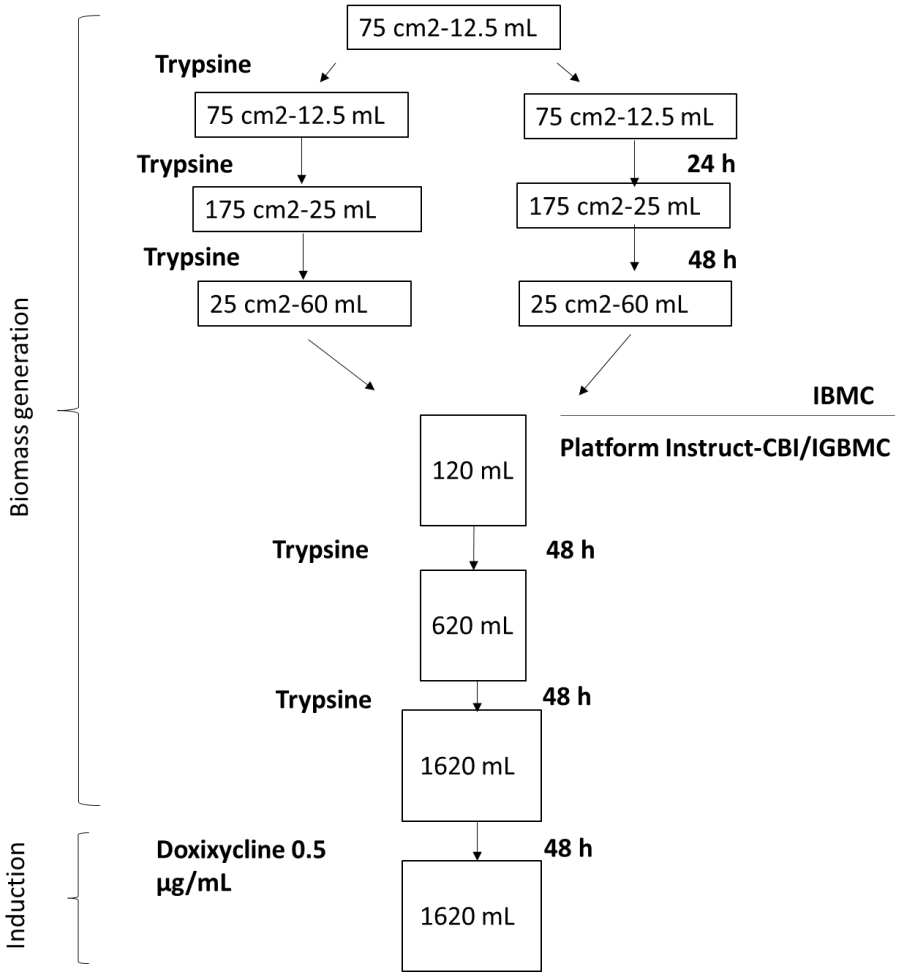

Figure 19 Flowchart of expression in suspension

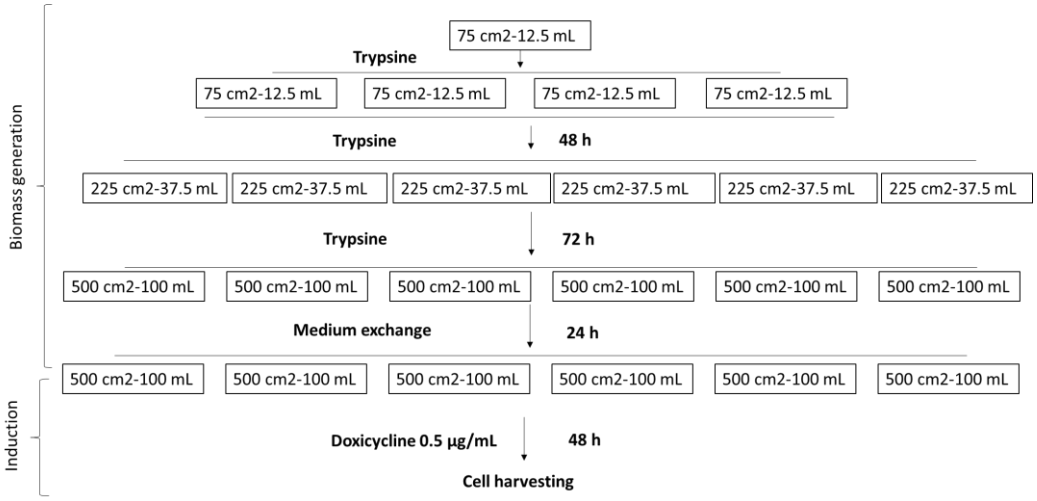

Figure 20 Flowchart of expression adherent culture

2.2.1.2 Recombinant protein purification

2.2.1.2.1 Bacterial SelenoN purification

11 g of cell pellet were resuspended in 200 ml of lysis buffer. The lysate was transferred to ultracentrifuge tubes and centrifuged for 1h at 100 000 g at 4°C. The supernatant which constitute the soluble extract was collected avoiding any disturbance of the pellet.

The soluble extract was batched with 4 ml of Ni-NTA matrix, preequilibrated in the lysis buffer, for 1 h at RT. Then the batch was transferred onto a column, and the flow through was collected by gravity flow. The batch was then washed twice with 5 bed volumes of lysis buffer containing 20 mM imidazole.

The matrix was then batched twice with 5 bed volumes of chaperones removal buffer and incubated for 30 min at 37°C on a rotating wheel. The batch was then transferred onto a column and the wash was collected by gravity flow. The batch was repeated for 15 min and fractions thus collected constitute ATP washes.

The protein was eluted with 750 mM imidazole in the lysis buffer without proteases inhibitors

The eluate from the IMAC purification of bSelenoN produced in *E coli* was concentrated to a volume of 2 mL with pressure dialysis using 50 mL concentrators with cut-off of 30 kDa. Recommended speeds for Amicon Ultra concentrators were followed.

The IMAC purified bSelenoN protein was polished using the Hiload Superdex 200 16/60 GL column on an AKTA purifier system. The Superdex 200 column was first washed with 2 bed volume of water then with at least 2 bed volume of buffer. 2 mL of purified bSelenoN were loaded onto the Superdex 200 16/60 column. Elution of protein was followed by measuring the absorbance at 280 nm. Aliquots corresponding to the A_{280} peaks were analyzed by SDS-PAGE.

2.2.1.2.2 Zebrafish SelenoN purification

Cell pellet was resuspended to 30% (weight/volume) into the lysis buffer containing 100mM Tris

HCl pH 8.0, 10% glycerol, EDTA free tablet protease inhibitor and 0.5 mM TCEP. After homogenization, cells were sonicated at 4°C during 3 min using the following features: pulse on 2sec, pulse off 2sec, amplitude 40%.

The lysate was centrifuged for 20 min at 12000 rpm (17400g) at 4°C. The membrane pellet thus obtained was resuspended in the lysis buffer supplemented with 150 mM NaCl and 0.25% β-DM. The expressed zSelenoN was solubilized from the membrane under mild agitation at 4°C during 1h.

After centrifugation (20min at 12000rpm), the solubilized membrane fraction was loaded in batch with 1mL Ni-IDA column with a flow 0.5 mL/min.

After washing the matrix with 10CV solubilization buffer, the protein was eluted over a gradient of Imidazole from 0 to 400 mM Imidazole.

After checking fraction enrichment on a SDS-PAGE gel, fractions containing zSelenoN were concentrated to 4 mL using an amicon with the cut off 50KDa. After centrifugation to pellet the insoluble aggregates, the sample was loaded on a Superdex 200 10/300. The run was carried out at 4°C with buffer composed of 50 mM TrisHCl pH 8.0, 150 mM NaCl, 0.5 mM TCEP, 10% Glycerol (zSelenoN Buffer) supplemented with 0.025% β-DDM.

2.2.2 Biophysical methods

2.2.2.1 Small Angle X-ray Scattering (SAXS) in line with Size Exclusion Chromatography (SEC)

2.2.2.1.1 SAXS data acquisition

SAXS is a method used to characterize biological macromolecules in solution. It is applicable to a broad range of particle size. The basic principle of the method is the following: a sample (macromolecule in solution) is illuminated with an x-ray beam andthe randomly oriented molecules in solution will scatter the radiation (**Figure 21**). Data acquisition is split up in multiple frames which were merged resulting in a 1D curve. The analysis will provide different information on the macromolecule like: Structural changes in different conditions, the molecular weight, the radius of gyration, the degree of folding, denaturation, disorder, as well as a low-resolution shape of the molecule (**Figure 22**). Scattering of the solvent must be subtracted to get the scattering from the dissolved molecule.

The most important requirement for the measurement is the sample quality. Basically, the sample must be as homogenous as possible (monodisperse) and free of any aggregation. Two ways of measurements are possible: the static measurement andthe High Pressure Liquid Chromatography coupled to SAXS (HPLC-SAXS). The HPLC-SAXS has the advantage that the preceeding size exclusion chromatography separates different oligomers and aggregation, and then all particles leaving the column are analyzed separately by SAXS according to their elution volume.

2.2.2.1.2 SAXS data processing and interpretation

Data obtained are 1-dimensional scattering function. The scattered intensity is related to the diffusion vector q or momentum transfer with the equation

$$q(\text{ Å}^{-1} \text{ or } \text{nm}^{-1}) = 4\,\pi\,\sin\theta/\lambda$$

Where 2θ is the angle between direct and diffused beam and λ the wavelength of the beam (**Figure 21**).

Data are processed using the package ATSAS 2.8.0 (D Franke et al. 2017). After selecting frames of

the peak within the same R_g range, buffer signal is subtracted. The resulting frames are scaled and averaged. The averaged curve is used for the Guinier as well as for the P (r) analysis.

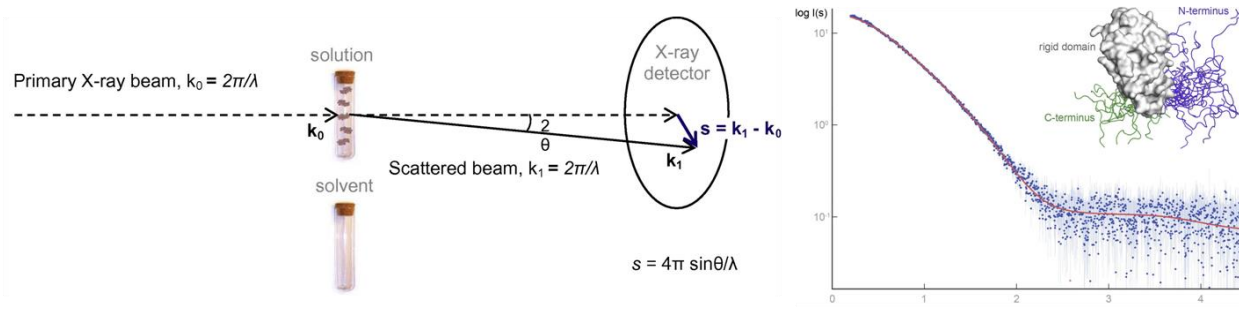

Figure 21: Schematic representation of a SAXS experiment.

Molecules randomly oriented in solution scatter an incoming beam. The resulting signal is translated in a 1-dimensional scattering curve which analysis can provide structural parameters and can be used for an initio modeling of an envelope of the molecule (Kikhney and Svergun 2015b).

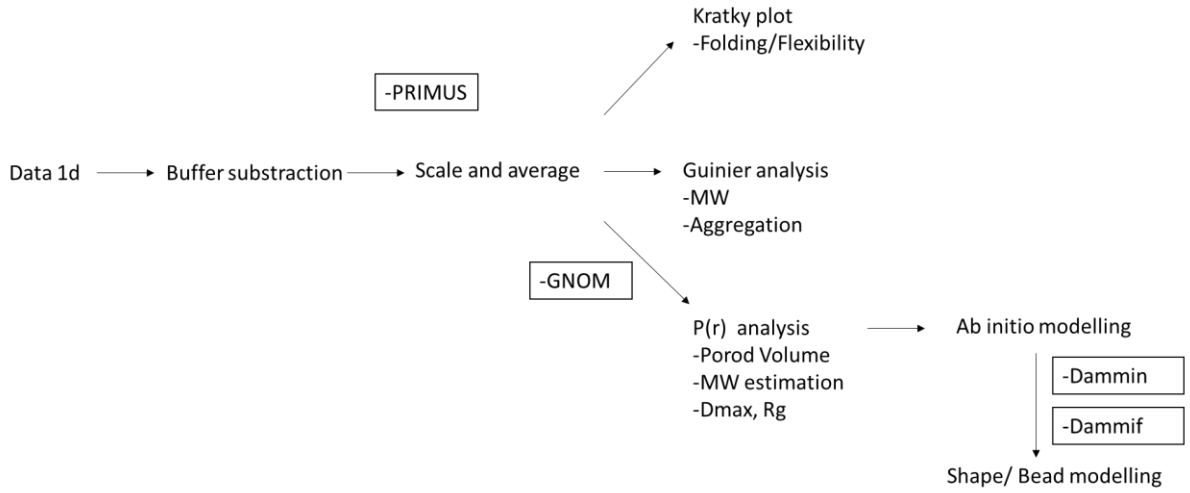

Figure 22: Workflow used for SAXS data processing.

2.2.2.1.3 Guinier Analysis

The Guinier analysis corresponds to the analysis of the SAXS curve at very small scattering angles. Its approximation enables the intensity calculation through the relation (Guinier and Fournet 1955):

$$LnI(q) = LnI(0) - q^2 * R_g^2/3$$

$LnI(q)$ *is* a function of the diffusion vector*q*and enables to determine the protein radius of gyration R_g of the protein from the linear part and enables the extrapolation of diffused intensity at zero angle *I(0).* The radius of gyration R_g is defined as the mass distribution of the macromolecule around its center of gravity. It is a powerful parameter to evaluate protein structural or conformational changes upon different conditions

The analysis of the Guinier trace enables to assess the quality of the sample as the linearity at low angle is a proof of absence of aggregatesor interpaticle interferences (**Figure 23**).

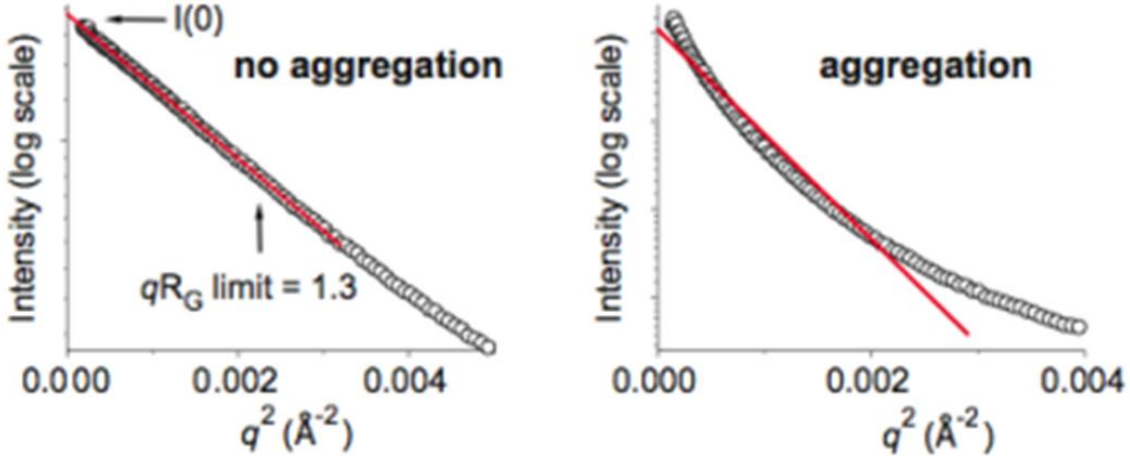

Figure 23 example of Guinier traces of a sample with aggregate Vs no aggregation (Putnam et al. 2007)

2.2.2.1.4 Kratky plot analysis

The Kratky plot is the representation of $q^2I(q)$ as a function of q (Glatter and Kratkt 1982). The profile of this curve gives information about the degree of folding, flexibility, as well as the

presence of more than one domain in the protein.

The bell shape is characteristic of a globular protein, a bell shape followed by a shoulder is characteristic of a multidomain protein, a bell shape followed by a plateau will characterize a partially folded protein or a protein with flexible linkers, and a plateau will characterize an unfolded protein (**Figure 24**).

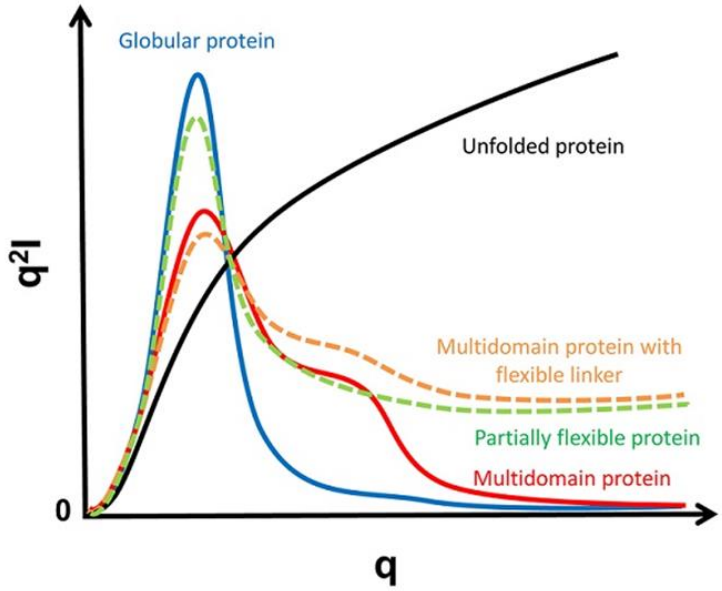

Figure 24: different Kratky traces that describe different protein shapes

(https://www-ssrl.slac.stanford.edu/~saxs/analysis/assessment.html)

2.2.2.1.5 Distance distribution function: P(r) versus r analysis

The pair distance distribution function or P(r) function is the real space representation of the SAXS curve. Its trace is supposed to be smooth, non-negative and approaching zero at the maximum dimension of the particle usually called D_{max}. In general, the pair distance distribution describes the paired-set of all distances between points in an object. When applying the principle to macromolecules, point of an object can be translate to electrons of the molecule. Thus, from this function, one can monitor structural changes even in few residues in a macromolecule since structural change implies a change of distance between electrons.

2.2.2.1.6 SAXS experiment with bacterial and zebrafish SelenoN

SAXS measurements were conducted on the Beam Line 29 (BM29) (Pernot et al. 2010) (**Table 11**)

at the European Synchotron Radiation Facilities (ESRF) in Grenoble-France with an X-ray beam of 12 KeV. For SelenoN proteins analysis, 70 µL of highly pure recombinant SelenoN concentrated at 4-15mg/mL was used for the HPLC-SAXS (**Table 19**). The sample was loaded on a Superdex 200 10/300 GL coupled in line with SAXS. The elution of the protein was monitored by a UV and SAXS detectors. And SAXS data were processed with softwares of ATSAS package (**Table 20**) following the framework described in **Figure 22**.

Table 19: SAXS SelenoN sample details

Organism	*Candidatus Poribacteriae*	*Danio rerio (zebrafish)*
Source	Purified from *E. coli*	Purified from HEK 293 Trex cells
Molar extinction coefficient E 0.1%	1.6	1.2
M from chemical composition (Da)	64772	62670
SEC SAXS column	Superdex 200 10/300	Superdex 200 10/300
Loading concentration (mg/mL)	15	10 or 4.5
Injection volume (µL)	70	70
Flow rate (ml/mL)	0.5	0.5

Table 20:Software employed for SelenoN SAXS data reduction analysis and interpretation

SAXS data reduction	PRIMUSqt from ATSAS 2.8.0 (Petoukhov et al., 2012)
Data basic analysis	PRIMUSqt from ATSAS 2.8.0 (Petoukhov et al., 2012)
Bead modelling	DAMMIF (Franke & Svergun, 2009) and DAMMIN (Svergun, 1999) via ATSAS online (https://www.embl-hamburg.de/biosaxs/atsas-online/)
Three-dimensional graphic model representation	PyMOL (DeLano, 2003)

2.2.2.2 Secondary structure studies using circular dichroism spectroscopy

Circular dichroism spectroscopy (CD spectroscopy) is based on the difference in absorption of the left and the right handed circularly polarized light (***Figure 25***). The circular dichroism signal is observed when a molecule contains one or more light absorbing group (chiral chromophores). Biological macromolecules are chiral for instance, the twenty-common amino acid that form proteins are chiral themselves. The CD spectroscopy has been used to assess the secondary structure of the recombinant proteins. Secondary structure elements such as alpha helix and beta sheet have a particular CD signature (**Figure 25**). Measurements made in the far UV (below 260 nm) can be used to predict the percentage of each of those elements in a protein. The obtained CD spectra contains information on percentage of each structural element and analysis with specific algorithms designed for fitting protein CD spectra will provide insight into the secondary structure. Folded and unfolded roteins will have a different CD spectra profile (**Figure 26**).

For the measurements, 100 µL of protein solution concentrated at 0.1-0.3 mg/mL was used in 1mm cuvettes. Buffer were first exchanged using amicon concentrator to 3 mM Tris, 15 mM NaCl 0.5 mM TCEP for the bacterial SelenoN, and to the same buffer supplemented with 2 mM EDTA, 2 mM EGTA, 0.05% β-DDM for the zebrafish SelenoN.

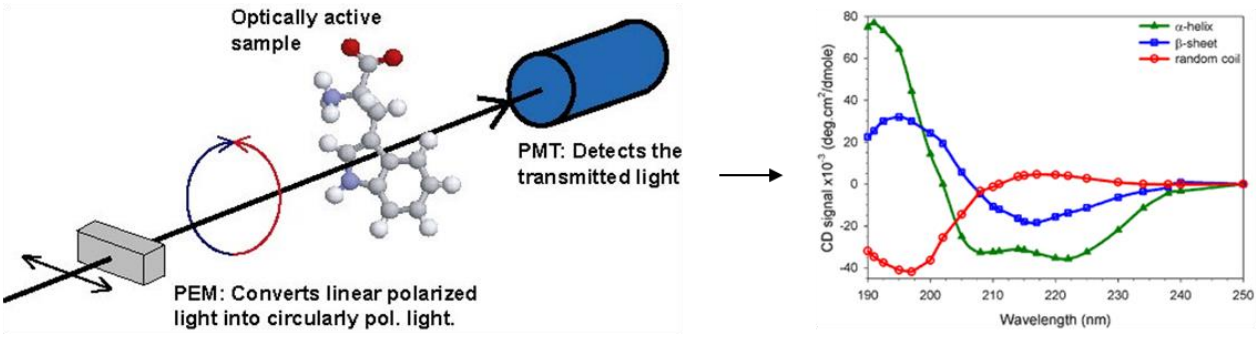

Figure 25: circular discroism spectroscopy principle and Circular dichroism spectra of α helices, β-sheet and rancom coil

CD spectra characteristic from each secondary structure are presented on the right panel: red = random coil, green = α-helix, blue = β-sheet

(http://www.isa.au.dk/facilities/astrid2/beamlines/AU-cd/images/CD-principle-1200px.png and http://www.fbs.leeds.ac.uk/facilities/cd/images/1.png)

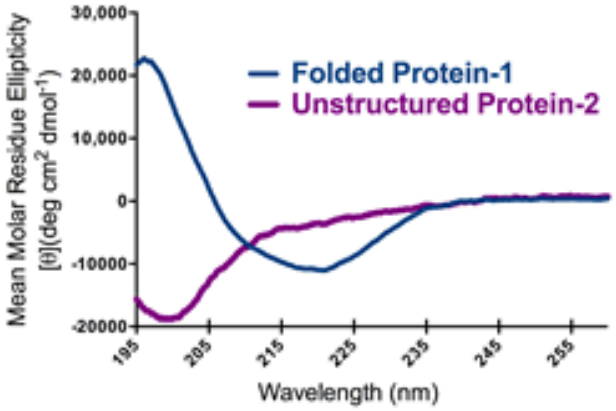

Figure 26: Circular Dichroism spectra profiles of a folded vs unfolded protein (https://www.urmc.rochester.edu/structural-biology-biophysics/services/biomolecular-characterization.aspx)

2.2.3 X-ray crystallography

Obtaining a protein structure using the x-ray crystallography is a long and empirical process that can require several years of intensive research. The prerequisite to this technique is obtaining a pure homogenous protein solution. The concentrated protein sample is submitted to different parameters and conditions that leading to the bulding of protein crystals. Crystals are submitted to x-ray diffraction experiments. Each element of the crystal (protein and solvent) and each electron of the protein will contribute to the diffraction (**Figure 27**). The diffraction pattern is therefore characteristic of the protein. From the collected data, an electron density map can be calculated and the position of each atom that constitutes the studied protein can be determined.

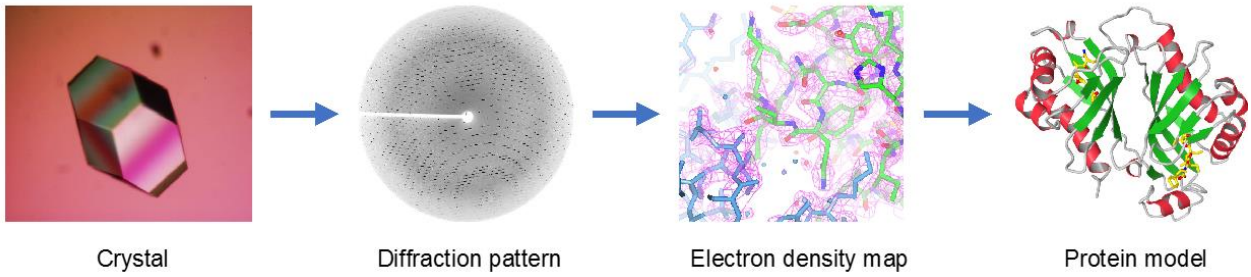

Figure 27: Workflow to assess a protein model using x-ray crystallography https://www.creative-biostructure.com/images/X-ray-Crystallography-Platform-1.png)

2.2.3.1 Crystallogenesis

2.2.3.1.1 Protein crystal definition

A crystal can be defined as periodical packing of molecules in three dimensionalspaces. The elementary unit of a crystal is called a unit cell that is characterized by three vectors a, b, c and three angles α, β, γ. The crystal lattice is built from the unit cell through the relation:

$$\vec{t} = m\vec{a} + n\vec{b} + p\vec{c}$$

Where m, n, and p are integer numbers.

The unit cell contains all information about symmetry operations like rotation, translation. The smallest unit in the unit cell is the asymmetric unit generating the complete unit cell by all symmetry operations of the space group.

A protein crystal is a periodical repetition of a unit cell and a motif where the motif is the protein. Inside the crystal, proteins are not compactly packed as there is a part of the crystal volume that is occupied by solvent. This solvent volume is calculated by the so-called Matthews coefficient (Matthews 1968). It is admitted that the proportion of the Solvent in the crystal varied between 30 and 75%. This percentage gives information about the number of protein molecules that constitute the motif.

2.2.3.1.2 Parameters that influence protein solubility in solution

Crystallization is the process in which a molecule evolves from a soluble state to a 3D organized solid state. Two main steps constitute this process: the nucleation and the crystal growth. In the case of protein, crystallization can occur when its solubility in solution gradually decreases according to different parameters such as:

- The protein concentration
- The nature of the precipitant and its concentration
- The pH of the solution that can influence the protein charge and stability
- The Ionic strength
- The Temperature that can affect stability and solubility of the protein.

- Additives, effectors, and ligands that can induce conformational change on the protein that can lead to a higher stability or compactness of the protein.

2.2.3.1.3 The Phase Diagram

The phase diagram is obtained by varying one of the parameters that influence the protein solubility, for example here the precipitant concentration as a function of the protein concentration. This leads to three main regions that represent the state of the molecule from soluble state to crystal (**Figure 28**).

- The area under the solubility curve represents an undersaturated solution where no crystallization is possible.
- The metastable zone limited by the solubility and the precipitation curves is important for the crystallogenenis as the nucleation and the crystal growth are possible only in that zone. The solution is then supersaturated.
- The precipitation zone is the zone where the protein and the precipitant concentrations are too high and that leads to a protein precipitation that can be non-reversible

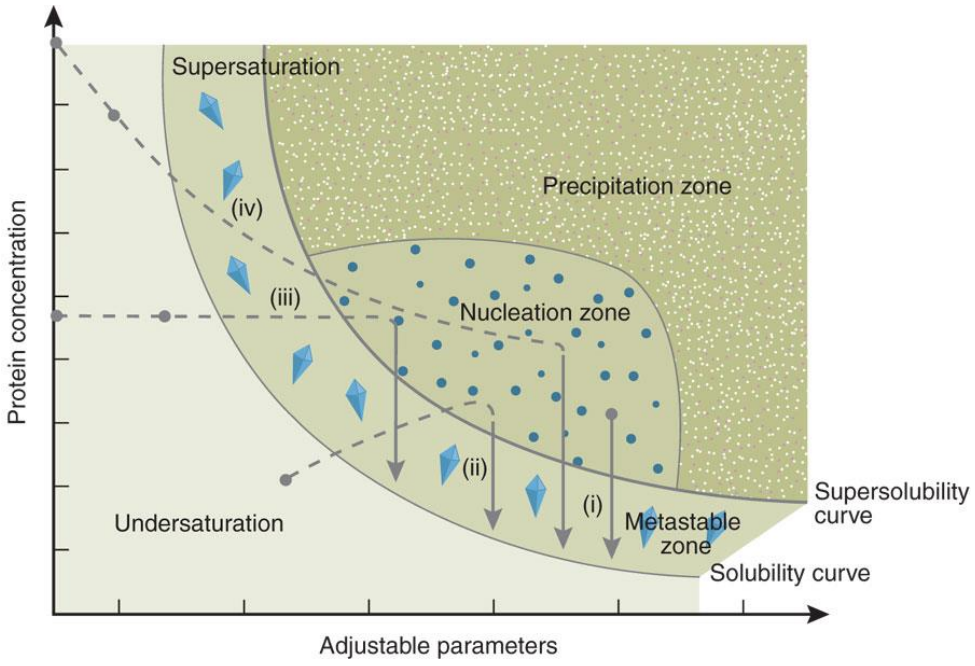

Figure 28: Phase diagram representing the protein concentration against any adjustable parameters (Khurshid et al. 2014)

2.2.3.1.4 Vapor diffusion technique: the hanging and the sitting drops

Many techniques for the protein crystallization have been developed, however the vapor diffusion technique associated to either the hanging or the sitting drop is the most popular and the aim is to bring to solution to a supersaturated state. The principle of the hanging drop is the following: a drop mixed of concentrated protein and precipitating agent is mounted on a cover slip that is the used to close a greased well containing the reservoir solution. The reservoir solution contains the precipitant agent at a higher concentration than in the drop. Due to the gradient concentration, the water will evaporate from the drop towards the reservoir thus, lowering the drop size and increasing the protein concentration and bringing the drop to the supersaturated state. If the other parameters as the pH, ionic strength, temperature are appropriate, nucleation followed by crystal growth can occur until the equilibrium between the drop and the reservoir is reached. The principle of the sitting drop is the same except that the drop is not hanging on a cover slip but is sitting on a smaller well adjacent to the reservoir well (**Figure 29**).

2.2.3.1.5 Crystallization of bacterial and zebrafish SelenoN

In our experiments, the vapor diffusion technique has been used. The bacterial as well as the zebrafish selenoN where concentrated to 10-12mg/mL before the buffer was exchanged to remove the glycerol prior to the crystallization set up. For the bacterial SelenoN, 2µL drops where set up with a protein to precipitant ratio of 1:1. Different cocktails of crystallization solutions where tested using a 24 well plate. Most of the condition tested where self-designed by varying the PEG 6000 concentration as well as the nature of the buffer at pH 6.5.

In the contrary for the zSelenoN, only the sitting drop in 96 well plates was used. The protein was first concentrated followed by an overnigth deglycosylation at room temperature using the endoglycosydase F1 (suitable for native deglycosylation). Different commercial and self designed screens were tested.

2.2.3.1.6 Selenomethionine-bSelenoN crystallization setups using microseeding

Selenomethionine-bSelenoN crystals were grown by combining vapor diffusion technique with microseeding technique (D'Arcy, Mac Sweeney, and Haber 2003). Native bselenoN crystals were harvested and placed in a tube containing 50 µL reservoir solution and a small crushing ball. The

seeding material was prepared by crushing them through vortexing the preparation. Then serial dilutions of the seed material were made as described in Figure 30.

For the crystallization, the same reservoir solution (same composition with the seed material) was used and seed material was used to set-up crystallization drops in a ratio of 1:1 with the SeMet-bSelenoN (**Figure 30**).

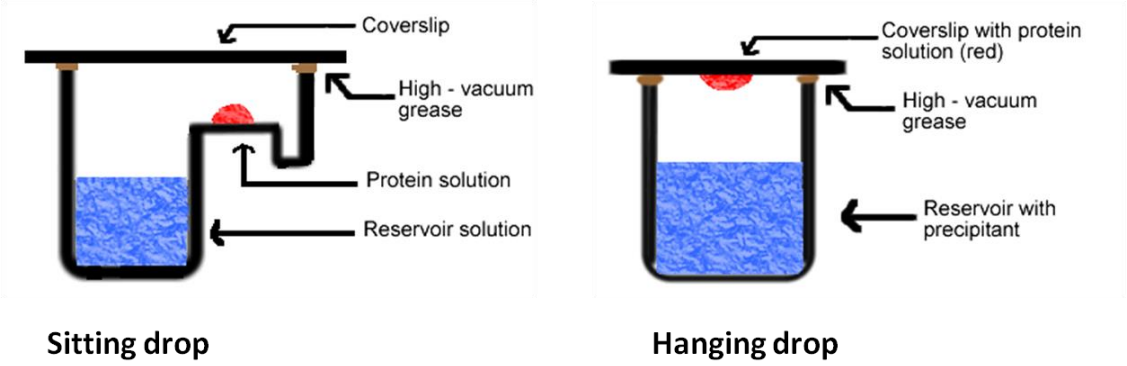

Figure 29: Crystallization by vapor diffusion technique (http://soft-matter.seas.harvard.edu/images/1/17/Drop2.gif)

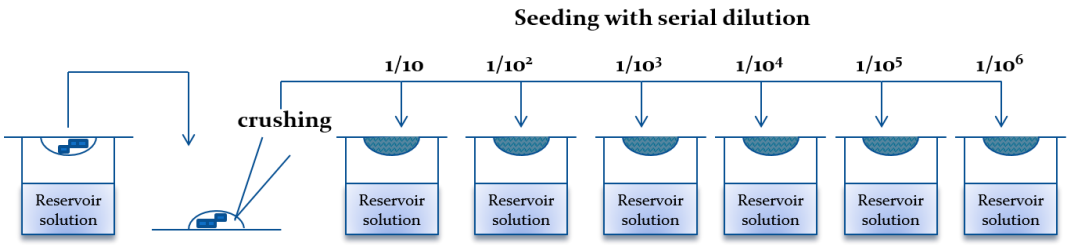

Figure 30: Principle of microseeding technique

2.2.3.2 X-ray diffraction and data analysis

2.2.3.2.1 X-ray diffraction Principle

X-rays are high energy electromagnetic radiation. Their diffraction is the result of their interaction with electrons of protein atoms.

The diffraction is possible when the Bragg law is respected. This Bragg law suggests that if an incoming beam with a wavelength λ hits with an angle θ a family of parallel lattice planes with a spacing distance d between them, the diffraction is possible when the following relation is respected:

$$2d*\sin\theta = n\lambda$$

Where n is an integer number.

When the equation is respected, diffractedwaves in phase will be summed and this results on a diffraction spot that will be recorded by the detector during the data collection. Each spot is characterized by a triplet of coordinates h,k,l which are called Miller indices. In the crystal, set of equivalent and equidistant lattice planes are defined by the Miller indices which are integer numbers of intercepts of a set of lattice planes with each of the unit cell axes.

2.2.3.2.2 X-ray diffraction data quality assessment parameters

Data quality is appreciated according to different parameters such as:

- The resolution corresponds to the minimum distance than can be distinguished between two points. It is expressed in Å.
- The R_{symm} factor can be defined as the disagreement between intensities of equivalent reflections. The lower the R_{symm} value is the better the data are.
- The completeness which is the percentage of experimentally measured number of reflections compared to the expected number of reflections.
- Multiplicity is the number of measurements made on a unique type of reflection. It determines how significant the statistics, in particular the R_{symm} values, are.
- R_{merge} which is a merged data quality assessment can be defined as the consistency of

measurements made on a unique reflection according to the multiplicity

- I/δ(I) represents the signal to noise ratio.

2.2.3.2.3 The Electron density map calculation and the phase problem

Interaction of x-rays with proteins electron results on an electron density map that is specific of each protein. The calculation of this map is translated by the equation

$$\rho(x,y,z) = \left(\frac{1}{V}\right)\sum_{h}\sum_{k}\sum_{l} F\,(h,k,l)e^{-2\Pi i(hx+ky+lz)}$$

Where V is the unit cell Volume, F (h, k, l) is the structure factor of the diffracted wave, xyz position coordinates of a point in the asymmetric unit cell.

The structure factor can be defined by the relation:

$$F(h,k,l) = \sum_{j} f(j)e^{2\Pi i(hx(j)+ky(j)+lz(j)}$$

This can be also written$F(h,k,l) = |\ F(hkl)|\ \ e^{i\varphi(hkl)}$

Where f(j) is the structure factor of each atom j of the unit, $|\ F(hkl)|$ is the amplitude of the diffracted wave which is proportional to its intensity and $\varphi(hkl)$ the phase of the diffracted wave. During the data collection, the phase information is not measured, only the intensity is directly accessible which makes the direct calculation of the electron density map not possible. Nevertheless, there are indirect methods used to recover the phase information. In the following chapter, I will present the two main methods used, the molecular replacement and the experimental phasing.

2.2.3.2.3.1 Molecular replacement

Molecular replacement is based on the use of the phase information protein template to calculate the electron density map of atarget protein. This method is applicable only when the target protein has a highier sequence homology with the template usually more than 30%. The resulting structure factor will be characterized by the template phase and the target amplitude.

In this method, Patterson functions are calculated for both the template and the target then are compared and oriented according to 3 angles of the space that are called Euler angles. The aim of this procedure is to maximize the numbers of superposed peaks that could correspond to intermolecular vectors. This first step defines the so-called Rotation function. Patterson maps that contain correlation vectors from the first step are later superposed to define three vectors in the space. The use of Euler angles and vectors in combination will help to position the template protein inside the unit lattice of the target protein.

2.2.3.2.3.2 Experimental phasing

2.2.3.2.3.2.1 Principle of experiment phasing

Experimental phasing is based on the determination of a marker atom substructure. The marker atom will provide a difference in data that will be used to determine its location and extend it to the rest of the protein. Marker atoms are generally heavy atoms that will provide data with a so-called anomalous signal.

Anomalous signal comes from the fact that a part of the energy of an incoming beam with a wavelength λ that correspond to the absorption threshold of the marker atom will be absorbed by electrons of its inner shell and this will result on the transition of those electrons to an outer shell. This transition will generate an electronic difference compared to other atoms which implies a different and more complicated structure factor thus a different phase and amplitude.

The wave diffracted by the heavy atom will be different from the other and its structure factor is then described by the equation

$$f = f0 + f'(\lambda) + if''(\lambda)$$

Where $f0$ is independent from the wavelength λ,f'' and f' are structure factors which their values will be dependent on the nature of the heavy atom and the wavelength of the incoming beam. f' is in phase with $f0$ but not with f''. Because of the imaginary number i, there is a phase shift of between f' and f''.This phase shift leads to the non-respect of the Friedel's Law which says that structure factors of equivalent reflections (h, k, l) and (-h, -k, -l) are also equivalent in other terms

$$|F(h,k,l)| = |F(-h,-k,-l)| \text{ or } |\mathrm{F}(+)| = |\mathrm{F}(-)|$$

In the case of anomalous difference, $|\mathrm{F}(+)| \neq |\mathrm{F}(-)|$

This difference of structure factors of equivalent reflections describes a function that is called anomalous difference and is written

$$\Delta|F|ano = (|F(+)| - |F(-)|)f'/2f''$$

The calculation of the Patterson map is based on this anomalous difference and aim to determine position of marker atoms that are responsible of the anomalous signal.

2.2.3.2.3.2.2 Isomorphous replacement

Isomorphous replacement requires crystals which are individually derivatized with one or more heavy atoms. The heavy atom is characterized by a strong electron density. Like other atoms it contributes to the overall diffraction intensity.

Experimentally, derivatized crystals can be obtained by two ways: one way is to soak a native crystal in a solution containing heavy atoms. The second way is by co-crystallization which means, setting up crystallization drops with heavy atoms.

The most important factor in this technique is that native and derivatized crystals should be isomorphouswhich means that they should belong to the same space group and have the same cell parameters. The difference of the intensity signal between native and derivatized crystals enables to determine heavy atoms position. Their position is then used to calculate their structure factors and phases and later extend it to the protein.

2.2.3.2.3.2.3 Single or Multiple Wavelength Anomalous Dispersion

The method consists on recording data from the same crystal at different wavelengths close to the normal anomalous wavelength. This enables to determine atoms that are responsible of the anomalous signal and to position them. Their position as for the MIR will be used to calculate their phase and extend it to the protein.

The advantage of the technique is that it can be achieved using one single crystal therefore,

overcome potential problems of non-isomorphism.

2.2.3.2.4 From the electron density map to the structural model

Once calculated, the electron density map can be ameliorated by flattening solvent which aim at reducing the noise and increasing the protein signal this step is called density modification.

Once ameliorated, the atomic model can be build inside the map. The final model is obtained after cycles of building and refining and is described by a set of calculated structure factor $Fcalc$ of each atom and an experimental observation for each structure factor amplitudes $Fobs$.

Refining steps consist on modifying the model so to get the highest accuracy with the experimental data. Structural parameters of the model such as the model coordinates, B-factors, bulk solvent correction will be refined against experimental data to obtain the best fit between the observed structure factor amplitude $Fobs$ and the computed model structure factor amplitude $Fcalc$.

The quality of the overall fit between the final model and the diffraction data can be translated by two main parameters which are the R factor and the R_{Free}factor. Both factors are calculatedfrom the same equation which is

$$R = Rfree = (\sum_{hkl} | Fobs - Fcalc|)/(\sum_{hkl} | Fobs|)$$

Where F is the structure factor.

The difference between both factors is that R is calculated for all reflections whereas $Rfree$ is calculated with 5% of non-refined reflections.

In other say, R factors will translate in percentage the agreement between the observed phase from the experiment and the calculated phase by the model. The lower the R factor, the more accurate the model is.

2.2.3.2.5 SelenoN X-ray diffraction data processing and phasing and structural model

Data were collected using MxCuBE program (Gabadinho et al. 2010) at different beamlines of the ESRF Synchontron (**Table 11**). After testing for the X-ray diffraction quality by a characterization step, the data processing quality was automatically generated by the program EDNA (Incardona et al. 2009). Collected data were processed using Mosflm (Leslie and Powell 2007). Later, POINTLESS (Phil Evans 2014) and SCALA (Philip Evans 2006) program were used to identify the space group and to scale data respectively. Molecular replacement was made using MOLREP (Vagin and Teplyakov 2010) and also PHASER MR (McCoy 2007) from Phenix (Adams et al. 2010). Experimental phasing was made using in the pipeline CRANK 2 (Ness et al. 2004) or the SHELX (Sheldrick 2008; Schneider and Sheldrick 2002) program containing SHELX C, D and E to determine the number of marker atoms, determine and refine their positions respectively. Protein model was built with BUCCANEER (Cowtan 2006). Refinement was made using COOT (Emsley and Cowtan 2004) and REFMAC5 (Murshudov et al. 2011) programs.

3 Results

3.1 Bioinformatic analysis of bacterial and zebrafish SelenoN amino acid sequences

To determine the degree of identity and similarity between the human, zebrafish and bacterial SelenoNs, amino acid sequences of the proteins were aligned using the BLASTP program (Altschul et al. 1997). The alignment showed 67 % identity between the human and zebrafish proteins, covering 96% of both sequences. The bacterial and zebrafish protein sequences (**appendix 1**) displayed 37% identity but in this case, the alignment was limited to one common region containing Sec residue and encompassing position 382-507 of the zebrafish and 229-355 of the bacterial SelenoN. The N-terminal domain of the human and zebrafish SelenoN was not found or conserved in the bacterial SelenoN however, there is an additional C-terminal domain in the bacterial SelenoN corresponding to a thioredoxin fold which is not found in zebrafish and human SelenoN (**Figure 31**).

To identify proteins with similar structures or domains, amino acid sequences of both bacterial and zebrafish proteins where analyzed with the online program SWISSMODEL (Biasini et al. 2014; Bordoli et al. 2009; Arnold et al. 2006; Guex, Peitsch, and Schwede 2009). Identified structural information can be later used as template to solve the structure by molecular replacement.

First, the bacterial sequence was provided as an input to search for similar domains. When using the full-length sequence, only the thioredoxin fold corresponding to the C-terminus was encovered by the search. This domain corresponds to 26% of the sequence and the closest structure identified was the thiol disulfide interchange protein from *Bacteroides sp* (PDB accession number 2LRN) which displayed 32.62% identity with the bacterial SelenoN C-terminal domain from position 409 to 558. Next, the sequence corresponding to that domain was omitted and the remaining SelenoN sequence was submitted to search for homologues. This time, four additional close structures were found (**Figure 32B**) corresponding respectively to the C-terminal domain of a protein of unknown function from *Archeoglobus fulgidus* (PDB accession number 3DT5) covering the position 33 to 85, G coupled receptor kinase 1 from *Bos taurus* (PDB accession

number 3C5O) position 137 to 182 and the UAS domain of the human UBX domain containing protein 7 (PDB accession number 2DLX) covering position 229 to 355.

The zebrafish sequence was analyzed using the same workflow. First the full sequence was investigated to search for similar structures. In this case, two main domains were covered respectively, the EF-Hand domain and a C-terminal domain from position 381 to 507 corresponding to the sequence aligned with the bacterial SelenoN which has 15% identity with the UAS domain of the human UBX domain containing protein 7 (PDB accession number 2DLX). UAS domain which is found in both the bacterial and zebrafish sequences is a thioredoxin fold of unknown function. In UBX domain containing protein 8, this domain was found to bind fatty acid leading protein oligomerization. Then, the two zebrafish domain sequences were removed, and the remaining sequence was resubmitted. This time, additional close structures were disclosed and without surprise are different from the bacterial hits (**Figure 32A**).

Only one common domain could be identified between bacterial and zebrafish SelenoNs. That domain aligned with a thioredoxin fold of unknown structure and contains the putative catalytic site SCUG with the only Sec residue. The diferent domains notably the EF-hand and transmembrane domain for the zebrafish and the additional C-terminal thioredoxin-fold for the bacterial suggest an evolution of function probably resulting from an adaptation process to the organism.

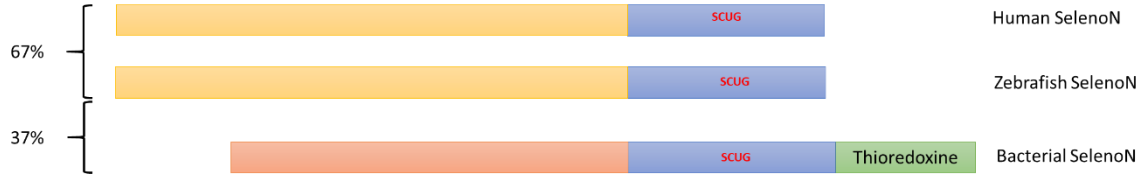

Figure 31 : Schematic representation of the alignment between zebrafish, human and bacterial SelenoN proteins.

Amino acid sequences of all three proteins where aligned using the BLASTP program. In blue is the common sequence to all three organisms, in green is the additional C-terminal thioredoxin fold found only in bacterial SelenoN sequence; in orange is the C-terminal sequence found only in zebrafish and in humal SelenoNs and in red is the C-terminal bacterial sequence. Percentages represent the degree of identity between sequences.

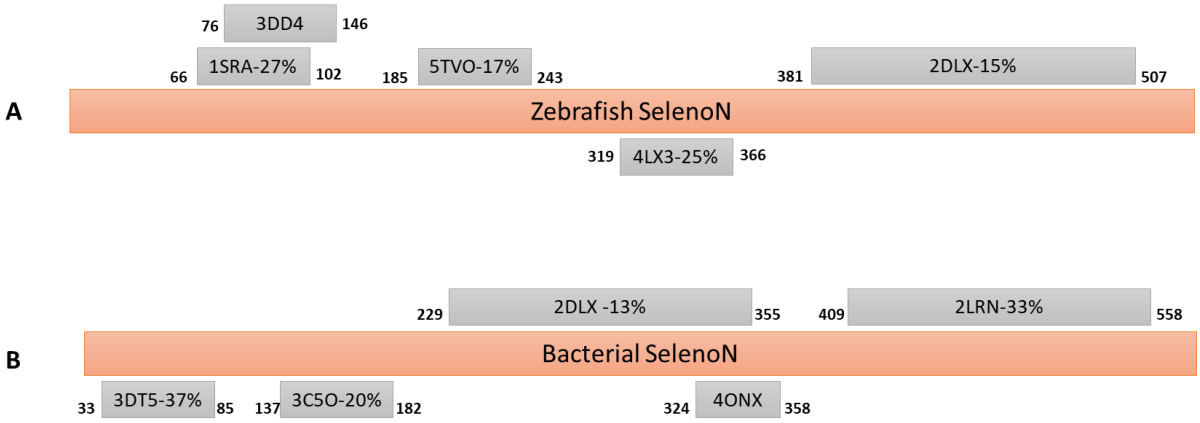

Figure 32 Schematic representation of bioinformatics analysis of zebrafish and bacterial SelenoN amino acid sequences with the program SWISSMODEL online

Numbers represent positions of amino acid that where covered by the alignment. In grey are PDB identifications of template structures and the identity percentage with SelenoN.

3.2 Results on zebrafish selenoN

3.2.1 Overexpression, purification and biophysical characterization of zebrafish SelenoN

3.2.1.1 Overexpression of the zebrafish SelenoN in mammalian cells HEK293

To produce large amount of zebrafish SelenoN or zSelenoN, an inducible stable cell line expressing the protein was engineered. To improve its expression in human cultured cells, the zebrafish SelenoN sequence was optimized for translation efficiency and the residue Sec was mutated into Cys. For purification purpose by affinity, the sequence of a His_8 tag was added at the C-terminus of zSelenoN sequence. The optimized sequence was cloned into pcDNA5 vector where the protein expression is under control of the human cytomegalovirus promoter (CMV) and inducible by addition of tetracycline or its stable analogue doxycycline. This construct was transfected into the Flp-IN HEK 293Trex™ cell line that allows the directed insertion of the expression vector at one genome position using the FLP recombinase. Stable recombinant clones were successfully selected and isolated (made by Melanie Thamy-Braye in Strasbourg).

The recombinant HEK 293Trex cells expressing zSelenoN were grown in DMEM medium containing 10% fetal bovine serum, either as suspension or adherent cultures. Biomass was increased as described in the previous chapter before induction of zSelenoN expression by addition of doxycycline to the growth medium. In suspension, it was observed that cells tend to form large aggregates although variable in size (**Figure 33B**). This aggregation resulted of a high cell density in the culture. It was hypothesized that this aggregation could limit the expression level of zSelenoN because cells within the aggregates have less access to oxygen therefore a reduced metabolism and secondly, limited accessibility to the inducer compared to cells on the surface.

To alleviate this problem, cell adaptation to synthetic medium designed for suspension culture, such as the CD293 medium without Fetal Bovine Serum was tested. However, cell viability dropped drastically when DMEM medium concentration was below 50%. Finally, cells did not survive the adaptation and died at a medium composition 75% CD293 and 25% DMEM.

Since the adaptation to synthetic medium for suspension culture was not possible, the expression protocol was optimized for adherent culture. No difference in expression level and in biomass quantities was observed between suspension and adherent culture (data not shown). This expression method presented the advantages of using fewer amount of medium and requires limited manipulations, therefore avoiding risks of contamination.

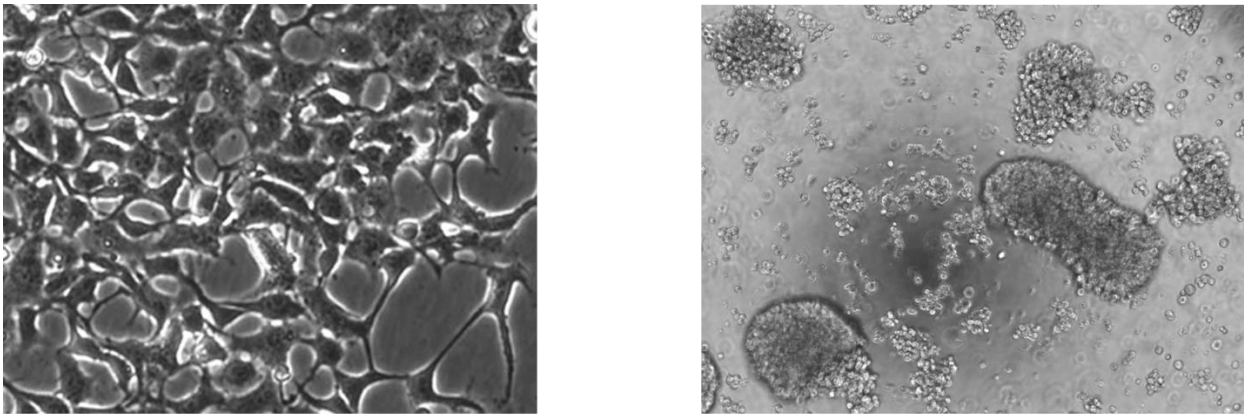

Figure 33 : Mammalian HEK 293T cells in adherent and in suspension cultures.

A: HEK cells in adherent culture at 80% confluence grown in DMEM medium and Fetal Bovine Serum.

B: HEK cells aggregates in suspension culture at a density of 10^6 cells/mL. Magnification is different in the two views.

3.2.1.2 Detergent and additives screening

Three grams of induced cells expressing zSelenoN where used for this purification test. Cells were resuspended in a hypotonic lysis buffer, and lysed by six cycles of freeze and thaw. Membrane fraction was resuspended and divided into 3 equal fractions. Different detergents were added in these fractions at final concentrations: 0.25% Dodecyl-β-Maltoside (DDM), 2% Decyl-β-Maltoside (DM), 6% CHAPS. After incubation, the solubilized membrane fraction was purified by affinity chromatography using a loaded Ni-IDA matrix in batch. Flow through were collected and matrix washed in buffer containing 80mM Imidazole. The bound protein was eluted with 400 mM Imidazole.

Analysis of the eluted fraction by SDS-PAGE showed that elution fractions of the DM are more concentrated and more homogenous than the others (**Figure 34**). This might be attributed to two interpretations: first the DM better solubilized the zSelenoN, secondly the binding of the protein to the matrix is more efficient in the presence of DM compared to the other detergents, possibly because of a better accessibility of the tag.

To test the stability of the protein in the different detergents combined with different additives, eluted fractions of each detergent experiment were concentrated. Afterwards, the fractions were divided into four fractions then, EDTA+EGTA were added at final concentration of 2 mM, in one hand and on the other hand $MgCl_2$ or $CaCl_2$ were added at final concentration of 10 mM. In addition, DM fraction was incubated with Octyl-glucoside (OG) at final concentration of 2.5% before being divided into four fractions that were prepared also as described before. After incubation for 4h at 4°C, purified protein status was analyzed on a Clear Native PAGE gel (Wittig and Schägger 2005, 2008).

Comparing the “control” lanes with detergents without additives, it appears that DM tends to better stabilize the protein than the other (**Figure 35**). Indeed, in the presence of the DDM, the purified zSelenoN migrated as a smear on the top of the gel and a band of lower molecular weight (MW), whereas in the presence of DM, it migrated as two discrete bands and less smear. The

CHAPS condition seems to have same effect as the DDM. DM appears to be the best condition in this case. The addition of 10mM $MgCl_2$ seems to have no significant effect on the migration. In contrary, in the presence of 10 mM $CaCl_2$, the lower MW decreased in intensity and is converted into the higher MW bands. Again, in the presence of DDM, CHAPS or OG, the band appeared as a smear whereas with DM, it corresponded to more resolved band. In the presence of EDTA and EGTA, DDM was no significantly different compared to the "control", whereas in DM and CHAPS conditions, the lower MW band appeared to be predominant and well resolved. Altogether, combination of DM and 2mM EDTA+EGTA seemed to be the most suitable for the protein homogeneity and stability (**Figure 35**)

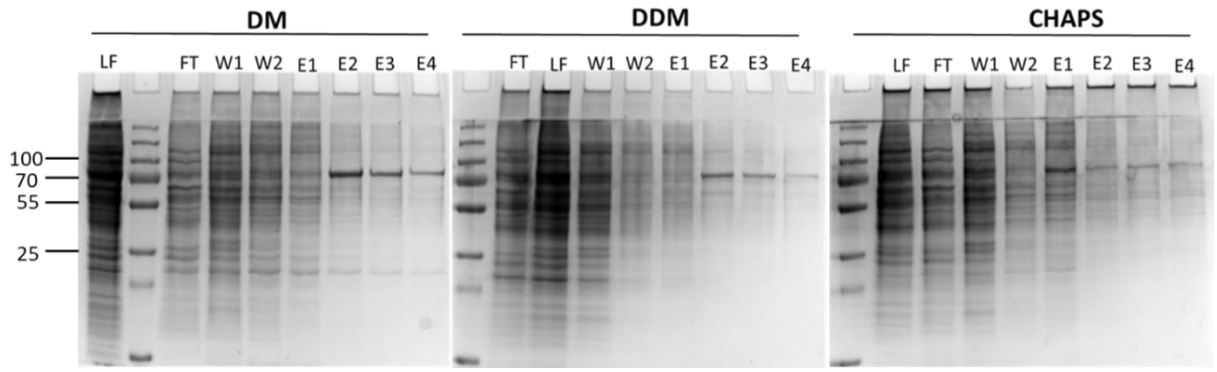

Figure 34: zSelenoN solubilization and purification using different detergents.

2% Decyl-β- Maltoside (DM), 0.25% Dodedyl-β-maltoside (DDM), 6% CHAPS.

Affinity purification visualization using an 8% SDS PAGE gel which was Coomassie stained. LF: Loaded Fraction, FT: Flow Through, W: washes with 80 mM Imidazole, E: Elution fraction.

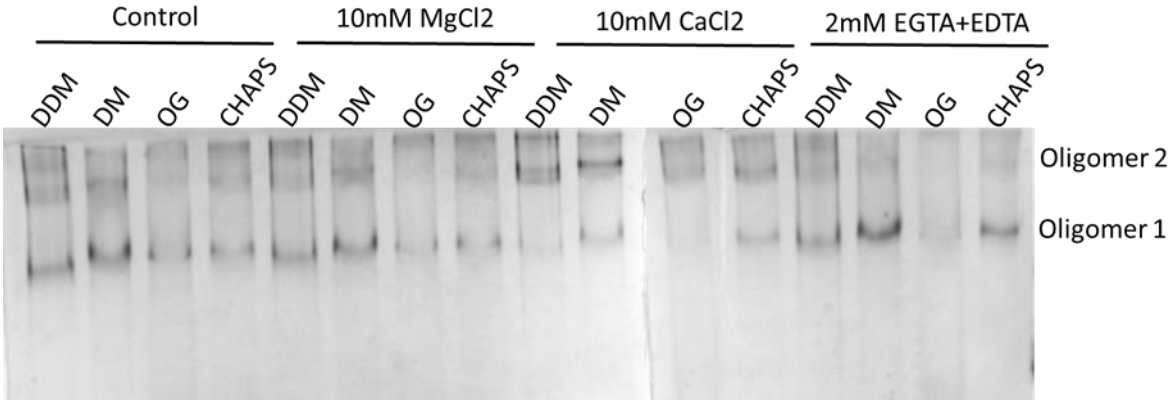

Figure 35 :Detergent/ additives screening

Results were visualized on an 8% Clear Native PAGE gel which was coomassie stained.

3.2.1.3 Optimization of the purification protocol

Induced HEK 293 cells expressing zSelenoN were collected and lysed. Membrane fraction was sedimented by centrifugation and the membrane proteins were solubilized with 0.5% Decyl-β-maltoside as described.

Then the zebrafish recombinant SelenoN was purified from the solubilized membrane fraction in two steps: a Ni-NTA affinity using DM containing buffers followed by a size exclusion chromatography using DDM containing buffers. The first step of the purification enabled to remove most contaminants from the protein extract. The binding of the protein on the Ni affinity column was efficient as the band corresponding to zSelenoN is absent in the flow-through (**Figure 36B**). The recombinant protein was with an imidazole gradient. Two peaks were obtained. Analysis on a SDS-PAGE gel of the fractions showed that zSelenoN was mainly eluted in the second peak and was purified close to homogeneity (**Figure 36A and 36B**). Fractions of the second peak were pooled, concentrated, and then loaded on a Superdex 200 10/300 for a polishing step by size exclusion chromatography. As shown on **Figure 36C and 36D,** the loaded fraction was eluted in 2 peaks, both corresponding to the recombinant zSelenoN. The first and enlarged peak came out directly after the void volume (8 mL for the column used), the second sharp and monodisperse peak came out at a volume that theoretically corresponded for this column to a molecule of about 150 kDa. It is important to keep in mind that the eluted particle corresponded to a protein-detergent complex. ZSelenoN elution in two peaks could be explained by the purification of two different conformations or two different oligomers. One could also hypothesize the eventual presence of a binding partner in one of the two peaks. However, similar amount of protein was recovered in both peaks which, were further analyzed individually.

In conclusion, 3 mg of pure recombinant zSelenoN protein equally distributed in two size exclusion peaks as shown in (**Figure 36D)** were obtained from 3 g cultured cells in a two-steps purification procedure.

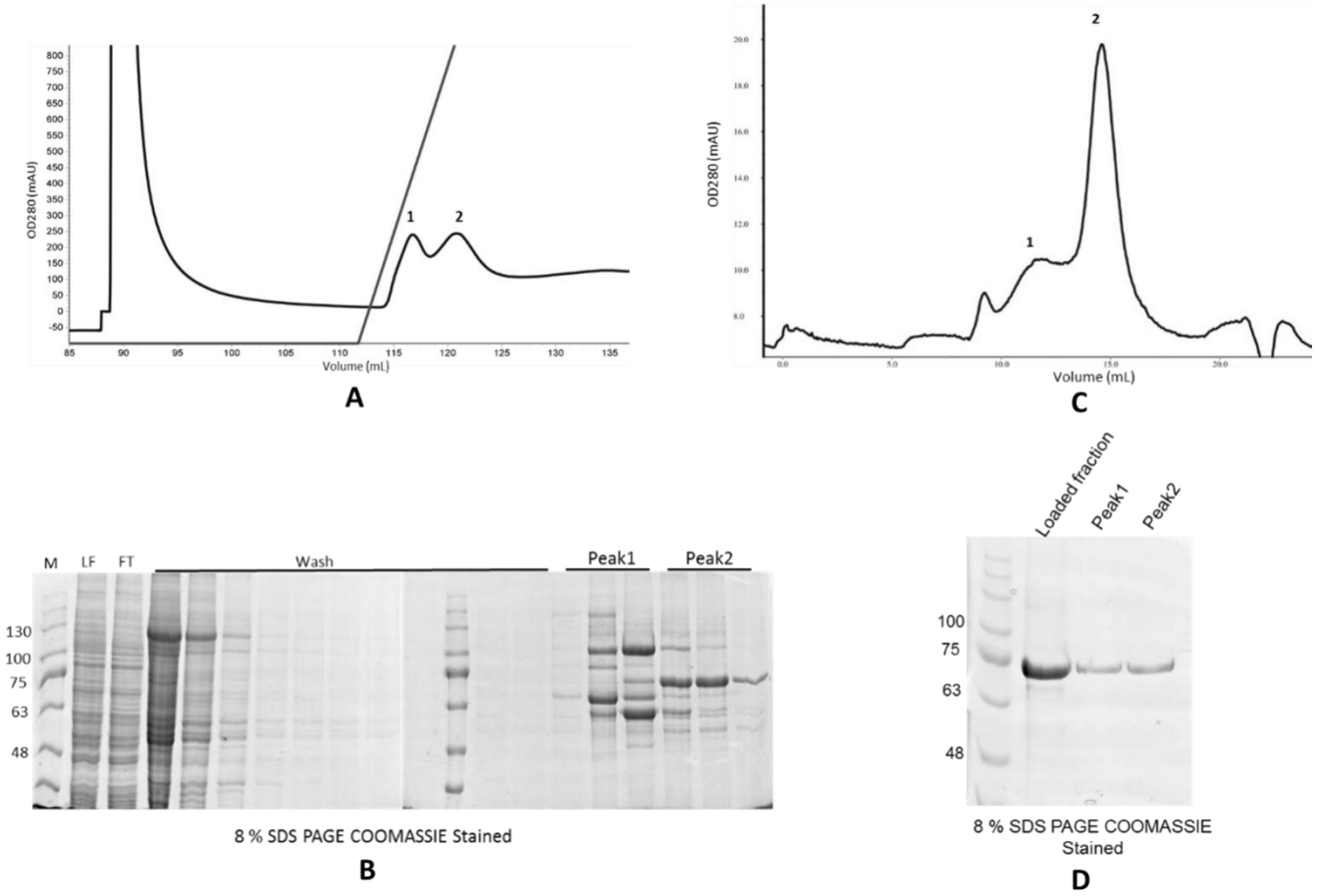

Figure 36 :Chromatography purification of zebrafish SelenoN

The recombinant zebrafish SelenoN was solubilized from the cell membrane fraction, and then purified by Ni-NTA affinity followed by a size exclusion chromatography. As required for membrane proteins, detergent was maintained in the buffer during the whole process. The solubilization and the affinity were performed using DM as in size exclusion DDM was used as detergent.

The SDS-PAGE gel **(B)** and chromatogram **(A)** show the elution profile over an imidazole gradient through a 1mL Ni-NTA column. The protein came out in the second peak that eluted at approximately 140 mM Imidazole.

The SDS-PAGE gel **(D)** and chromatogram **(C)** show the elution profile through a superdex 200 10/300. The peak 1 elute after but close to the void volume and displayed a flat shape, the sharp peak 2 elute between 14 and 15 mL elution volume. Both peaks contained equal amount of the recombinant pure zSelenoN as seen on the SDS-PAGE gel

3.2.1.4 Effect of bivalent ion

Since the eukaryotic SelenoN contains a conserved calcium binding Ef-hand domain, effect of bivalent ions on zSelenoN conformation was tested by native gel analysis. Second peak recovered from the size exclusion chromatography was first dialyzed to remove EDTA and EGTA.

Fractions were prepared by addition of EGTA and increasing amount of $CaCl_2$ or $MgCl_2$, as well as a combination of both $CaCl_2$ and $MgCl_2$. Samples were then incubated for 4h at 4°C, and fractionated on an 8% clear Native PAGE gel. The separation of proteins of different entities was visualized by a western blot using an antibody directed against zSelenoN (**Figure 37A**).

Two forms were detected. In the control fraction without any additives, the two entities were present, and the faster migrating band was predominant. With increasing concentrations of magnesium, the lower form was increasing in intensity and above 0.5 mM $MgCl_2$, the higher band was disappearing. In contrary, the lower form was converted to the higher one with increasing Ca^{2+} concentrations. Moreover, third higher-migrating band was appearing with increasing Ca^{2+} concentrations (**Figure 37A**). This suggests a conformational rearrangement effect of bivalent ions notably, in presence of Ca^{2+} zSelenoN tends to form higher oligomer and in the presence of Mg^{2+}, the reverse effect is observed.

To estimate the apparent molecular weight of the previously visualized entities, the purified protein fractions incubated with the different additives were analyzed on a Coomassie stained Blue Native PAGE (Wittig, Braun, and Schägger 2006; Wittig and Schägger 2008). The migration profile appeared like the one obtained with the Clear Native PAGE although the two higher bands were less defined. The lower band migrated at an apparent mass of about 140 kDa if the particle is globular, and the second form migrated at a position around 250 kDa (**Figure 37B**).

Binding parameters of the Ca^{2+} with zebrafish protein was investigated using the Microscale Thermophoresis. EGTA was used as negative control to compare the dose-response signal amplitude in both conditions. Several ranges of Ca^{2+} concentration (nanomolar, micromolar and millimolar ranges) were covered in the experiment but unfortunately, no interpretable result

could be obtained (result not shown). However, all attempts to add Ca^{2+} in a concentrated zSelenoN sample resulted in an irreversible precipitation of the protein therefore, all following characterization of zebrafish SelenoN were made in presence of EGTA.

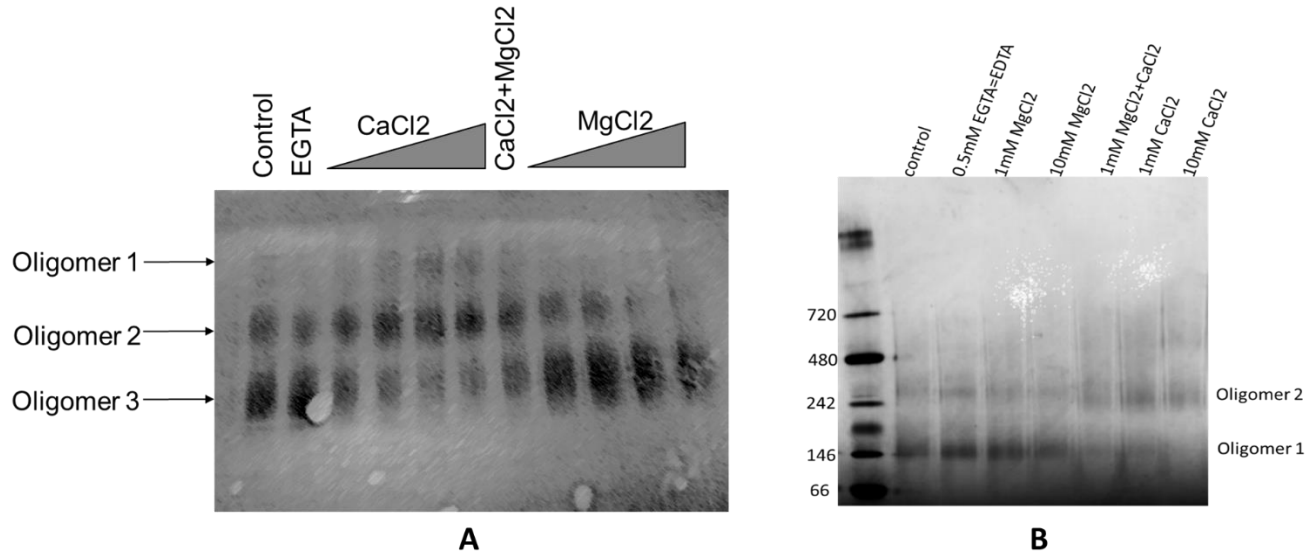

Figure 37: Effect of bivalent ions on zSelenoN oligomeric status.

The second peak of the size exclusion chromatography was dialyzed to remove EDTA and EGTA, before being used for these experiments.

Gel A: after incubation at 4°C with either 1 mM EGTA, MgCl2 or CaCl2 at final concentrations of 0.25, 0.5, 0.75, 1mM or 0.5mM $CaCl_2$ + 0.5 mM $MgCl_2$., zSelenoN samples were fractionated on an 8% clear native PAGE gel then analyzed by a western blot using an anti-zSelenoN antibody.

Gel B: after incubation at 4°C with 0.5 mM EDTA+EGTA, 1mM and 10mM of $CaCl_2$ or $MgCl_2$, 1mM $MgCl_2$+$CaCl_2$., zSelenoN samples were fractionated on a 3-12% Blue native PAGE gel and revealed by coomassie stain.

3.2.1.5 Biophysical parameters from the SAXS measurement

In order to calculate structural parameters as well as to obtain a low-resolution model of zSelenoN, SAXS coupled to a preceding High-Pressure Liquid Chromatography (HPLC-SAXS) was performed.

Seventy µL of pure recombinant zSelenoN concentrated at 10 mg/mL from the purification peak 2 or 4.5 mg/mL from the purification peak 1 (**Figure 36C and 36D**) were used for HPLC-SAXS. Samples were loaded separately on a Superdex 200 10/300 GL coupled in line with SAXS. The elution of the protein was monitored by UV and SAXS detectors at the beamline BM29 of the European Synchrotron Facility (ESRF) in Grenoble.

The purification peak 1 yielded a profile with 3 peaks recorded by the UV detector at 280nm and 4 peaks (**appendix 2B**) recorded by SAXS detectors corresponding to different molecule sizes. The purification peak 2 on the other hand displayed one main peak recorded by the UV at 280nm and two peaks recorded from SAXS detectors and corresponding to two main populations of molecules with different sizes (**see appendix 2 A and 2C**). For the subsequent analysis, only data from the purification peak 2 were processed.

The R_g and I(0) traces (**Figure 38A**) as a function of frame number showed that the sample was highly pure as expected from the purification profile. The profile exhibited two peaks. The first was identified as a protein-detergent complex according to its UV absorption at 280 nm (**see appendix 3**) and the second peak corresponded to detergent micelles as no UV absorption was detected at the wavelength 280 nm (Slotboom et al. 2008). Buffer frames where subtracted from frames 1960 to 2000 (see highlighted frames on **Figure 38A**) that corresponded to the highest I(0) with a similar R_g. After buffer subtraction, intensities of the frames were averaged for subsequent analysis.

Averaged data were first analyzed with the program SHANUM (Konarev and Svergun 2015; D Franke et al. 2017) to determine the s range with the minimum signal to noise ratio. Following this first analysis, data were cut to s_{max}=4nm^{-1}.

The LogI(s) versus s plot (**Figure 38B**) represents the primary averaged SAS data of the selected frames, with Guinier plot (Konarev P.V., et al 2003) shown as inset. The Guinier plot was linear to the first measured s values (with a R2 = 0.9974) which indicates the absence of aggregation. Analysis provided a radius of gyration (Petoukhov et al. 2007) of about 4.18 ± 0.03 nm .

The Kratky plot (**Figure 38C**) display a bell-shaped curve as expected for a predominantly folded particle.

The distance distribution analysis (D I Svergun 1993) (**Figure 38C**) gave the values of the maximal particle size: D_{max} was 14.80 nm and the Porod volume described as the scattering particle volume (Porod, 1951) is 334.53 nm^3. The P(r) versus r was well defined as it displayed a smooth and concave approach to zero at r=0 and r= D_{max}. The calculated R_g in the real space was similar to the Guinier analysis.

Molecular weight (MW) was evaluated using different approaches. The calculation according to the Porod volume (Vp) provided a value of 209 kDa assuming a ratio Vp to MW of 1.6 (Whitten et al, 2017). MW estimation according to the MoW indicated a mass of 156.8 kDa (**Table 21**).

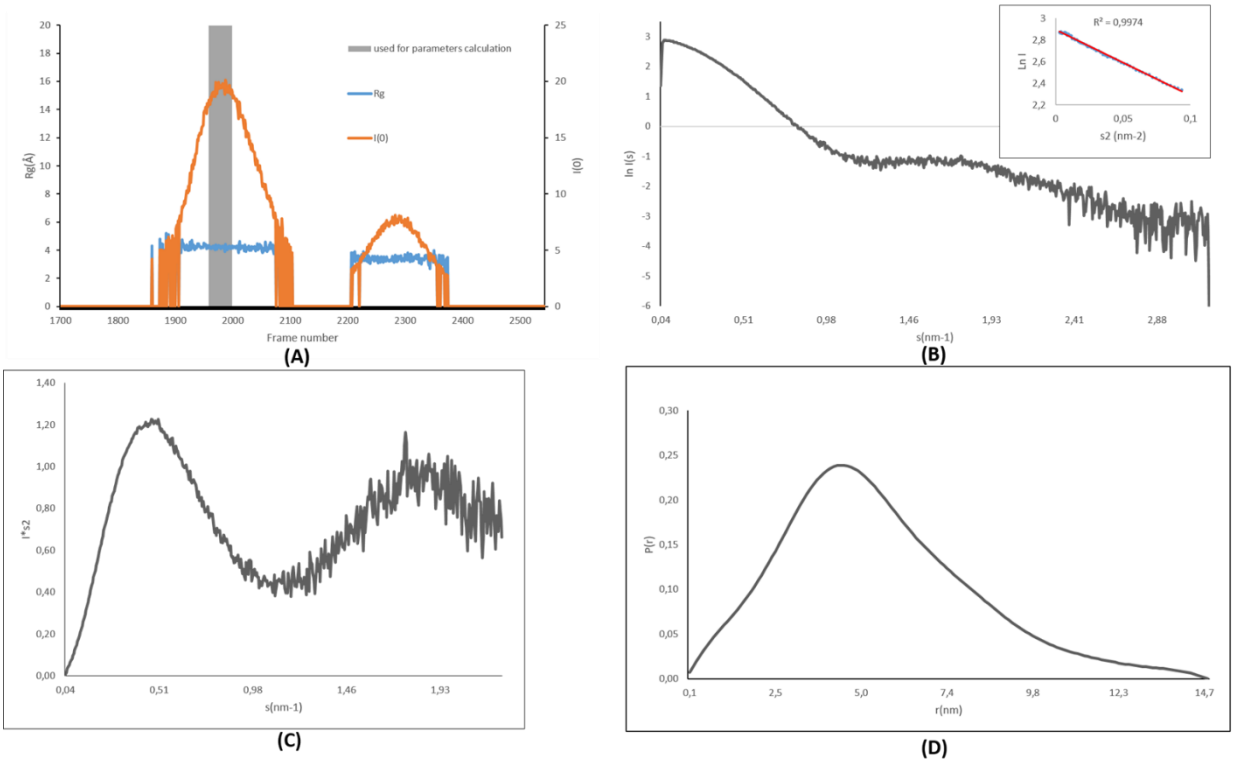

Figure 38 Curves and Structural parameters derived from HPLC-SAXS performed on zebrafish SelenoN.

(A) Plot showing I(0) as a function of frame. Frames are proportional to the time and therefore to the elution volume for the SEC-SAXS run. One frame was recorded per second with a flow of 0.5mL/min. Therefore, it represents 120 frames per mL of elution Volume. Highlighted data frames were selected for averaging to obtain the ln(I) versus s**. (B)** Ln I(s) versus s plot with the inset showing Guinier plot. **(C)** Kratky plot from the data in (B) represented for s< 3nm-1. **(D)** P(r) versus r profile from the data in (B).

Table 21 Structural parameters calculated from the HPLC-SAXS of the purification peak 2 of the zebrafish SelenoN

Guinier Analysis	
I(0) (nm^{-1})	17.77 ±0.05
R_g (nm)	4.18 ±0.03
sR_g range	0.68 – 1.3
Correlation coefficient R^2	0.997
P(r) analysis	
I(0) (nm^{-1})	17.8±0.3
R_g(nm)	4.29±013
D_{max}(nm)	14.80
s range (nm^{-1})	0.17-4.23
X^2 (total estimate from GNOM)	0.969 (0.868)
Porod Volume (nm^{-3})	334.5
Molecular Weight estimation (kDa)	
Theoretical MW of the monomer	72
MW by DATMOW	156.8
MW calculated from porod volume (ratio Vp to MW)	209 (1.6)

3.2.1.6 *Ab initio* modelling of zSelenoN

Ab initio modeling conducted using two different approaches was made. DAMMIF (Daniel Franke and Svergun 2009) was run twenty times with parameters assuming that the molecule is a dimer of zSelenoN. Models generated were grouped into 4 main clusters (**appendix 3**) with a χ^2 between 1.054 and 1.111. Distance between the different generated models is named Normalized Spatial Discrepancy (NSD). It translates the degree of similarity between generated models and therefore the stability or confidence of the average model. Similar model will typically have a NSD less or close to 1. The DAMMIF NSD value was 1.976, indicative of a high distance between all the twenty models. The fourth cluster included most of the models obtained and is presented in **Figure 39**.
Modelling in space based on diffusion curves did not lead to a unique solution. Therefore, the DAMMIN program (Dmitri I Svergun 1999) was run twenty times independently. Models thus obtained were grouped into clusters and compared using the DAMAVER program (Volkov and Svergun 2003) to evaluate the distance between the different solutions. In our case, the NSD varied between 0.494 to 0.663 which indicates a good correlation and a good stability of the average solution.
The average and refined solution was then used as input for one last DAMMIN run. The experimental diffusion curve was then compared to the theoretical DAMMIN model and the fit between both is estimated by the factor χ2 (D I Svergun 1993). In our case, the χ2 value was 21.65 which is very high and unexpected (**Table 22**).

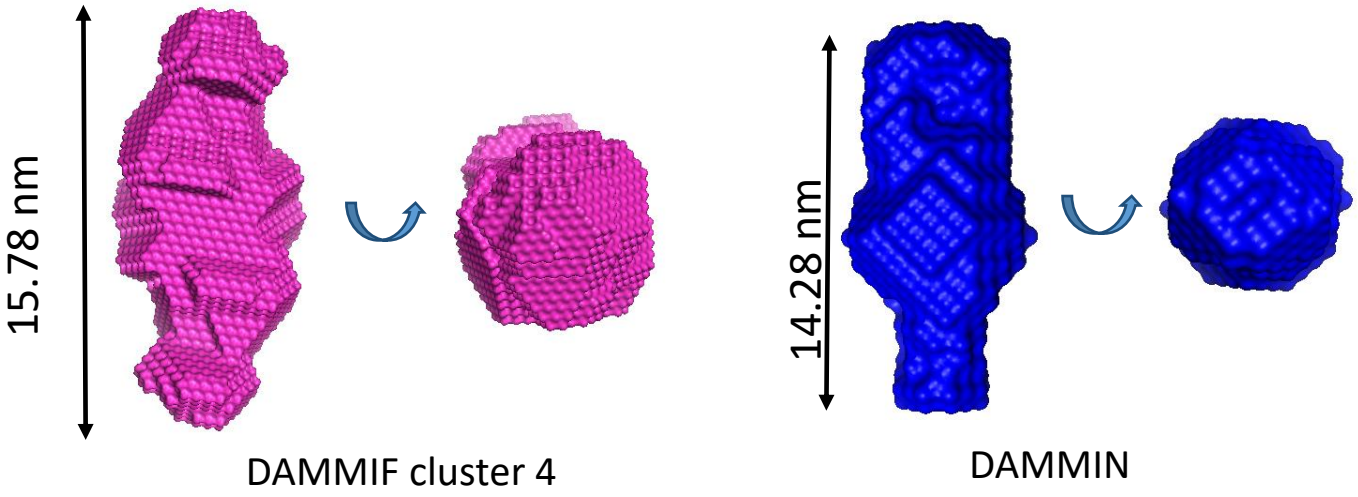

Figure 39 : Ab initio modelling of zSelenoN

Bead models where generated with DAMMIN and with DAMMIF programs. Picture of the models where made by PYMOL

Table 22: Shape calculation and model-fitting result of zSelenoN

DAMMIF	
q range for fitting ($Å^{-1}$)	0.02 - 0.2
NSD (standard deviation), No of cluster	1.976 (0.248), 4
X2 range	1.054 – 1.111
MW of the model (kDa)	188
Resolution (Å) from SASRES	69 ± 3
DAMMIN	
X2	21.65
volume of the model (nm^{-3})	286.43
Resolution (Å) from SASRES	37± 3

3.2.1.7 Secondary structure studies

The percentage of the different secondary structure elements was evaluated using the Circular Dichroism (CD) spectroscopy (Whitmore and Wallace 2008). For this purpose, 200 µL of protein solution at 0.1-0.3 mg/mL concentration was used in a 1 mm cuvette. Prior to measurements buffer was exchanged to 3 mM Tris-HCl, 15 mM NaCl 0.5 mM, 2mM EDTA, 2 mM EGTA, 0.05% DDM.

After collecting the raw signal, the buffer signal was subtracted and the data were processed on-line using the DICROWEB server (Lobley, Whitmore, and Wallace 2002; Whitmore and Wallace 2004, 2008). The signal above 190 nm was too noisy (**Figure 40**). Therefore, Protein data sets smp180 (Abdul-Gader, Miles, and Wallace 2011) and SP175 (Lees et al. 2006) specific for membrane proteins were used for calculation using the algorithms SELCON3 (Sreerama and Woody 1993; Sreerama, Venyaminov, and Woody 1999), CONTIN LL (Provencher and Gloeckner 1981; Van Stokkum et al. 1990) and CDSSTR (Compton and Johnson 1986; Manavalan and Johnson 1987; Sreerama, Venyaminov, and Woody 2000). Results of the calculation obtained were averaged for each secondary structure element.

In parallel, a bioinformatic prediction tool: PHYRE2 (Kelley et al. 2015) based on the amino acid sequence of the protein was run to calculate the theoretical value of the secondary structure elements and compare to the experimental data.

By comparing theoretical CD spectra of folded Vs unfolded protein (***Figure 26***), one could see that zSelenoN CD spectra profile corresponded to a well folded protein (Figure 40). However, the experimental values obtained were very different from the theoretical one. CD spectra analysis indicated that the protein is α-helical rich with about 56% of the overall protein and contains only 12% β-sheet. The PHYRE2 program predicted a lower α-helical content and corresponding higher β-sheet content.

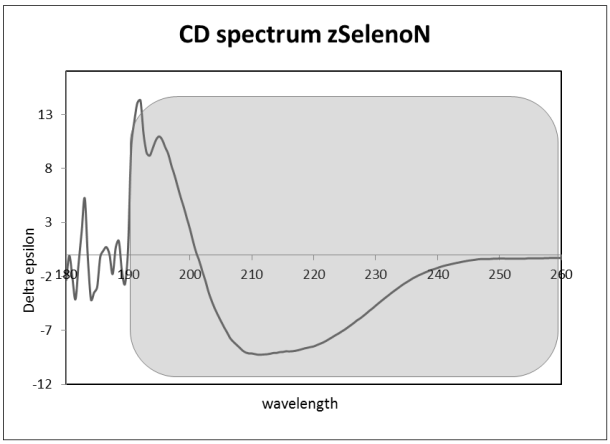

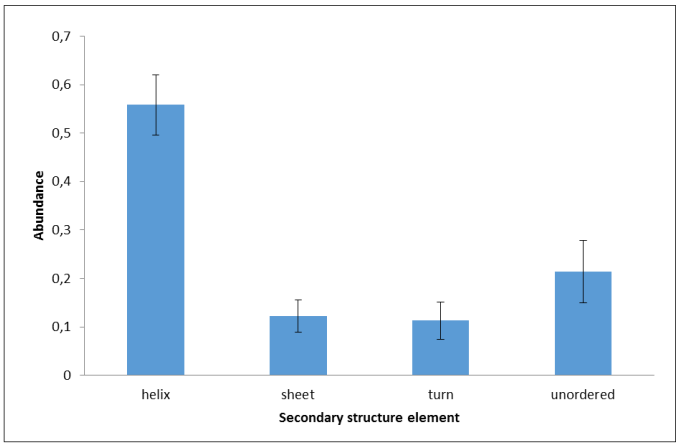

	α-helix	β-sheet	turns	unordered
Prediction(Phyre 2)	37%	23%	14%	26%
experimental	56%±6.3	12%±3.3	11%±3.9	21%±6

Figure 40 :Evaluation of the secondary structure of the recombinant zSelenoN using CD spectroscopy

The curve presented is the zebrafish SelenoN CD spectra after buffer spectra subtraction. The highlighted area is the range of wavelengths used for the secondary structure calculation. Data were processed on-line using Dicroweb. SELCON, CONTIN LL and CDSSTR algorithms and protein sets smp180, SP175. Obtained results were averaged. The table presents the comparison between the experimental averaged values and the theoretical values obtained using the on-line prediction tool PHYRE2.

3.2.2 Crystallization of zebrafish SelenoN and optimization

The purified zSelenoN protein was concentrated to 10-12 mg/mL and glycerol was removed by buffer exchange using amicon concentrators prior to crystallization trials. Both peaks (**Figure 36D**) were crystallized separately. Phenix robot was used to generate nanodrops in 96 well plates as described by Müller and Lancaster in 2013. Different commercial screens designed for membrane proteins were initially tested. No crystals were observed under those conditions.

Eukaryotic SelenoN is a glycosylated transmembrane protein of the endoplasmic reticulum and sugar moiety of glycosylated proteins can behave as floppy extremities that prevent nucleation and crystallization (Mesters and Hilgenfeld 2007). To tackle this problem, zSelenoN was assayed for native deglycosylation using different endoglycosidases notably endo F1, F2 of the NDegly kit (Sigma^{TM}). The main asset of the tested endoglycosidases is that they present a small size and therefore they can easily access inside a folded protein to cut glycoside residues. Among the enzymes tested, Endo F1 was the only one to remove sugar residues from zSelenoN in native conditions. Comparing EndoF1 deglycosylation on the native with PNGase on the denaturated zSelenoN confirmed that Endo F1 removed all glycoside groups of zSelenoN (**Figure 41A and 40B**). Assays were made to determine the efficiency of native deglycosylation at room temperature to limit the protein stress. Results showed that an overnight incubation at room temperature with the enzyme is enough to deglycosylate the protein (see endo F1 Vs PNGase F on **Figure 41**).

Native deglycosylation was carried out on a dilute sample (1-2 mg/ml) at room temperature overnight. Then, the protein sample was subjected to centrifugation using a 50 kDa cut off amicon concentrator to wash out the endo F1 glucosidase (32 kDa) and the glycerol prior to concentration and crystallization screen. First hits were obtained. Spherulites were observed after a few weeks of incubation at 18°C in a condition containing 0.1% Na cacodylate pH 6.5 and 30% PEG 2000.

Then, different additives ($CaCl_2$, $MgCl_2$, and ZnCl) were added to the screens. Different conditions containing $CaCl_2$ and $MgCl_2$ gave rise to spherulites (**Figure 42**) that were transferred to cryoprotectant solution composed of the crystallization condition supplemented with glycerol and

then flash-frozen in liquid nitrogen. X-ray experiments using these spherulites exhibited low resolution diffraction at 15 Å.

Those spherulites were used as seed material using same reservoir solutions. Small crystals with a size between 20 and 25µm (**Figure 43**) grew in conditions containing 0.1 M MES or MOPS pH 6.5, 0.2 M $CaCl_2$, 6.5% PEG 2000 at 18°C. Unfortunately, X-ray experiments showed no diffraction from these obtained crystals.

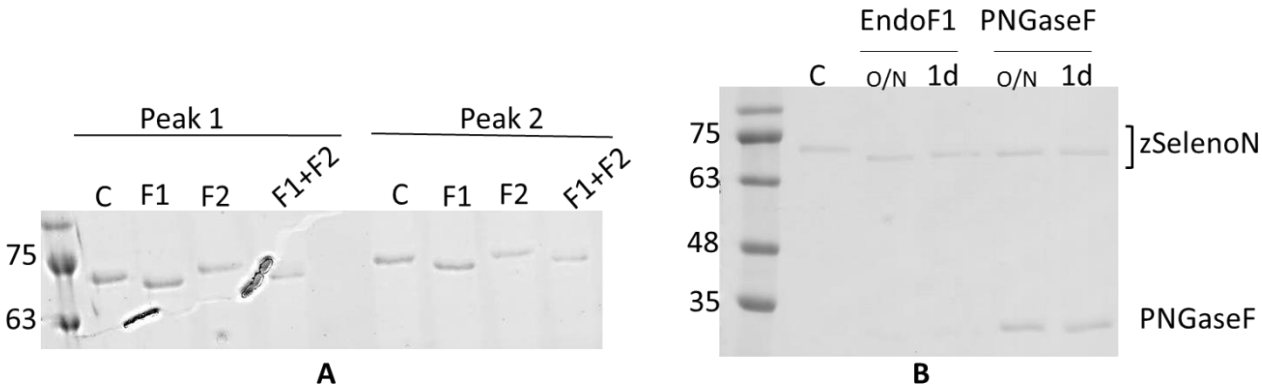

Figure 41 :zSelenoN deglycosylation essays

Gel A: Visualization of the native deglycosylation of zSelenoN using differents endoglycosydases: F1, F2 and F1+F2. C= control, Peak1=size exclusion peak1, Peak2= size exclusion peak 2.

Gel B: Optimization of native deglycosylation condition. Endo F1 was tested either overnight or for 24 hours. The efficiency of the deglycosylation is evaluated by comparison with the denaturing deglycosylation using PNGaseF.

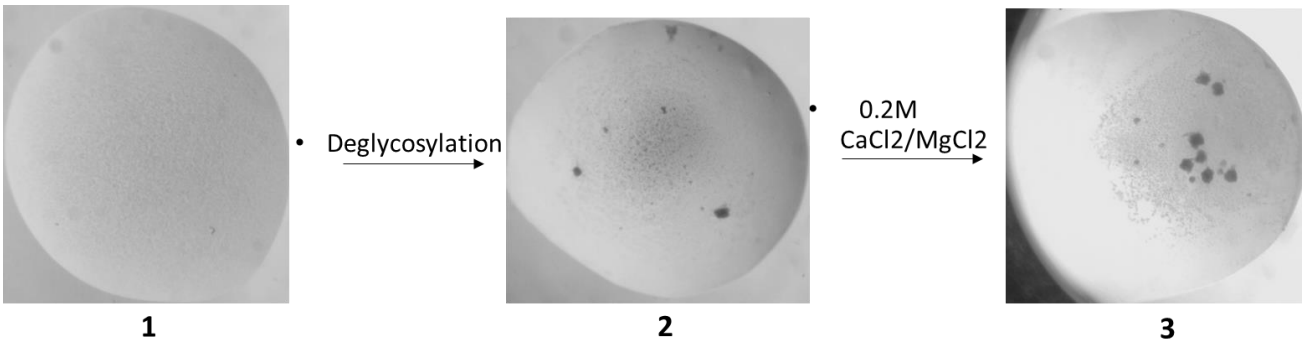

Figure 42: Optimization of zSelenoN crystallization trial.

Pictures 1, 2 and 3 are crystallization drops of zSelenoN Peak 2 in the condition 0.1M Na cacodylate pH 6.5, 30% PEG 2000. 1=glycosylated zSelenoN, 2= deglycosylated zSelenoN, 3= deglycosylated zSelenoN + additives

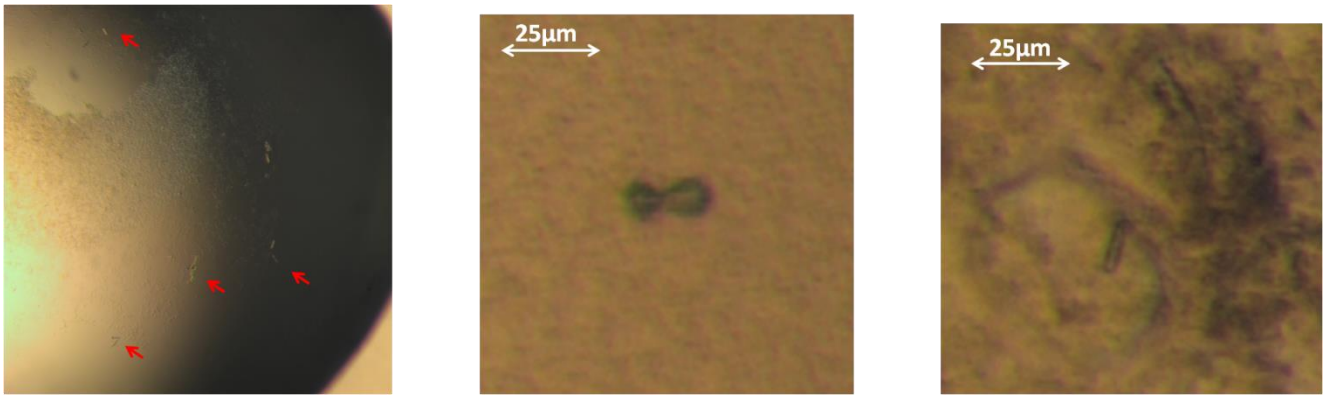

Figure 43 : zebrafish SelenoN crystals obtained after seeding

Crystals were obtained using deglycosylated protein and seeding material. The crystals grew in conditions 0.1M MES or MOPS pH 6.5, 6.5% PEG2000 and 0.2M $CaCl_2$.

3.3 Results on Candidatus poribacteriae SelenoN

3.3.1 Overexpression, purification and biophysical characterization of bacterial SelenoN

3.3.1.1 Overexpression and purification

The *Candidatus poribacteria* SelenoN sequence optimized for expression in *E. coli* was cloned into the pQE70 vector to generate a C-terminal fusion with a His_8 tag expressed under the control of the bacterial T5 promoter. This construct was transformed into *E coli* XL1-Blue-pGRO7 (Cam^r) that co-expressed the chaperons GroES and GroEL to improve SelenoN solubility. The expression was performed in LB medium containing first arabinose to induce the expression of chaperones, then IPTG was added to induce SelenoN expression.

Recombinant bacterial SelenoN (bSelenoN) was purified from the soluble extract in two chromatography steps beginning with Ni-NTA affinity, followed by a size exclusion chromatography. The first step of the purification resulted in the removal of most contaminants from the protein extract (**appendix 4A**). bSelenoN was eluted from the resin with 750 µM imidazole. After concentration, the eluate was then loaded on a Superdex 200 16/60 column for a polishing step by size exclusion chromatography. As show on **Figure 44A,** the loaded fraction was eluted in two peaks, both corresponding to the recombinant bSelenoN. The first peak came out directly with the void volume (40 mL for the column used) and is likely to correspond to large complexes or to aggregatesof bSelenoN. The second peak is monodisperse and eluted at an elution volume between 70 and 80 mL. Eluted fractions corresponding to the two peaks were analyzed by SDS-PAGE, the majority of bSelenoN is retained within peak 2, suggesting that the protein preparation was homogenous.
Overall, 6 mg of pure recombinant bSelenoN protein (**Figure 44)** were obtained from 11 g cells cultured in 6 L LB medium, in a two-step purification procedure.

In order to confirm the monodispersity and also appreciate the apparent molecular weight of the recombinant bacterial SelenoN, a blue Native PAGE analysis was carried out. The protein eluted

in the second peak (**Figure 44A),** was monodisperse and monomodal as only one single band was detected. Surprisingly, this band migrated at a position between 66 and 146 KDa (**Figure 44C**) as the calculated mass is 64 kDa.

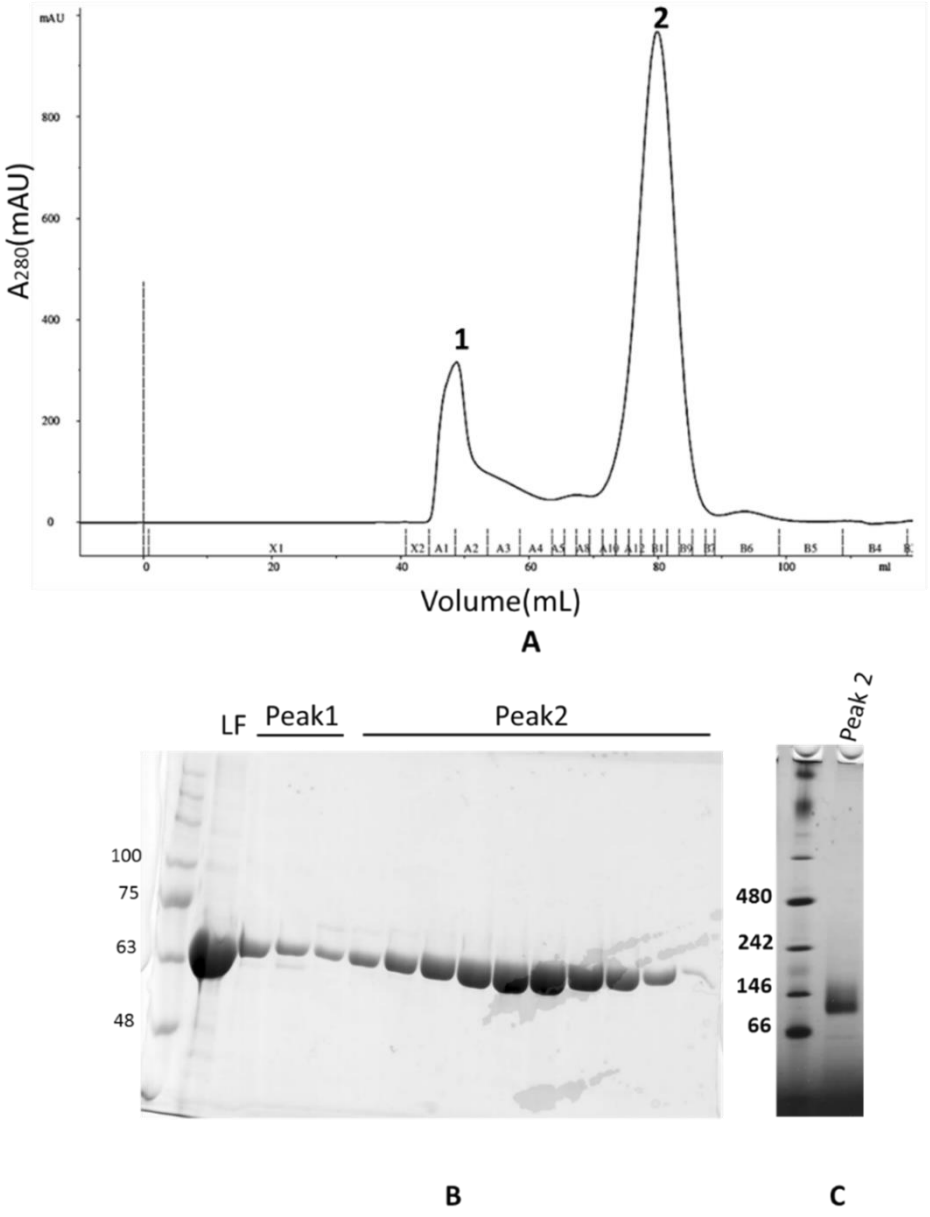

Figure 44 :Purification of the* Candidatus poribacteriae *SelenoN

The bacterial recombinant SelenoN was purified by affinity followed by a size exclusion chromatography. **(A)** The chromatogram showed the elution profile through a superdex 200 16/60. **(B)** The peak 2 eluted between 70 and 80 mL and contained bSelenoN as a pure sample as seen on the SDS PAGE gel. **(C)** The Native Blue PAGE showed that the protein fraction is monomodal as only one band or one oligomer was detected on the gel

3.3.1.2 Biophysical parameters from the Size exclusion chromatography coupled with Small Angle Light Scattering measurement

In order to calculate structural parameters as well as a low-resolution model, SAXS coupled to a preceding HPLC (HPLC-SAXS) was conducted.

Seventy µL of highly pure recombinant bSelenoN concentrated to 15 mg/mL was loaded on a Superdex 200 10/300 GL coupled in line with SAXS. The elution of the protein was monitored by UV and SAXS detectors. Frames corresponding to the single peak (see **appendix 5**) were scaled and averaged. Data were analyzed with the program ATSAS 2.8.0 from the EMBL Hamburg. The resulting averaged scattering curve (see below) was then used for further analysis.

The R_g and I(0) traces (**Figure 45A**) as a function of frame number showed that the sample was highly pure as expected from the purification profile. The protein eluted as one single peak with a linear R_g profile. Buffer frames where subtracted from frames 1814 to 1824 that corresponded to the highest I(0) and similar R_g. After buffer subtraction, intensities of the frames where averaged for subsequent analysis.

Data where first analyzed with the program SHANUM to determine the s range minimizing signal to noise ratio. Following this first analysis, data where cut to s_{max} of $4nm^{-1}$.

The LogI(s) versus s plot (**Figure 45B**) represents the primary averaged SAS data of the selected frames, with Guinier plot shown as inset. The Guinier plot was linear to the first measured s values (with a R^2 = 0.998) which suggested the absence of aggregation. Analysis provided a radius of gyration of about 3.66±0.14 nm.

The Kratky plot (**Figure 45C**) displayed a bell-shaped curve as expected for a predominantly folded particle.

The distance distribution (**Figure 45D**) analysis gave the values of the maximal particle size D_{max} which is 12.82 nm and the Porod volume 113.5 nm^3.The P(r) versus r was well defined as it showed a smooth and concave approach to zero at r = 0 and r = D_{max}. The calculated R_g in the real space

was higher than the one using the Guinier approach.

Molecular weight was evaluated using different approaches. The calculation according to the Porod volume (Vp) gave a value of 72 kDa assuming a ratio Vp to MW of 1.5. MW estimation according to the MoW and the Volume of correlation gave respectively 83 and 73 kDa (Table 23.

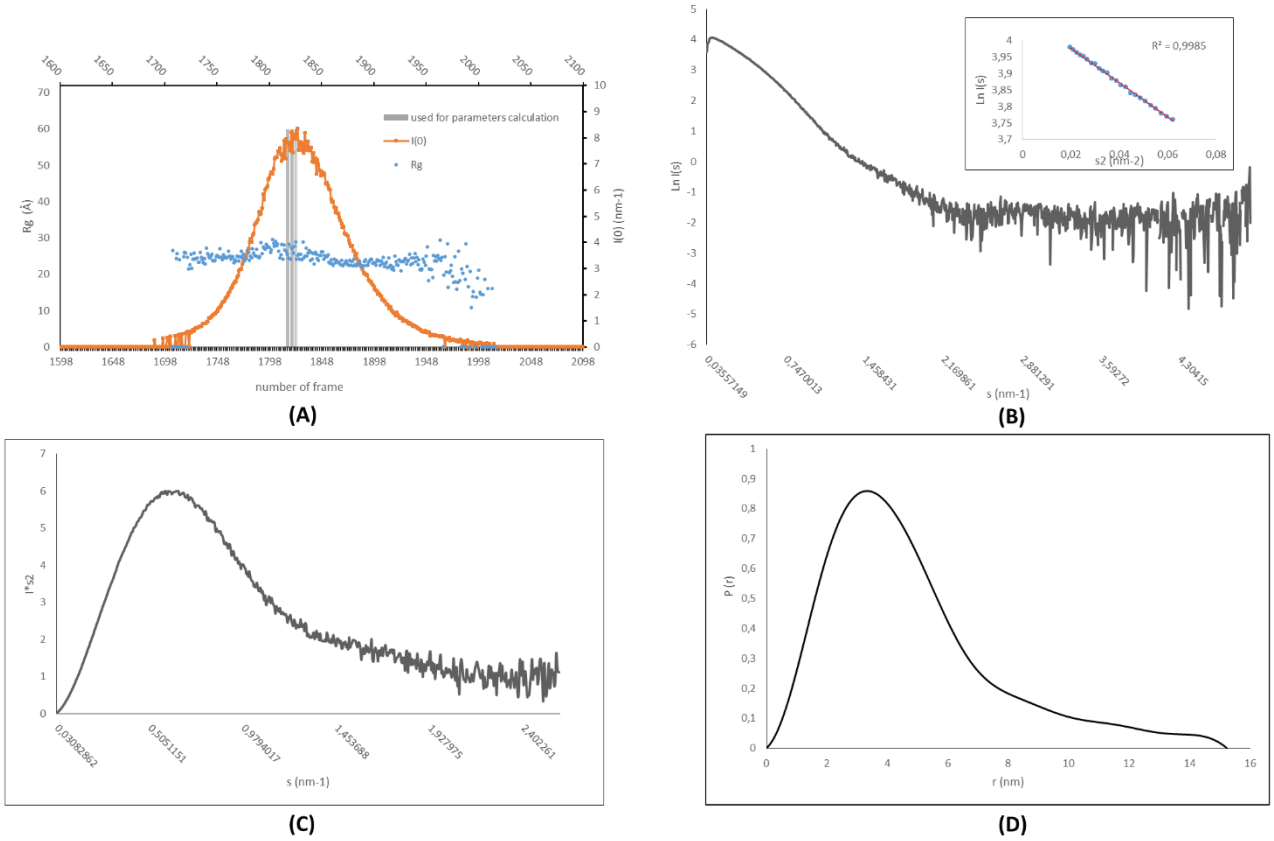

Figure 45 Curves and Structural parameters derived from HPLC-SAXS analysis of the bacterial SelenoN.

(A) Plot of I(0) as a function of frame number. Frames are proportional to the time and therefore to the elution volume of SEC-SAXS run. One frame was recorded per second with a flow of 0.5mL/min. This represented 120 frames per mL of elution Volume. Data frames between 1814 and 1824 were selected for averaging to obtain the ln(I) versus s.**(B)** Ln I(s) versus s plot with the inset showing Guinier plot. **(C)** Kratky plot from the data in (B) represented for $s < 2.5$ nm^{-1}. **(D)** P(r) versus r profile from the data in (B).

Table 23: Structural parameters calculated from the SAXS data analysis of the bacterial SelenoN.

Guinier Analysis	
I(0) (nm^{-1})	56.94 ±0.11
R_g (Å)	3.66 ±0.14
sR_g range	0.74 – 1.17
Correlation coefficient R^2	0.998
P(r) analysis	
I(0) (nm^{-1})	57.77±0.16
R_g(nm)	3.94±0.019
D_{max}(nm)	15.24
s range (nm^{-1})	0.17-4
X^2 (total estimate from GNOM)	0.997 (0.426)
Porod Volume (nm^{-3})	113.8
Molecular Weight estimation (KDa)	
Theoretical MW of the monomer	64
MW by DATMOW	83.2
MW by DATVC	73.2
MW calculated from porod volume (ratio Vp to MW)	72.4

3.3.1.3 Ab initio modelling of bacterial SelenoN

The Ab initio modeling workflow was the same used for zSelenoN. DAMMIF was run twenty times with parameters assuming that the molecule is a monomer. From this run, four main clusters were obtained with a χ^2 between 1.337 and 1.441. The NSD was close to 1 indicative of a high degree of a similarity between models. All models were grouped into one single cluster (**Figure 46**).

DAMMIN program was also run twenty times independently. The NSD varied between 0.562 and 0.640, which again indicated a good correlation between the different generated models.

The average and refined solution was then used as input for a last DAMMIN run and the resulting χ2 was 4.761 (**Table 24**), indicative of a poor agreement between the solution and the experimental data.

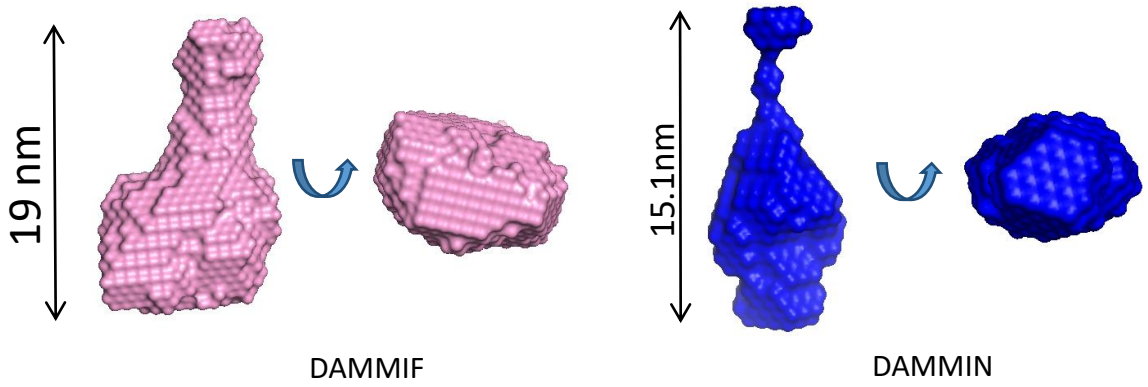

Figure 46 Ab initio modelling of the bacterial SelenoN using two approaches

Table 24: Shape calculation and model-fitting results of bacterial SelenoN

DAMMIF	
q range for fitting ($Å^{-1}$)	0.02 - 0.2
NSD (standard deviation), No of cluster	1.021 (0.105), 1
X2 range	1.337 – 1.411
MW of the model (kDa)	78.4
Resolution (Å) from SASRES	45 ± 3
DAMMIN	
X2	4.761
volume of the model (nm^{-3})	139.8
Resolution (Å) from SASRES	35 ± 3

3.3.1.4 Secondary structure studies

As carried out for the eukaryotic SelenoN, the percentage of the different secondary structure element was evaluated by Circular Dichroism (CD) spectroscopy analysis. To achieve this goal, 200-300 µL of protein solution was used at 0.1-0.3 mg/mL in 1 mm cuvette. Buffer was exchanged to 3mM Tris, 15mM NaCl and 0.5mM TCEP prior to measurements.

Data were processed like described above for the zebrafish SelenoN. The same algorithms were run but protein reference sets 3, 4 and 7 (Sreerama and Woody 2000) were used.

The first observation was that, comparing to theoretical CD spectra of folded vs unfolded protein, the profile of the bacterial SelenoN CD spectra corresponded to a well folded protein (**Figure 47**). After processing, values obtained experimentally for the different structural features were not significantly different from the theoretical one predicted by the PHYRE2 program. The protein showed an enriched α-helical contain (40 - 45%) for only 20% β-sheet.

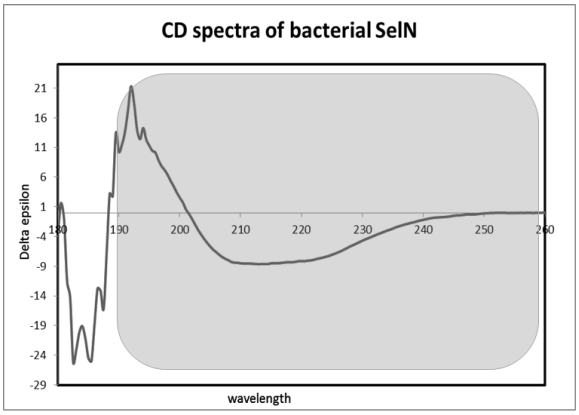

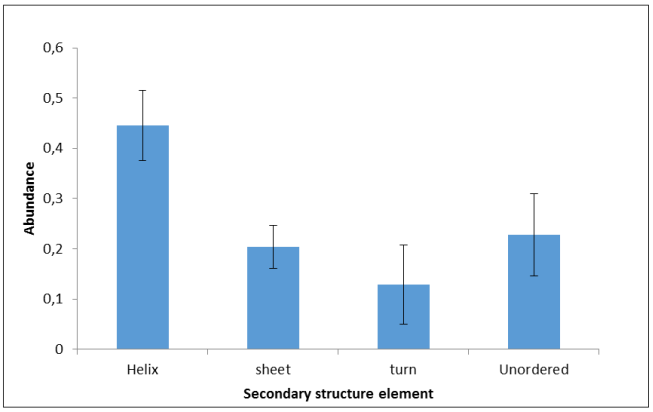

	α-helix	β-sheet	turns	unordered
Prediction (Phyre2)	40%	23%	14%	23%
experimental	45%±6.9	20%±4.3	13%±8	23%±8

Figure 47 :Evaluation of the secondary structure of the recombinant bacterial SelenoN using CD spectroscopy

The curve represents the bacterial CD spectra obtained after subtracting the buffer spectra. The highlighted area represents the range of wavelengths that was used for secondary structure calculation. Data where processed on-line using Dicroweb. SELCON, CONTIN LL and CDSSTR algorithms were used with protein sets 3, 4 and 7. Results of all calculations were averaged. The table presents the comparison between the experimental averaged values and the theoretical values obtained using the on-line prediction PHYRE2 program.

3.3.2 Crystallization of bacterial SelenoN and X-ray diffraction experiments

3.3.2.1 Crystallization of native SelenoN

The protein was concentrated to 10-12 mg/mL before the storage buffer was exchanged using amicon concentrator to a buffer close to physiological conditions (30 mM Tris-HCl pH 7.5 and 150 mM NaCl) prior to crystallization screening.

Initial screens were performed with sitting drops using the vapor diffusion technique. Drops were made by mixing protein solution and reservoir solution to a 1 to 1 ratio using the Phenix robot at a nanoliter scale (100-200nL). Several commercial screens designed for 96 well plates were used, and plates were incubated at 18°C. No crystal grew directly when using commercial screen instead, crystalline precipitate was observed in some conditions. Volume of those conditions was scaled-up to 2 µL drops in 24 well plates. Fragile crystals grew in one of the conditions containing 0.1M HEPES pH 6.5 and 20% PEG 6000. Next, a screen of different buffers and PEG6000 concentrations was made around that condition in a 24 well plate format.

Crystals grew under different conditions of the screen after incubation ranging from 5 days up to several months. Crystallization conditions included 0.1M of different buffers: MES, Tris-HCl, Sodium cacodylate, at pH 6.5 and PEG 6000 or 3350 with percentages of 20, 30, and 35 %. Crystals obtained displayed a needle-like shape with sizes between 50 and 100 µm (**Figure 48**). Some conditions were reproducible but gave tiny crystals of poor quality notably, the X-ray diffraction pattern showed double lattice profile and poor resolution.

After collecting several datasets at different ESRF beamlines, data were processed using Mosflm (Leslie et al, 2011). The processing failed at early stage for most of the dataset and indexing was not possible. Those that were successfully processed resulted in different space groups but in some case with poor resolution.

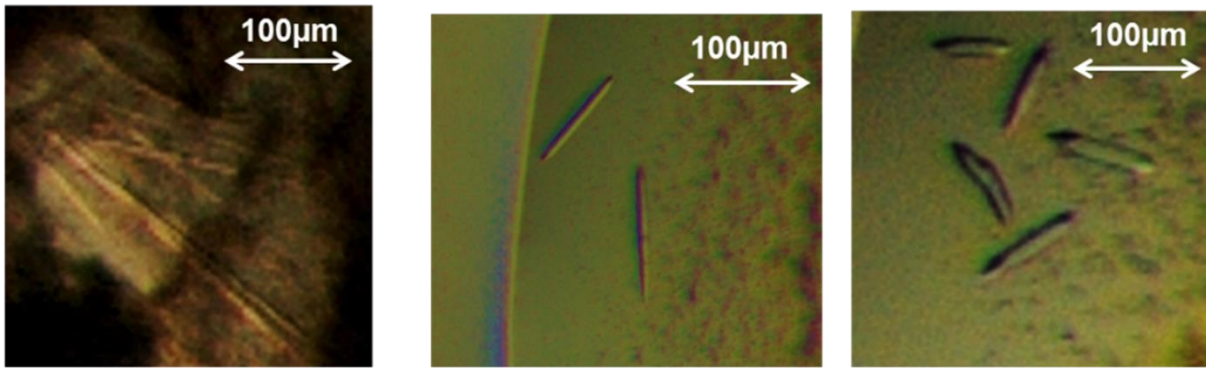

Figure 48: Crystals of bacterial SelenoN were obtained in different conditions.

Crystals of SelenoN1 grew in different conditions. A = 0.1M MES pH 6.5, 30% PEG6000, B= 0.2M Ca acetate, 20% PEG3350, C= 0.1M Na cacodylate, 20% PEG6000.

Table 25: Data statistics after autoprocessing by EDNA of different bSelenoN crystals

	A	B	C
Beam line(ESRF Grenoble)	ID 23.1	ID 23.1	ID 23.1
Wavelength (Å)	0.979	0.979	0.979
Resolution(Å)	2.27	1.98	3.02
Space group	P1 2 1	$P4_2\,2_1\,2$	$P4_1\,2\,2$
Unit cell parameters: a, b, c (α,β,δ)	46.4 (90.0)	67.6 (90.0)	81.98 (90.0)
	149.6 (91.6)	67.6 (90.0)	81.98 (90.0)
	66.5 (90.0)	85.1 (90.0)	163.0 (90.0)
Completeness(Inner shell, Outer shell, Overall)	92.40	99.60	99.00
	91.60	99.70	100.00
	92.70	99.90	100.00
Rsymm(Inner shell, outer shell, Overall)	9.30	6.20	7.60
	42.30	105.50	230.50
	15.80	18.00	37.90

The best diffracting crystal defined after data processing grew in the condition 0.2M Calcium acetate and 20% PEG3350 but unfortunately, this condition was not reproducible. Crystals were soaked in cryoprotectant solution composed of reservoir solution supplemented with 20% glycerol before being flash-frozen in liquid nitrogen. X-ray experiments were made at the beam line ID 23.1 of the ESRF in Grenoble. Data were collected until 1.9 Å resolution (**Table 25**). Processing was made using Mosflm. Crystals of this condition belong to space group $C222_1$ with cell parameters a=b=95.686 Å c=85.240 Å, α=β=ɣ=90°.

Data were scaled using the program SCALA (Kabsch 1988) and cut at a resolution of 2.3 Å according to the I/δ(I) and R_{merge} recommended limits that must be respectively over 2 and under 50% for further use. The data statistics table below (**Table 26**) summarizes the crystal quality at the end of the scaling process.

Table 26: Best crystal of bacterial SelenoN data statistics after processing with Mosflm

Space group	$C222_1$
Unit cell constants	a=b=95.686Å c=85.240Å, α=β=ɣ=90°
Resolution	33 -2.3 Å (2.42 -2.3)
Completeness	99.2 % (99.8)
I/δ(I)	5.6 (1.95)
Rmerge	0.133 (0.392)
Reflections	82143 (11981)
Unique reflections	17568 (2553)
Multiplicity	4.7 (4.7)
Mosaicity	0.25

In brackets are values fort he outer shell

3.3.2.2 SeMet-SelenoN purification, crystallization and crystals derivatization

For the purpose of experimental phasing, selenomethionine labelled bacterial SelenoN was produced following an adapted protocol derived from the native expression one. After removing chaperones expressing medium, cells were washed with cold water before being resuspended in a Selenomethionine labelling medium. The selenomethionine was added prior to protein induction with IPTG. Surprisingly, a higher amount of cells where obtained compared to the native protein expression. In fact, 30g of expressing cells where obtained from 6L expressing medium.

The purification protocol and buffers were all the same to those used for the native bacterial SelenoN. The yield was also on the same scale.

Similarly, to what was observed for the native protein purification, most of contaminants were removed during the first step of the purification (**appendix 4B**). The selenomethionylated protein also eluted in the second peak of the size exclusion chromatography. It appeared monodisperse and monomodal as only one single band was detected. To confirm the monodispersity and also appreciate the apparent molecular weight of the selenomethionine labelled bacterial SelenoN, a native Blue PAGE analysis was conducted. The same migration profile was observed for the native protein (**Figure 49**).

Initial crystallization screens were made again using the same conditions described previously for the native protein. The same commercial and self-prepared screens were tested but no crystal was obtained.

Crystals grew in self-prepared conditions containing 0.1M MES or MOPS pH 6.5 and 20-30% PEG 6000 only when combining hanging drop vapor diffusion with seeding technique (**Figure 30**). Crystals of the native protein were crushed and used as seeding material at different dilutions 10^{-1} to 10^{-6}. Selenomethionine-labelled SelenoN crystals were tested at the ID23.1 beamline of the ESRF where the wavelength is tunable.

Crystals were first tested for their X-ray diffraction properties. The best of them diffracted to 2.8 Å (**Figure 50**). Then, the selenium signal was searched by an energy scan. Unfortunately, the signal

was very weak (result not shown) for all crystals tested and collecting data at selenium edge was not possible.

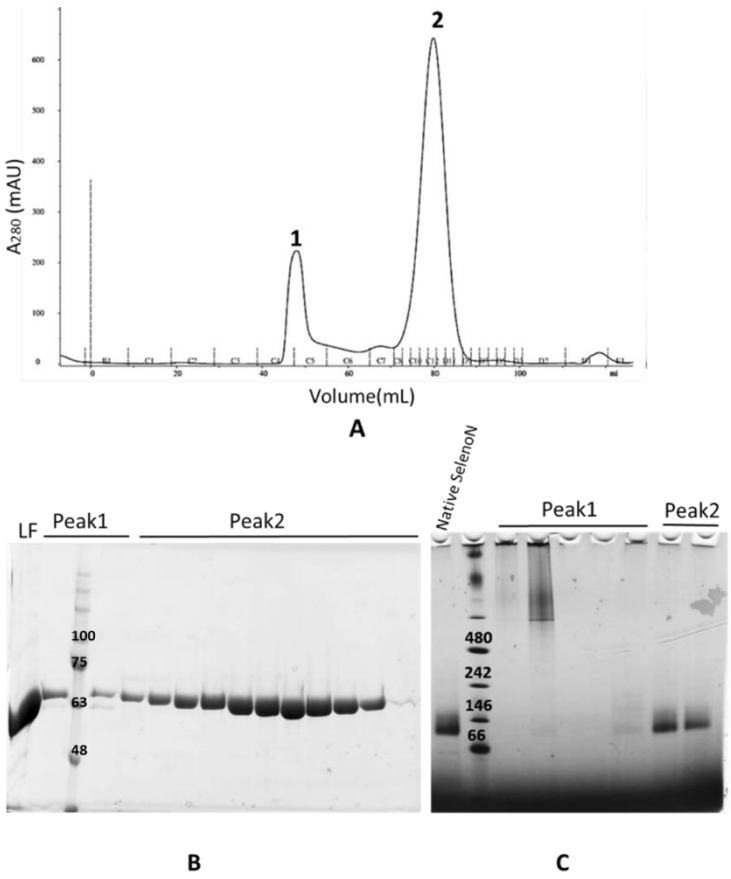

Figure 49: Purification of the Selenomethionine labelled bacterial SelenoN

The chromatogram **(A)** shows the elution profile of the labelled protein over a superdex 200 16/60. The peak 2 eluted between 70 and 80 mL and contains Selenomethinine labelled SelenoN as a pure sample as depicted on the coomassie stained SDS PAGE gel **(B).** The coomassie stained Native PAGE **(C)** showed that the protein fraction was monodisperse and that its migration profile is similar to as the native protein.

In order to introduce marker atoms to enable experimental phasing, selenomethionine-labelled SelenoN crystals were soaked in Ta_6Br_{12} (Knäblein et al. 1997).

Powder of the cluster was added to the crystallization drop. The crystal was considered efficiently soaked when turned greenish (**Figure 51**). After collecting, the soaked crystal was washed in the reservoir solution containing 20% glycerol before flash-cooling in liquid nitrogen. X-ray diffraction measurement were performed at the Ta and Br edges. Data were collected at peak, inflection and low remote wavelengths using an adapted collection strategy automatically calculated by the EDNA program and further processed with Mosflm.

Data collected at the Ta edge were of a very poor quality and completeness. In fact, indexing was not possible for the peak and remote data set. Data collected at the inflection point showed a strong anomalous signal only at a very low resolution around 7Å.

Data collected at Br edge were of a better quality and exhibited an anomalous signal at a better resolution than Ta. Inflection and peak datasets were successfully processed using Mosflm.

Statistics of data collected at peak and inflection point at the Bromide edge are presented (**Table 27).** Those data exhibited anomalous signal but have a poor resolution that is under 3.4 Å. Crystals belong to a different space group and have different unit cell parameters compared to the native. They belong to the space group $P2_12_12_1$ and have the following unit cell parameters, a = 43.92 Å b = 78.32 Å c = 93.63 Å, α= β = ɣ = 90°. The absence of isomorphism with the native crystal excludes the possibility of phasing using isomorphous replacement methods. The only method that will be trying are therefore based on anomalous dispersion and will be discussed later in the discussion chapter.

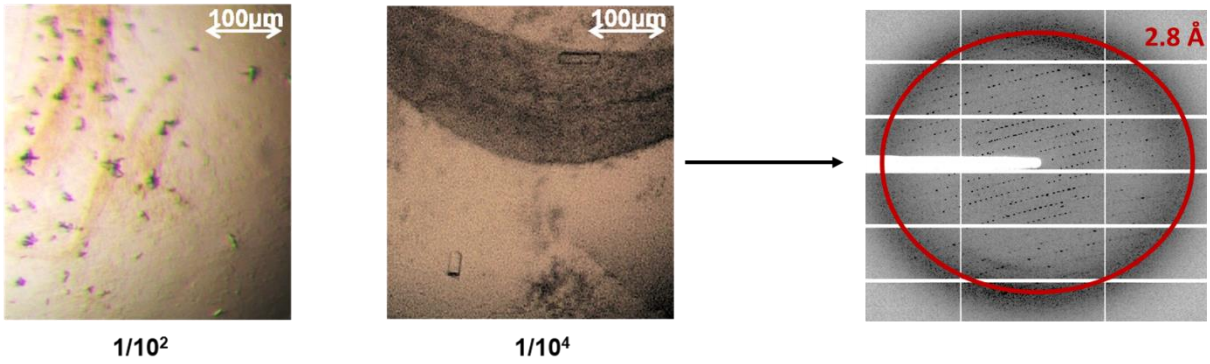

Figure 50: Crystal of bacterial SeMet-SelenoN and its x-ray diffraction.

Crystals grew when combining vapor diffusion with seeding using crushed native crystals as seeding material.

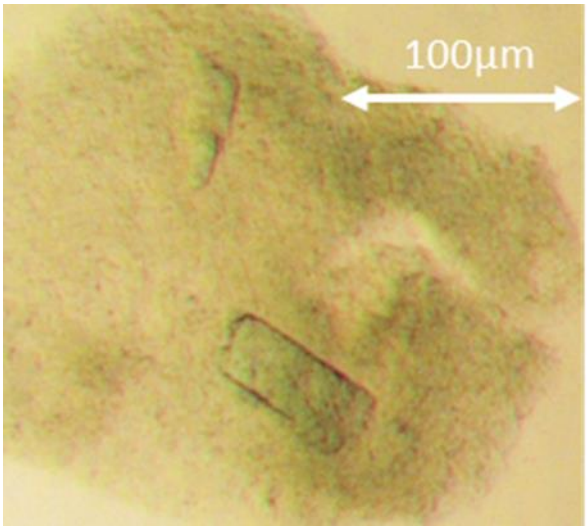

Figure 51: Crystals of Ta_6Br_{12} soaked bacterial selenomethionine-SelenoN

Table 27: Data statistics of Selenomethionine SelenoN crystal soaked in Ta_6Br_{12}.

Space group	$P2_12_12_1$	$P2_12_12_1$
Unit cell constants	a=43.92Å b=78.31Å c=93.63Å, α=β=ɣ=90°	a=44.208Å b=78.657Å c=94.136Å, α=β=ɣ=90°
Resolution (Å)	47.07-3.65 (4.00 -3.65)	46.77-3.40 (3.73 -3.40)
Completeness	98.8% (96.1)	99.4% (97.7)
Anomalous completeness	96.2 % (86.9)	95.9% (89.6)
Mean (I/sd (I))	7.0 (1.3)	8.7 (1.8)
Reflections	23395 (4871)	28260 (6320)
Unique reflections	3933 (886)	4762 (1080)
Multiplicity	5.9 (5.5)	5.9 (5.9)
Anomalous multiplicity	3.2 (3.1)	3.2 (3.2)
DelAnom CC (1/2)	0.475 (0.517)	0.486 (0.571)
Mosaicity	0.40	0.40
Wavelength (λ)	0.9197 (Peak)	0.9191 (Inflection point)

Data were collected at peak and inflection point wavelengths at the bromine absorption edge and were later processed with Mosflm and scaled with Scala. CC: correlation coefficient, Numbers in parentheses are for the outershell

3.3.3 Molecular replacement of the bacterial SelenoN

The UAS domain of human UBX containing protein 7 and thiol disulfide interchange protein from *Bacteroides sp* structures that represent respectively 13% and 33% degree of identity with two invidual domains of bacterial SelenoN could not be used as templates for the molecular replacement. However, the thiol-disulfide oxidoreductase protein (PDB accession number 4NMU) that represents a 28% degree of identity with the C-terminal thioredoxin-like domain of SelenoN was used. The program MOLREP (Vagin and Teplyakov 2010) was run using default parameters

and yielded a partial structure that was later optimized with iterative cycles of building in COOT (Emsley and Cowtan 2004) and refinement with REFMAC5 (Murshudov et al. 2011).

With no surprise, the solution was limited to the last 140 amino acids corresponding to the C-terminal thioredoxin-like domain (**Figure 15**). As expected, the model obtained displayed characteristics of thioredoxin-fold notably a core of β-sheets surrounded by α-helices. The R_{Free} was 52%, which is a high value for a molecular replacement solution. In our case, it is remarkable that 52% could be attributed, even though only 1/4th of the protein could be correctly covered with a low percentage identity. From the local geometry analysis (**Figure 52**), the partial structure fit well into the electron density map, but quality parameters were averaged over the whole structure. This is one possible explanation for the high value of the R_{Free} factor.

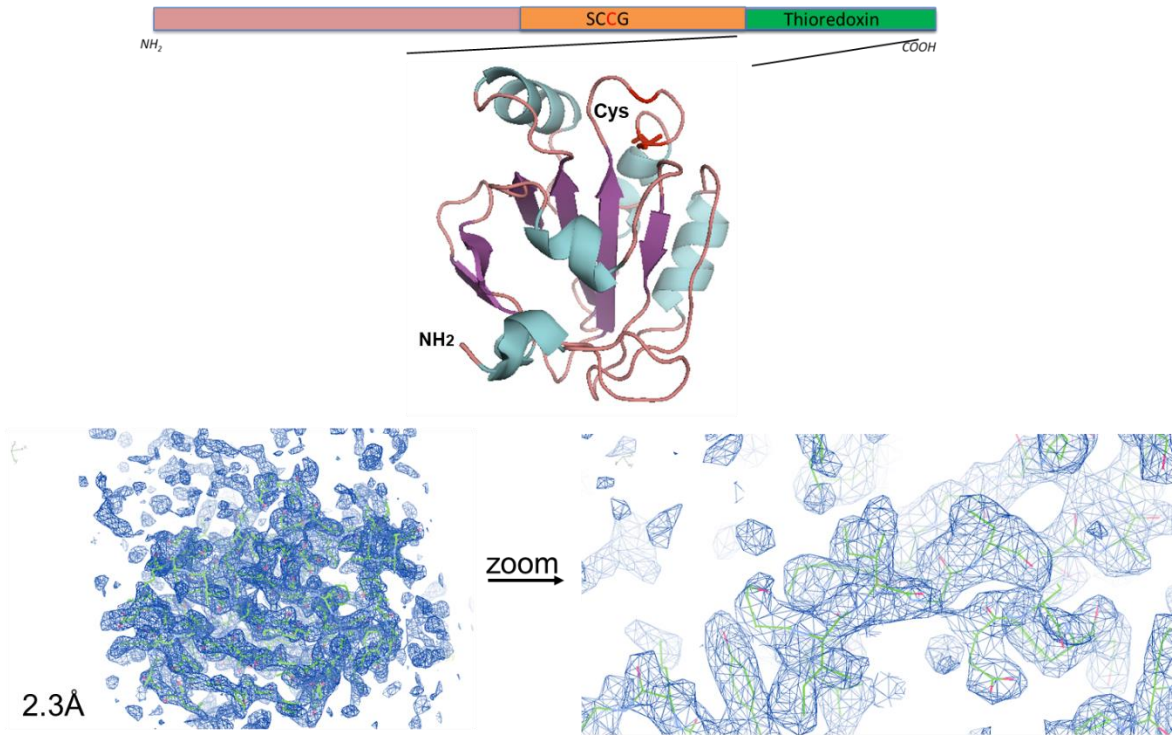

Figure 52: Molecular replacement of the bacterial SelenoN.

The upper panel shows the protein model obtained after molecular replacement covering the C-terminal thioredoxin-fold. The lower panel shows the fit of the protein model in the calculated electron density map.

4 Discussion

4.1 Bioinformatic analysis of bacterial and zebrafish amino acid sequences

It is important to note the degree of conservation between in the human and the zebrafish proteins on one hand and the zebrafish and the bacterial proteins on the other hand. Alignment yielded respectively 67% identity for the two eukaryotes and 37% identity between zebrafish and *Candidatus poribacteriae*. In addition, most of the differences are clustered within the transmembrane region in eukaryote and the additional thioredoxin fold in bacteria. Previous experiments demonstrated that manipulation of the zebrafish SelenoN is easier than its human counterpart, probably due to the high GC content of the human SelenoN DNA, and that the zebrafish SelenoN is expressed at a higher level in culture cell than its human homolog. The structure and domain conservation between both eukaryotes makes zebrafish a good alternative for SelenoN structural and functional studies.

Analysis of the zebrafish SelenoN amino acid sequence showed the presence at the N-terminus of a transmembrane domain organized in one α-helix from amino acids 43 to 53 and an EF hand domain which is a calcium binding domain. These two domains were not found in the bacterial sequence.

The 37% identity between the bacterial and the zebrafish sequence covers the conserved SelenoN sequence which corresponds to the UAS domain of a human protein of unknown function: the human UBX domain containing protein 7 (UBXD7) (PDB accession number 2DLX) that was identified in the analysis and presents 13 to 15% identity. From the structural point of view, this domain corresponds to a thioredoxin fold domain that was found to bind fatty acids and is responsible of protein UBXD8 oligomerization (Kim et al. 2013). The domain consists of 126 amino acids covering from amino acid 381 to 507 in zebrafish sequence and from 229 to 355 in bacterial sequence. The domain was modelled using the SWISSMODEL program on-line. It is organized in five α- helices and three β-sheets (**Figure 53A**). The hypothetic catalytic site is located at the end of one helix and the beginning of a turn (**Figure 53A**). The thioredoxin fold domain of the C-terminal bacterial sequence was also modeled (**Figure 53B**) using the disulfide interchange protein from

Bacteroide sp. (PDB accession number 2LRN) as template. It consists of six β-strands with four of them organized as a core surrounded by four α-helices.

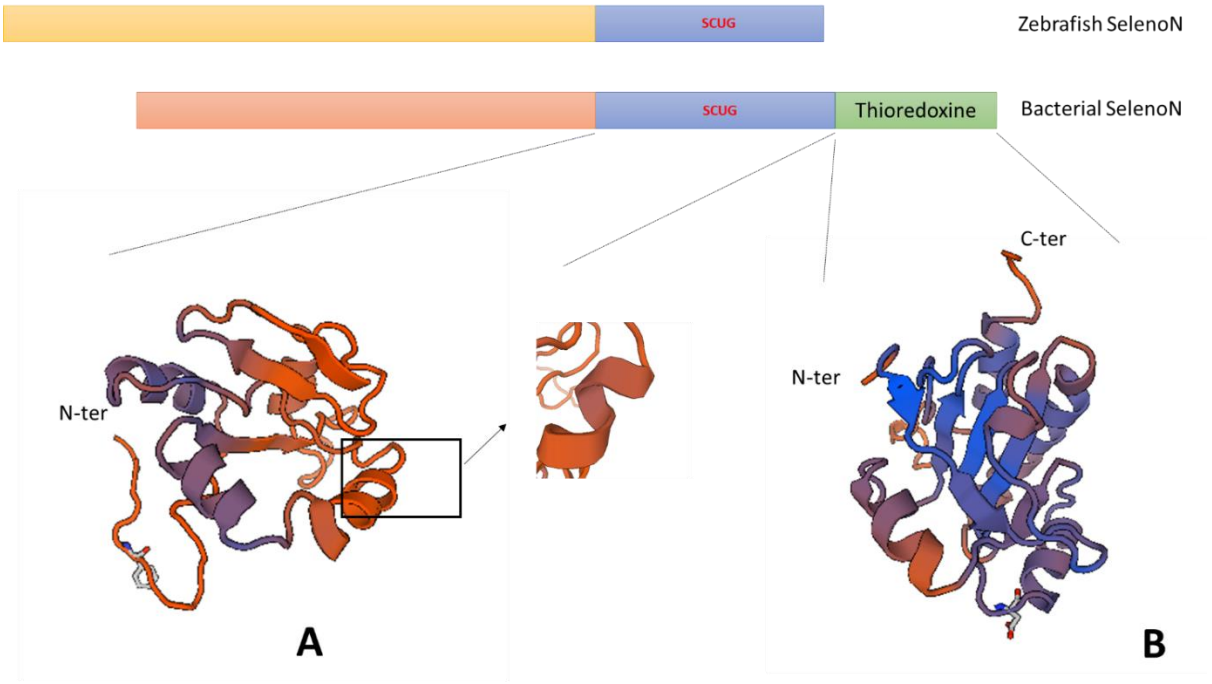

Figure 53: Models from SWISSMODEL of the two-main domain found on bacterial and zebrafish SelenoN.

A model of the UAS domain found in both bacterial and zebrafish sequence. The highlighted area is the hypothetical active site including the predicted catalytic motif, the SCUG sequence.

B model for the thioredoxin-like domain found at the C-terminus in the bacterial sequence.

4.2 Zebrafish SelenoN

4.2.1 Expression/Purification and biophysical characterization of the recombinant zebrafish SelenoN

In this study, the recombinant zSelenoN was expressed in mammalian HEK 293Trex cells as an integral membrane protein. The used stable transformed strain was specifically designed for inducible expression. Based on our result, this strain can be used for expression of zSelenoN as efficiently in suspension or adherent cell culture (results not shown). Therefore, to limit manipulations and avoid contamination, adherent culture was used as an expression system to produce zSelenoN. Screening different detergents showed that solubilization with decyl-β-maltoside (DM) condition yielded elution fractions with a higher purity and higher amount of protein compared to the dodecyl-β-maltoside (DDM) and CHAPS. In addition, screening of different cationic additives combined with the detergents on a Native PAGE gel showed a major oligomer that is more prominent when DM combined with EGTA and EDTA was used.

Because of the presence of an EF-hand domain, one would expect a destabilizing or stabilizing action of Ca^{2+} on the protein surprisingly, the result of the additive screening suggested that the protein is more stable when chelating Ca^{2+} from the buffer. One possible explanation is that Ca^{2+} binding is involved in the regulation of a catalytic activity and that cannot be reproduced in absence of the substrate.

The cell membranes containing the recombinant protein were isolated by differential centrifugation. Recombinant zSelenoN was successfully solubilized with DM and further purified in two chromatographic steps. Using a Hiload Superdex 200 10/300 GL size exclusion chromatography, the zSelenoN protein eluted in two peaks: a first flat peak followed by a second sharp peak. The elution volume of the second peak corresponded theoretically to a globular particle of 150 kDa. SDS-PAGE analysis showed that both peaks contained the protein without major contaminants and evaluation of the amount of protein in each fraction by absorbance at 280 nm showed that both fractions contained equal amount of zSelenoN. Interestingly, based on the difference between the migration on a denaturing gel and the expected size calculated from the amino acid sequence (72 kDa instead of 64 kDa as predicted by EXPASY) and also based on

the deglycosylation assay using PNGaseF, these data confirmed that the protein produced transited through the endoplasmic reticulum and has been post-translationally modified. Human SelenoN was shown to be glycosylated *in vivo* (Petit et al. 2003), and mass spectrometry analyses on zSelenoN demonstrated that the protein was N-glycosylated on two residues (communication from M. Baltzinger). This modification is believed to be important for protein solubility and folding, since its expression in presence of an inhibitor of protein glycosylation, tunicamycin, induced destabilization of the product. In addition, previous expression attempts in bacteria failed to produce any soluble protein even without the transmembrane domain.

Small angle X-ray scattering (SAXS) has emerged as an important tool to control the quality of a purified protein sample, to evaluate the structural parameters such as the maximum length and gyration radius of a particle as well as modelling a low-resolution structure in solution (Kikhney and Svergun 2015a). Such information collected could be useful to compare two proteins homologs such as, wild type vs. mutant, full length vs. truncated forms, and even a structural or a conformational modification in a protein resulting for example from a binding even with a partner.

SAXS experiments were performed in-line with a preceding separation step. Both peaks of purified zSelenoN were analyzed. The I(0) vs. N^{o} of frame trace of the flat peak suggested that the sample is a mixture of several zSelenoN oligomers whereas in the case of the sharp peak, only the protein-detergent complex peak and the detergent free micelles peak were detected. The detergent micelle peak was identified by comparing the I(0) curve to the A_{280} curve. On the I(0) curve, two peaks were identified and only the first one was also detected at A_{280}. As DDM presents a very low absorbance at A_{280} the peak corresponding to the detergent could clearly be identified. It is important to mention that the two peaks that were detected in this case where also detected when analyzing the purification flat peak (**appendix 2D**). Since the flat peak was showed to be polydisperse, further analysis and characterization was only made with the sharp and monodisperse peak.

The monodispersity and absence of aggregates in the zSelenoN sharp peak were confirmed by the SAXS analysis: the R_g trace was horizontal under the protein-detergent complex peak and the Guinier plot was linear for the first measured s values.

The Kratky plot displayed two bell-shaped peaks which tend to zero at the maximum values of s. This behavior suggested a well folded and multidomain particle. Keeping in mind that this analysis was carried out on a protein-detergent complex, the part of the protein surrounded by detergents monomers corona could appear as a domain different from the soluble remaining part of the protein. This could explain the Kratky plot profile. On the other hand, as suggested by it amino acid sequence analysis, zSelenoN was predicted to contain more than one domain.

The molecular weight and oligomer status were calculated using different approaches. Based on the on SDS-PAGE migration, the denaturated glycosylated monomer is 72 kDa while the calculated value in native conditions is within the range of 150-210 kDa. This value is 2 to 3 times higher than the monomer value without detergent. This result is in favor of a compact trimer or dimer. When combining the results with the estimation from the retention volume on the superdex 200 10/300 column which is 150 kDa one can conclude that the protein-detergent complex contains a compact dimer of zSelenoN and several monomers of DDM.

zSelenoN secondary structure content was investigated by circular dicroism (CD) spectroscopy. Experimentally, the protein was found to be well folded as only 21% of residues were calculated as unordered. This result is consistent with the bioinformatics prediction using the program PHYRE2 on-line. However, experimental and bioinformatics analyses were divergent concerning the percentage of secondary structure contents of: α-helices and β-sheets. The percentage of α-helices calculated experimentally is 56% and only 37% for the bioinformatics estimation whereas, 23% of β-sheets were estimated bioinformatically and only 12% experimentally. One should keep in mind that the bioinformatics analysis is based only on the amino acid sequence and do not take in account several parameters such as post-translational modification, oligomerization or presence of detergent. Hence, the difference observed between the calculated and theoretical values could be attributed to such parameters. To be able to compare more accurately with the theoretical values, one should first evaluate the secondary structure of the deglycosylated and truncated protein without the transmembrane domain.

4.2.2 Ca^{2+} effect on zebrafish SelenoN

As the EF-hand domain of zSelenoN is localized in the ER Lumen, one would expect that the binding site is active and that the protein structure and/or function is sensitive to the Ca^{2+} concentration. In order to investigate the effect of the bivalent ion on the protein, it was required to determine and control its binding parameters. First the effect of the binding was analyzed on a native PAGE gel to test for an induced-change of conformation. In the presence of EGTA, the protein migrated as a 140 kDa globular particle whereas, in the presence of Ca^{2+}, it migrated to a higher molecular weight. This result suggested that the protein was sensitive to the Ca^{2+} environment and that its conformation/oligomerization was controlled by Ca^{2+}. The binding constant was investigated using microscale thermophoresis (MST) (Jerabek-Willemsen et al. 2011), and EGTA was used as negative control. Several concentration of Ca^{2+} were tested. In the case of binding, one would expect the signal amplitude of the Ca^{2+} conditions to be higher than the EGTA condition and that the Ca^{2+} binding curve displays a sigmoid shape. Surprisingly, no difference could be observed between Ca^{2+} and EGTA conditions. This result gives rise to three hypotheses: first, due to its conformation, the EF hand domain of zSelenoN was not active and did not bind the Ca^{2+}. Indeed, the Calcium binding protein 4 (CaBP4) presents in its amino acid sequence four EF Hand domains but the second one, eventhough presenting a classic EF-hand motif is not able to bind Ca2+ due to its conformation (Park et al. 2014). Secondly, regarding the fact that incubation with Ca^{2+} led to oligomerization of the protein as was seen on the native PAGE gel, one can suggest that the Ca^{2+} binds, but that for some reason, this binding cannot be monitored by thermophoresis. The third hypothesis is that the protein aggregated in presence of Ca^{2+}, resulting in the absence of a signal. In the Ca^{2+} binding superfamily, there are proteins such as the Calbindin D28K which is a highly conserved Ca^{2+} binding protein with six EF-hand domains. Oligomerization of four of the binding sites was proved to be mediated by Ca^{2+} binding, whereas the binding on the sixth one which has a low Ca^{2+} affinity leads to severe aggregation of the protein (Cedervall et al. 2005).

Ca^{2+} binding could not be further investigated since the binding constant could not be calculated using MST. It is important to mention that all attempts to add Ca^{2+} in concentrated zSelenoN

samples led to protein precipitation. Therefore, further characterization of zebrafish SelenoN was only conducted in presence of EGTA.

4.2.3 Crystallization and structural studies in solution of the zebrafish SelenoN

Characterization of zSelenoN purified from HEK 293 Trex cells showed that the protein was well folded and that the protein sample was of a good quality for crystallization trials. Crystals were initially obtained after intensive optimization. The difficulty in the crystallization of zSelenoN resides in the fact that it is a glycosylated membrane protein. On one side, the requirement of detergent to keep the protein in solution is a first limit to the crystallization since, detergents in solution can form phase separation thus reducing the possibility or probability of nucleation and crystal growth (Papers, Garavito, and Ferguson-miller 2001; Newby et al. 2009). The second hurdle for the crystallization is the glycosylation. Glycan residues are in one hand necessary to support the corect folding of the protein during expression, on the other hand they are conformationally flexible, thus minimizing the probability for crystal contacts (Tang et al. 2005; Kalisz et al. 1990; Mesters and Hilgenfeld 2007).

With no surprise, no crystalline precipitate was obtained in the first screens using the glycosylated protein. Only when removing sugar residues from the protein spherulites could be obtained although with a very weak diffraction to 15 Å. Those spherulites were used later as seeding material and small crystals could be obtained. X-ray diffraction experiments of those crystals showed no diffraction. They are either of a poor quality due to their size or due to internal disorder. Alternatively, their quality could have been impaired during the cryoprotection treatment. zSelenoN crystals size and quality should be optimized for example using iterative seeding (D'Arcy, Mac Sweeney, and Haber 2003; D'Arcy et al. 2014). If no increase in size could be obtained, one should try to make in situ measurements using a small beam.

Low resolution models were calculated using DAMMIN and DAMMIF programs. Models with D_{max}

values of 14.85 nm and 15.78 nm were obtained respectively, which in the case of DAMMIN was in a good agreement with the calculated value from the P(r) function. The molecular weight and volume of the models were also in a good agreement with the P(r) function. The DAMMIN model and the dominant cluster of the DAMMIF model displayed the same shape. When taken individually, the twenty shape models generated by DAMMIN program displayed χ^2 values in agreement with the scattering data and the different models obtained presented low distance between each other. Therefore, the average model was expected to be within the same χ^2 range. The high χ^2 value of DAMMIN model can be attributed to the presence of detergents or glycan residues. In the case of a protein of known structure, it would have been interesting to generate a model and fit it into the SAXS shape but in our case, the identity with aligned protein templates is very low. Therefore, models generated would be of a very poor quality and not reliable.

4.3 *Candidatus poribacteriae* SelenoN

4.3.1 Expression/Purification and biophysical characterization of the recombinant bacterial SelenoN

The recombinant bacterial SelenoN was expressed in *E. coli* and purified using a two-step protocol. This protocol was optimized and SDS-PAGE analysis of the purified bacterial SelenoN showed that the full-length protein was expressed and purified without significant proteolysis. Using a Hiload Superdex 200 16/60 GL size exclusion chromatography, the peak of the recombinant bacterial SelenoN eluted at a volume corresponding to a globular particle of 75 kDa. The migration on a blue native PAGE confirmed the monodispersity and monomodality of the bacterial SelenoN fraction, and showed an approximate molecular weight of 80 kDa. Based on the difference in mobility on the native and the denaturing PAGE, it is likely that the recombinant protein is either not globular and could form an elongated shape retarding its migration on the native PAGE compared to the SDS PAGE. Alternatively, it could form a very compact homodimer that migrates as a smaller molecule.

As for zSelenoN, the molecular weight in native condition could also be determined using SAXS experiments. It was evaluated in the range of 72-83 kDa which is 11 to 13% greater than the denaturated monomer. The result of this estimation is in good agreement with on the one hand the calculation using SEC in line with RALS, corresponding to about 76 kDa and on the other hand the mobility on the native PAGE gel.

The secondary structure content was experimentally determined and bioinformatically estimated. Results of both analyses are consistent. CD spectra displayed a profile of a well-folded protein and analysis estimated only 20% of unordered residues. The bacterial SelenoN is more likely to be α-helical enriched (40%) and with a percentage of 23% of β-sheets. This secondary structure report is the first for the bacterial SelenoN and as for zSelenoN, it can be used later to investigate structural rearrangements due to mutations or binding of interaction partners.

4.3.2 Structural studies of the recombinant bacterial SelenoN

Low resolution models were calculated using DAMMIN and DAMMIF approaches. Models displayed D_{max} values of 15.1 nm and 19 nm respectively, which in the case of DAMMIN was in a good agreement with the calculated value of the P(r) function. The molecular weight and volume of the models were also in a good agreement with the P(r) function. Both models displayed similar shapes but, according to the D_{max} values, the DAMMIN model seemed to be the most accurate.

Native bacterial SelenoN was crystallized at 18°C using the hanging drop vapor diffusion technique with a concentration of 12 mg/mL. Crystals of a needle shape with a size ranging between 50 and 100 µm were obtained under different conditions. They belonged to different space groups. Crystal quality was compared with their statistics after processing of the data obtained and the best of them was used for molecular replacement attempts.

Molecular replacement is a challenging method for the phasing of a protein of unknown structure such as SelenoN. As described for the obtained partial model, only limited part could be covered by the process and this yielded a result of a poor quality. It is more common and trustable for a protein of unknown structure to phase with the help of anomalous scatterer signals. The most problematic part when using this method is to efficiently insert the marker atom that will provide the data with an anomalous signal that is strong enough and so to keep a good resolution. There are several ways to insert a marker atom. The mostet common is to express and purify proteins including a Selenomethionine (SeMet) label. Through a specific expression process, the selenomethionine is inserted in place of methionine and the specific signal of the selenium later is used for the phasing. This technique was applied for the bacterial SelenoN. The SeMet labeled protein was efficiently expressed and purified yielding a sample of quality equivalent to the native protein. Diffracting crystals were obtained by vapor diffusion combined with seeding but unfortunately, those crystals displayed a very poor anomalous signal.

The other way to insert anomalous signal is, after growing crystals to soak them into heavy atoms solution. SeMet bacterial SelenoN crystals were used for this purpose. As the limit to our heavy atoms screening was the number of crystals, I choose to test the cluster Ta_6Br_{12} as first anomalous scatterer. The advantage of this cluster is that one can collect data for experimental phasing at

either Br or Ta edges, and also one can soak by directly adding the green powder over the drop containing the crystal. The crystal is considered efficiently soaked when it turns greenish, which happened in this case. As expected the anomalous signal was strong enough to be detected and data were collected at both Br and Ta edges. Attempts to phase using the so collected and processed data failed because of the poor resolution due to soaking treatment and, because the soaking yielded a modification of the space group and unit cell parameters therefore, the native crystal data could not be used for isomorphous replacement.

4.3.3 The bacterial SelenoN thioredoxine-like fold

The molecular replacement covered the last 140 C-terminal amino acid of the bacterial SelenoN. As predicted, this domain adopted a classical thioredoxin-fold constituted by four ß-sheets surrounded by alpha helices. The pecularity of the bacterial SelenoN is that the fold contains only one cysteine instead of two within the conserved C-X-X-C motif, the first cysteine being replaced by an asparagine. This situation suggested that this thioredoxin-like fold corresponds to either a monothiol glutaredoxin or to a one-cys peroxiredoxin. Structurally, peroxiredoxins are organized as a core of seven β-sheets surrounded by four α-helices whereas glutaredoxins are organized as a core of four β-sheets surrounded by three α-helices (Pan and Bardwell, 2006). The solution of the molecular replacement displayed a structural organization closer to that of the glutaredoxins. Therefore, we propose that the bacterial thioredoxin-like domain of SelenoN corresponds to a monothiol glutaredoxin (**Figure 54**). Glutaredoxins are as other thioredoxin family members electron donor involved in redox reactions. The reduced monothiol glutaredoxin exchanges electrons with gluthationylated proteins and later uses gluthatione to regenerate the oxidized form (**Figure 54**).

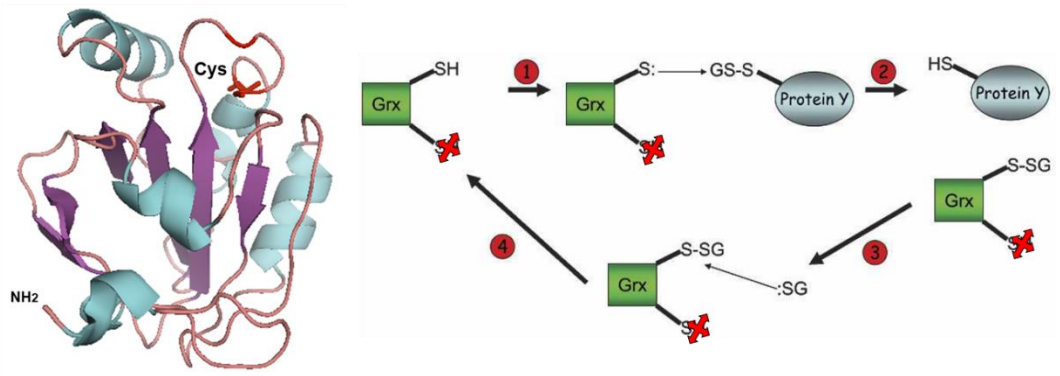

Figure 54: The C-terminal thioredoxine-like fold of the bacterial SelenoN

The left panel display the structure deduced from the X-ray diffraction interprated by molecular replacement. The left pannel is a schematic representation oft he enzymatic mechanisms catalyzed by monothiol glutaredoxin. Baseed on it structural organisation, the C-terminal thoioredoxin-like domain of the bacterial SelenoN is predicted to belongs to this group of reducing enzymes.

4.4 Comparison between bacterial and zebrafish SelenoN

Taken together, the results presented in this project stressed that eukaryotic and bacterial SelenoN share several features, but also present differences (**Table 28**).

In their amino acid sequence, bioinformatic analyses revealed a difference of domain composition: Zebrafish sequence contained at its N-terminus a transmembrane domain organized in one α-helix, followed by an EF Hand domain. Ca^{2+} binding was shown to influence the conformational organization of zebrafish SelenoN, but binding parameters could not be calculated.

A common domain was found in both organisms. This domain corresponding to the C-terminus domain of the zebrafish SelenoN contains the redox motif SCUG and aligned with the UAS domain of the human protein UBXD7. This domain was proved to bind fatty acid (Kim et al. 2013) and is suggested to be involved in cholesterol metabolism (Loregger et al. 2017). In Selenoprotein N, since it includes the predicted redox motif, this domain could correspond to a catalytic function.

Bacterial SelenoN was lacking the two first N-terminal domains and presented an additional C-terminal domain corresponding to a thioredoxin-fold. First X-ray analysis suggested that this C-terminal thioredoxin-fold might correspond to a monothiol glutaredoxin.

Both SelenoN proteins were found to be well folded and α-helical enriched, suggesting a common general organization. However, the zebrafish SelenoN behaved as a compact dimer whereas bacterial SelenoN behaved as an extended monomer. This latter observation was further confirmed by analytical ultracentrifugation analysis (result not shown). The difference observed could be the result of adaptability or an evolution of functions regarding the difference in domains composition and intracellular localization in respective organisms.

Table 28: Comparison of zebrafish and Candidatus poribacteriae SelenoN

	Bacterial SelenoN	Zebrafish SelenoN
Localisation	Cytoplasm Soluble protein	Endoplasmic reticulum Membrane protein
Predicted domains	-SCUG located in a thioredoxin-fold (reactiv center?) -UAS domain (fatty acid binding and cholesterol metabolism)	
	-C-terminal thioredoxin domain (maybe a monothiol glutaredoxin)	-EF-Hand domain (additional mechanism by calcium concentration) -Transmembrane domain (addressing to the ER and restriction activity to one cell compartment)
Results obtained during the PhD thesis		
Optimized steps for structural studies	-Expression in *E.coli* and purification -Biophysical characterization -Crystallization trials	-Expression in HEK 293 Trex cells , solubilization by detergent and purification -Biophysical characterization -Effect of Calcium -Impact of glycosylation in crystallization -Crystallization trials
CD Spectroscopy	α-helical rich and well folded	
SAXS analysis	Elongated shape	Compact structure
Oligomerization	Monomer (confirmed by AUC)	Proposed dimer ?

5 Conclusion and perspectives

The aim of this PhD project was to lay foundation for the structural studies of SelenoN to help in the understanding of its dysfunction in SELENON-related myopathies. The strategy to attain this goal was by working on the bacterial and the zebrafish SelenoN orthologs simultaneously. Once solved, the bacterial structure could be used as a template to solve the zebrafish SelenoN structure. Since the zebrafish SelenoN has 67% identity with the human protein, important structure information relevant to the pathogenic mutations could be derived. The structure solved would be a prerequisite for a better understanding of SelenoN function and its catalytic mechanism.

The zebrafish full-length SelenoN has been successfully expressed in HEK 293 Trex culture cells as a membrane protein to ensure the complete post-translational modifications necessary for its folding. The purification strategy made of affinity and size exclusion chromatography was optimized and yielded a first polydisperse fraction and a second monodisperse stable fraction. The second fraction was used to characterize the molecular weight, the shape and the secondary structure of the recombinant protein.

The monodisperse and stable fraction was more likely to correspond to a compact dimer that was experimentally characterized to be well-folded and α-helical rich with 56% of α-helices and only 12% β-sheet. Optimization of the crystallization condition by native deglycosylation, reservoir solution optimization and seeding yielded small crystals that were obtained with both polydisperse and monodisperse fractions. Their size and quality should be optimized as no X-ray diffraction could be observed with classical experimental technique. For the continuation of the project, one could envisage on first place iterative seeding but, if not yielding better and bigger crystals, in situ measurement could be made to limit the manipulation and therefore the stress of the crystals.

It was shown that zSelenoN is sensitive to the Ca^{2+} environment and that its oligomerization is mediated by Ca^{2+} binding. It was also observed that if not properly controlled, Ca^{2+} binding can lead to severe aggregation. Calculations of binding affinity by microscale thermophoresis failed. To further investigate this Ca^{2+} effect, we recommend investigating the

binding affinity using label free techniques such as Isothermal calorimetry and in parallel with analytical ultra centrifugation, to follow and characterize the oligomerization process.

The difficulty when working on the zefrafish recombinant comes from the fact that on one hand detergents are necessary for all steps which makes the interpretation of characterization results less accurate and on the other hand, the glycosylations which of course are necessary for the folding, but are not suitable for characterization as well as crystallization.

In the case of the bacterial protein, the recombinant soluble SelenoN was overexpressed in *E coli* using co-expression of GroES/GroEL chaperones, purified it using affinity and size exclusion chromatographies, and characterized its secondary structure content and shape. The so-produced protein is an elongated monomer that was found to be well folded and alpha helical rich with 40% of α-helices and 23% β-sheet content. Crystals of the protein that diffracted up to 1.9 Å were obtained using a purified fraction concentrated to 10 mg/mL, after few days to few weeks depending on the conditions. All crystals obtained presented same needle-like shape and belong to space groups $C222_1$ or $P2_12_12_1$. The molecular replacement yielded a partial model that covers $1/4^{th}$ of the protein corresponding to the additional C-terminal thioredoxin-fold domain. Later, phasing based on anomalous scatterers was tried. For this purpose, Ta_6Br_{12} cluster was used to derivate SeMet-bSelenoN crystals. Anomalous signal was successfully inserted but yielded a decrease in the crystal quality. Next, attempts to phase by single or multiwavelengths anomalous dispersion failed. The main reason for this unsuccessful phasing was that crystallization was very poorly reproducible so that, systematic screening for heavy atoms derivatives was not possible. Production of bacterial selenoN and initial crystallization conditions are now established. The only limit to get to the structure is to obtain a quantity of crystals large enough for more and efficient marker atoms screening in terms of type, concentration and soaking time.

It is important to rethink the initial strategy that was designed for SelenoN structure studies. As a reminder, one aspect of working with the bacterial construct was that, the solved structure of the bacterial SelenoN was to be used as a template for molecular replacement to solve zSelenoN structure. Regarding the experimental results of the characterization, once

zSelenoN crystals are obtained, it is recommended to introduce anomalous signal for the phasing, since too many differences between both recombinants were observed in terms of secondary structural element content, oligomerization behavior, shape and theoretical domain content according to their topology, suggesting that the degree of similarity is not extended. Even the only common domain between the bacterial and the zebrafish amino acid sequences, presents just 37% degree of identity. As previously seen, molecular replacement in this condition will yield a poor result that will cover only a part of the protein. Nowadays, new X-ray diffraction experiments and phasing methods with less stress on the crystals are being developed, notably, in situ measurements of small crystals using a very small beam combined with native SAD. The native SAD is based on anomalous scattering of chemical elements that are naturally found in the protein such as sulfur, iron, or calcium. This aims at avoiding the step of crystal derivatization and thus limit the probability of decreasing the crystal quality during the treatments.

Many questions of biological relevance are still opened concerning this project. Differences observed between the bacterial and eukarotic SelenoN are suggested to translate an evolution of the function as well as a specification in different organisms. Also, SelenoN-RM animal models as well as patients have a muscular phenotype. As this protein is present in higher eukaryotes but also in organism lacking any muscular organization, one can suggest that the function of the protein is broader than the muscle establishement and maintenance as suggested by studies on animal models. One can also suggest that the muscular function observed in higher eukaryots is the result of an evolution. Mutations leading to SelenoN-RM can be grouped into two main regions of the gene. Region covering exons 5 to 8 and the region covering exons 10 and 11 that correspond to the predicted catalytic center. Mutations in the first region can be suggested to lead to a structural reorganization leading itself to a loss of function or to a loss of binding with a partner. The second region mutations are indeed suggested to lead to a direct loss of function.

During my PhD work, we had the opportunity to use two different expression systems: first, the *E coli* system which is adapted for structural studies and second, a mammalian cells HEK 293 Trex culture which is less common than bacterial systems but more appropriate for eukaryotic recombinant protein harboring post-translational modifications. We could evaluate the

advantages and disadvantages of both systems: *E. coli* remains certainly a very good expression system to produce high quantities of protein, which is an advantage for a structural study, but is not capable of post-translational modifications that are required in certain case for proper eukaryotic protein folding and stability. Mammalians HEK cells on the other hand are capable of these modifications but are more time and money consuming and less easy to handle because of a higher risk of contamination and a higher sensitivity to stress.

This thesis was a collaboration between Dr. Lescure Alain of “Institut de Biologie Moleculaire et Cellulaire-IBMC” Strasbourg and Prof. Dr. Lancaster Roy of the “Zentrum Fur Human- und Molekulare Biologie” Homburg. Both laboratories brought to the project different and complementary expertises. The Strasbourg laboratory is a biomolecular and cellular biology lab which has the expertise in selenoproteins while the Homburg laboratory is a structural biology laboratory with expertise in membrane proteins studies using the X-ray crystallography. In Strasbourg, expression and purification protocols of both bacterial and zebrafish constructs were developed while the biophysical characterizations as well as the X-ray crystallography were conducted in Homburg.

6 Appendix

Appendix 1: amino acid sequences of bacterial and zebrafish SelenoNs

> Zebrafish_SelenoN

MATDVDKTPAGEQKDDHEDRGTPSSRRGRSRFTQISSLFIIAAIPVISFCIKYYLDIQFVKRHEAGLKALGADGL
FFFSSLDTDHDLYLSPEEFKPIAEKLTGVAPPPEYEEEIPHDPNGETLTLHAKMQPLLLESMTKSKDGFLGVSHS
SLSGLRSWKRPAISSSTFYASQFKVFLPPSGKSAVGDTWWIIPSELNIFTGYLPNNRFHPPTPRGKEVLIHSLLS
MFHPRPFVKSRFAPQGAVACIRATSDFYYDIVFRIHAEFQLNDVPDFPFWFTPGQFAGHIILSKDASHVRDFHI
YVPNDKTLNVDMEWLYGASETSNMEVDIGYLPQMELGAEGPSTPSVIYDEQGNMIDSRGEGGEPIQFVFEEI
VWSEELKREEASRRLEVTMYPFKKVPYLPFSEAFSRASAEKKLVHSILLWGALDDQSC**U**GSGRTLRETVLESSP
VLALLNQSFISSWSLVKELEDLQGDVKNLELSEKARLHLEKYTFPVQMMVVLPNGTVVHHINANNFLDQTSM
KPEDEGPGLSFSAGFEDPSTSTYIRFLQEGLEKAKPYLES

>Bacterial_SelenoN

MVDFNNTLSSTASVQVAAHWDPIENTANNLHRSTEEKFNRDKAQWQEPVEMTWEQWLEVFNPGPAHPL
KNYSTADFQVFLPPSTVNVADVWDLDTEGILPFLRQFHPSATMKLPRYGSIPSDQKDAKACLRALSPEYADIVF
RIHARFTLDASIDAYFMPAQFAGHLIINRNSRTIHQWTLSLPNRNSNVDIGAFRSHDIGFVPRMELCSVSETQP
ESIVWEAAITAEEADKKFQNSLYKFAEIEWTPIEEAVELAKASNRSIHAVLLFGVLDDESC**U**GTGKALRAGPLSS
PKVINLLNTHFVNVWVLLRELPALQTGAKGATAGTLATKLRQHYSDSVDILTLTADLEVIEHLPSKSLWHPDYL
PQSEWIPRYLELLTSSVDVEVVPQKPGELGKHGLSRRLVKAYEELGKPAPDFSATDLDGKPISLQQYRGKVVLL
DFWAVWNGFCIGDILRVKKIYNTYKDQGFDIIGVSLDTDETKLRNYLQENDISWRQIYSGLERQSPLAQQYDV
RSIPTRWLIDRDGKLIAHETHHKLISRKGRESDLEQVVAEAVVNKKSAESVKFAIIRDSDD

Appendix2: SEC-SAXS of zebrafish SelenoN

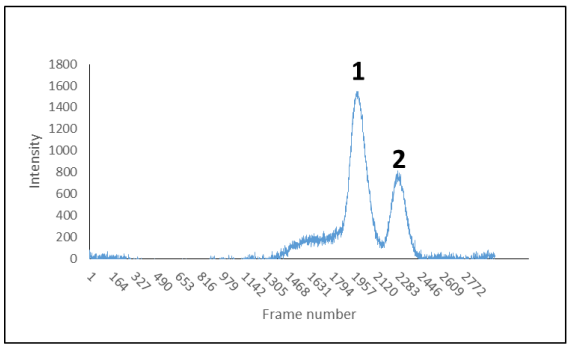

(A)

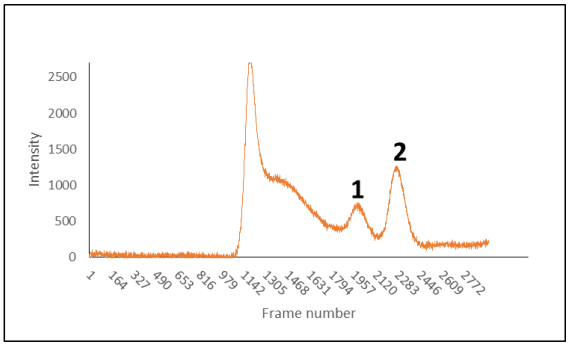

(B)

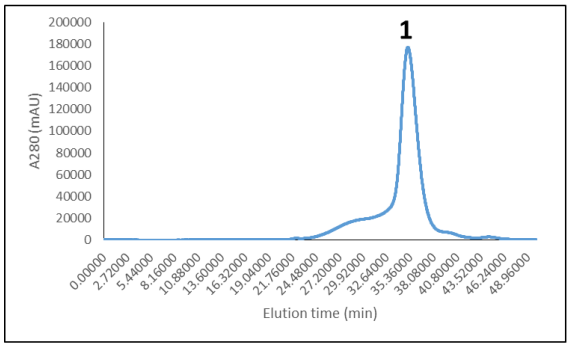

(C)

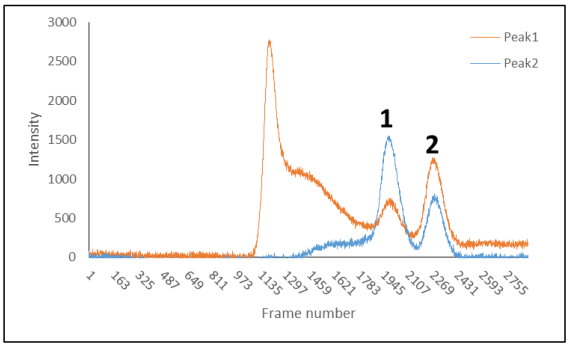

(D)

(A) intensity trace as a function of frame number of the Purification Peak2 (Figure 34 C and D)
(B) intensity trace as a function of frame number of the purification peak 1 (Figure 34 C and D)
(C) A_{280}nm trace as a function of elution time. of the peak
(D) Merge of intensity traces peak 1 (orange) and peak 2 (blue)
1 = protein-detergent complex, 2 = detergent micelle

Appendix 3 : representatives of zSelenoN clusters obtained after modelling with DAMMIN program

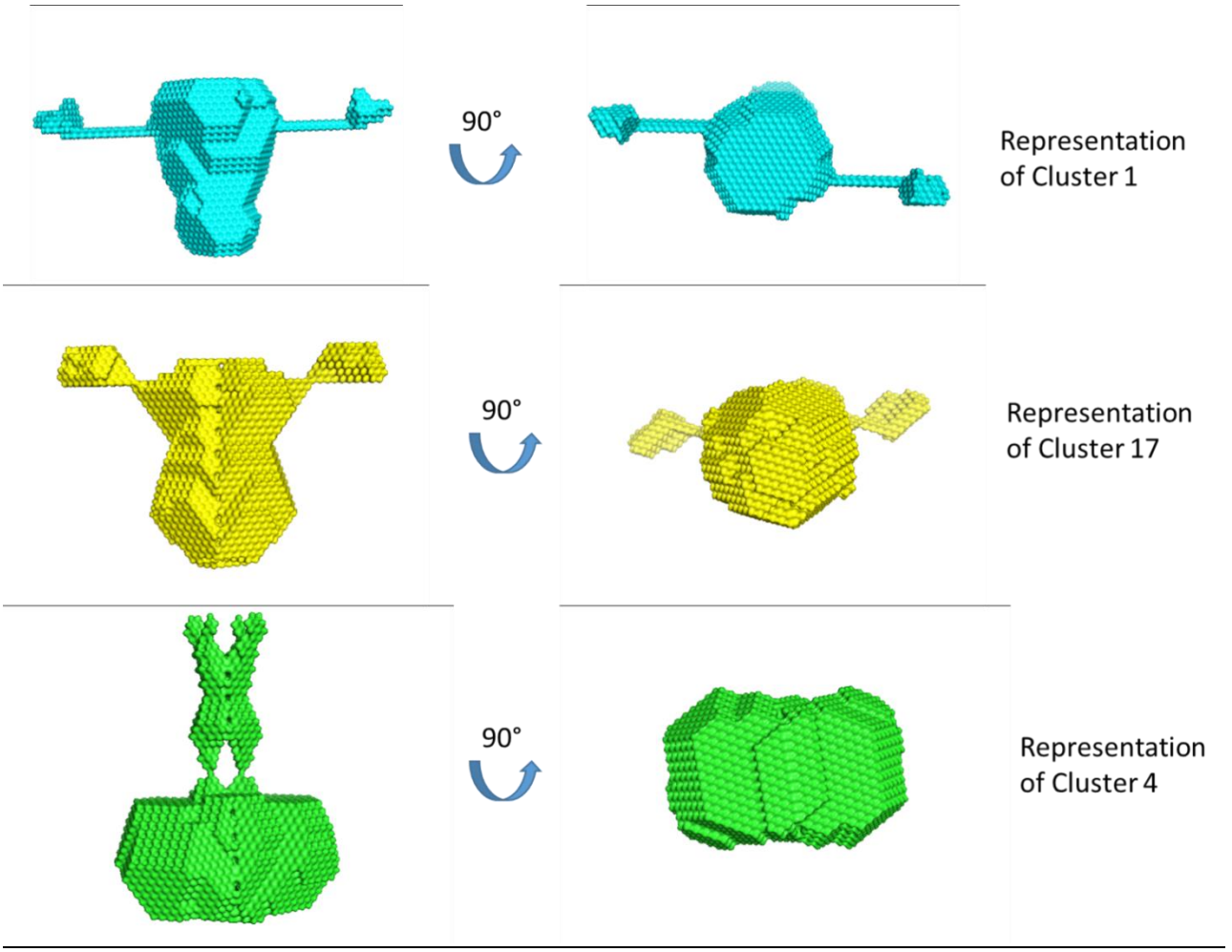

Appendix 4: Native and selenomethionine labelled bacterial SelenoN Imac purification

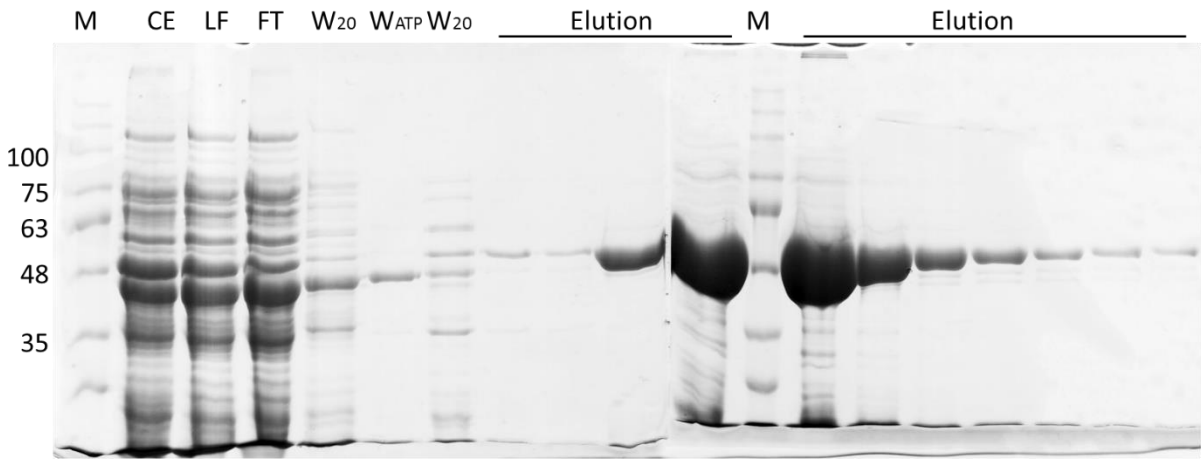

(A)

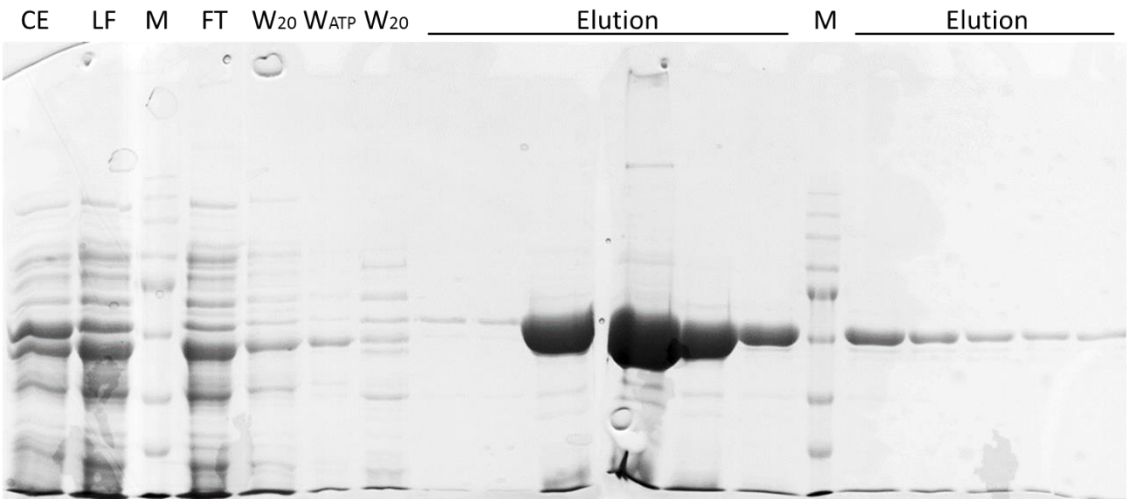

(B)

(A) Imac purification of bacterial SelenoN

(B) Imac purification of selenomethionine labelled bacterial SelenoN

M = protein marker, CE = Crude extract or lysate, LF = loaded fraction, FT = flow through, W_{20} = wash with 20 mM Imidazole, W_{ATP} = wash with 5mM ATP to remove chaperones, Elution=elution fractions

Appendix 5: SEC-SAXS of bacterial SelenoN

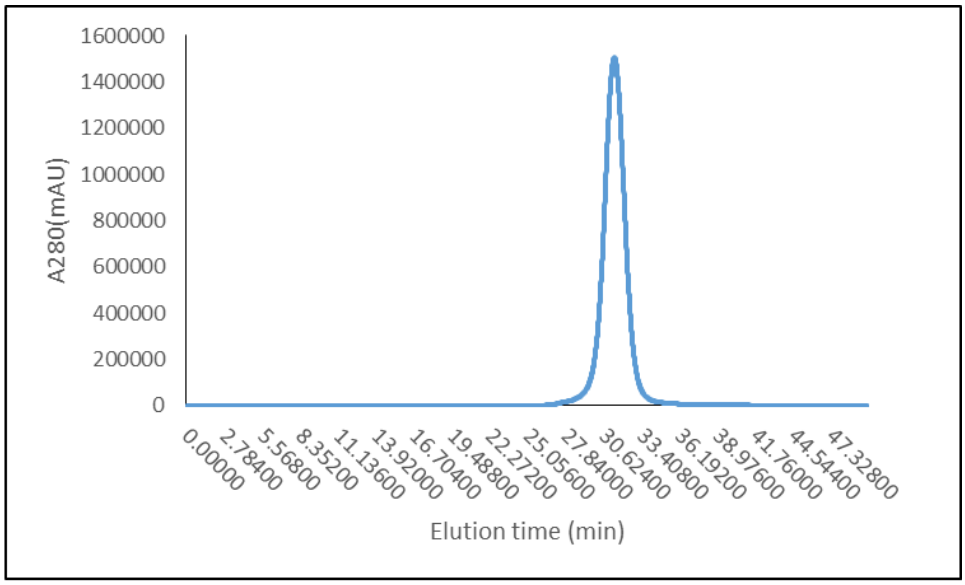

(A)

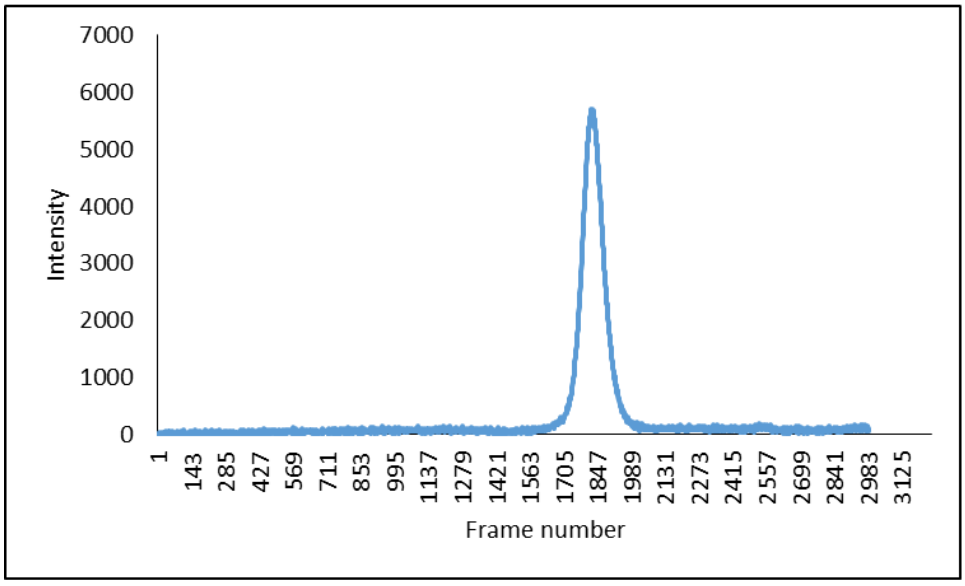

(B)

(A) Intensity as a function of elution volume of the bacterial SelenoN
(B) Intensity as a function of frame number of the bacterial SelenoN

7 References

Aachmann, Finn L., Dmitri E. Fomenko, Alice Soragni, Vadim N. Gladyshev, and Alexander Dikiy. 2007. “Solution Structure of Selenoprotein W and NMR Analysis of Its Interaction with 14-3-3 Proteins.” *Journal of Biological Chemistry* 282 (51):37036–44. https://doi.org/10.1074/jbc.M705410200.

Abdul-Gader, Ali, Andrew John Miles, and Bonnie A Wallace. 2011. “A Reference Dataset for the Analyses of Membrane Protein Secondary Structures and Transmembrane Residues Using Circular Dichroism Spectroscopy.” *Bioinformatics* 27 (12). Oxford University Press:1630–36.

Adams, Paul D, Pavel V Afonine, Gábor Bunkóczi, Vincent B Chen, Ian W Davis, Nathaniel Echols, Jeffrey J Headd, L-W Hung, Gary J Kapral, and Ralf W Grosse-Kunstleve. 2010. “PHENIX: A Comprehensive Python-Based System for Macromolecular Structure Solution.” *Acta Crystallographica Section D: Biological Crystallography* 66 (2). International Union of Crystallography:213–21.

Allamand, Valerie, Pascale Richard, Alain Lescure, Celine Ledeuil, Delphine Desjardin, Nathalie Petit, Corine Gartioux, Ana Ferreiro, Alain Krol, and Nadine Pellegrini. 2006. “A Single Homozygous Point Mutation in a 3’ Untranslated Region Motif of Selenoprotein N mRNA Causes SEPN1-related Myopathy.” *EMBO Reports* 7 (4). EMBO Press:450–54.

Altschul, Stephen F, Thomas L Madden, Alejandro A Schäffer, Jinghui Zhang, Zheng Zhang, Webb Miller, and David J Lipman. 1997. “Gapped BLAST and PSI-BLAST: A New Generation of Protein Database Search Programs.” *Nucleic Acids Research* 25 (17). Oxford University Press:3389–3402.

Arbogast, Sandrine, Maud Beuvin, Bodvaël Fraysse, Haïyan Zhou, Francesco Muntoni, and Ana Ferreiro. 2009. “Oxidative Stress in SEPN1-Related Myopathy: From Pathophysiology to Treatment.” *Annals of Neurology* 65 (6):677–86. https://doi.org/10.1002/ana.21644.

Arnér, Elias S J, and Arne Holmgren. 2000. “Physiological Functions of Thioredoxin and Thioredoxin Reductase.” *European Journal of Biochemistry* 267 (20):6102–9. https://doi.org/10.1046/j.1432-1327.2000.01701.x.

Arnold, Konstantin, Lorenza Bordoli, Jürgen Kopp, and Torsten Schwede. 2006. “The SWISS-MODEL Workspace: A Web-Based Environment for Protein Structure Homology Modelling.” *Bioinformatics* 22 (2). Oxford University Press:195–201.

Baba-Aïssa, Fawzia, Ludo Van Den Bosch, Frank Wuytack, Luc Raeymaekers, and Rik Casteels. 1998. “Regulation of the Sarco/endoplasmic Reticulum Ca 2+-ATPase (SERCA) 2 Gene Transcript in Neuronal Cells.” *Molecular Brain Research* 55 (1). Elsevier:92–100.

Baum, M K, G Shor-Posner, S Lai, G Zhang, H Lai, M A Fletcher, H Sauberlich, and J B Page. 1997. “High Risk of HIV-Related Mortality Is Associated with Selenium Deficiency.” *Journal of Acquired Immune Deficiency Syndromes and Human Retrovirology : Official Publication of the International Retrovirology Association* 15 (5):370–74. http://www.ncbi.nlm.nih.gov/pubmed/9342257.

Beck, M A. 1999. “Selenium and Host Defence towards Viruses.” *The Proceedings of the Nutrition Society* 58 (3):707–11. http://www.ncbi.nlm.nih.gov/pubmed/10604206.

Behne, D, H Weiler, and A Kyriakopoulos. 1996. “Effects of Selenium Deficiency on Testicular Morphology and Function in Rats.” *Journal of Reproduction and Fertility* 106 (2):291–97. http://www.ncbi.nlm.nih.gov/pubmed/8699413.

Benton, D, and R Cook. 1990. “Selenium Supplementation Improves Mood in a Double-Blind Crossover Trial.” *Psychopharmacology* 102 (4):549–50. http://www.ncbi.nlm.nih.gov/pubmed/2096413.

Bianco, Antonio C, Domenico Salvatore, Balázs Gereben, Marla J Berry, and P Reed Larsen. 2002. “Biochemistry, Cellular and Molecular Biology, and Physiological Roles of the Iodothyronine Selenodeiodinases.” *Endocrine Reviews* 23 (1):38–89. https://doi.org/10.1210/edrv.23.1.0455.

Biasini, Marco, Stefan Bienert, Andrew Waterhouse, Konstantin Arnold, Gabriel Studer, Tobias Schmidt, Florian Kiefer, Tiziano Gallo Cassarino, Martino Bertoni, and Lorenza Bordoli. 2014. “SWISS-MODEL: Modelling Protein Tertiary and Quaternary Structure Using Evolutionary Information.” *Nucleic Acids Research* 42 (W1). Oxford University Press:W252–58.

Bordoli, Lorenza, Florian Kiefer, Konstantin Arnold, Pascal Benkert, James Battey, and Torsten Schwede. 2009. “Protein Structure Homology Modeling Using SWISS-MODEL Workspace.” *Nature Protocols* 4 (1). Nature Publishing Group:1–13.

Bösl, Michael R, Kazuaki Takaku, Masanobu Oshima, Susumu Nishimura, and Makoto M Taketo. 1997. “Early Embryonic Lethality Caused by Targeted Disruption of the Mouse Selenocysteine tRNA Gene (Trsp).” *Proceedings of the National Academy of Sciences* 94 (11). National Acad Sciences:5531–34.

Boukhzar, Loubna, Abdallah Hamieh, Dorthe Cartier, Yannick Tanguy, Ifat Alsharif, Matthieu Castex, Arnaud Arabo, et al. 2016. “Selenoprotein T Exerts an Essential Oxidoreductase Activity That Protects Dopaminergic Neurons in Mouse Models of Parkinson’s Disease.” *Antioxidants & Redox Signaling* 24 (11):557–74. https://doi.org/10.1089/ars.2015.6478.

Broach, James R, Vicki R Guarascio, and Makkuni Jayaram. 1982. “Recombination within the Yeast Plasmid 2μ Circle Is Site-Specific.” *Cell* 29 (1). Elsevier:227–34.

Broach, James R, and James B Hicks. 1980. “Replication and Recombination Functions Associated with the Yeast Plasmid, 2μ Circle.” *Cell* 21 (2). Elsevier:501–8.

Castets, Perrine, Anne T. Bertrand, Maud Beuvin, Arnaud Ferry, Fabien Le Grand, Marie Castets, Guillaume Chazot, et al. 2011. “Satellite Cell Loss and Impaired Muscle Regeneration in Selenoprotein N Deficiency.” *Human Molecular Genetics* 20 (4):694–704. https://doi.org/10.1093/hmg/ddq515.

Castets, Perrine, Alain Lescure, Pascale Guicheney, and Valérie Allamand. 2012. “Selenoprotein N in Skeletal Muscle: From Diseases to Function.” *Journal of Molecular Medicine* 90 (10):1095–1107. https://doi.org/10.1007/s00109-012-0896-x.

Castets, Perrine, Svetlana Maugenre, Corine Gartioux, Mathieu Rederstorff, Alain Krol, Alain Lescure, Shahragim Tajbakhsh, Valérie Allamand, and Pascale Guicheney. 2009. “Selenoprotein N Is Dynamically Expressed during Mouse Development and Detected Early

in Muscle Precursors." *BMC Developmental Biology* 9:46. https://doi.org/10.1186/1471-213X-9-46.

Caton-williams, Julianne, and Zhen Huang. 2008. "Biochemistry of Selenium-Derivatized Naturally Occurring and Unnatural Nucleic Acids" 5:396–407.

Cedervall, Tommy, Ingemar Andre, Cheryl Selah, James P Robblee, Peter C Krecioch, Robert Fairman, Sara Linse, and S A Karin. 2005. "Calbindin D 28k EF-Hand Ligand Binding and Oligomerization : Four High-Affinity Sites S Three Modes of Action †," 13522–32. https://doi.org/10.1021/bi050861q.

Christensen, Lea Cecilie, Njal Winther Jensen, Andrea Vala, Jurate Kamarauskaite, Linda Johansson, Jakob Rahr Winther, Kay Hofmann, Kaare Teilum, and Lars Ellgaard. 2012. "The Human Selenoprotein VCP-Interacting Membrane Protein (VIMP) Is Non-Globular and Harbors a Reductase Function in an Intrinsically Disordered Region." *Journal of Biological Chemistry* 287 (31). ASBMB:26388–99.

Compton, Larry A, and W Curtis Johnson. 1986. "Analysis of Protein Circular Dichroism Spectra for Secondary Structure Using a Simple Matrix Multiplication." *Analytical Biochemistry* 155 (1). Elsevier:155–67.

Cowtan, Kevin. 2006. "The Buccaneer Software for Automated Model Building. 1. Tracing Protein Chains." *Acta Crystallographica Section D: Biological Crystallography* 62 (9). International Union of Crystallography:1002–11.

Cunniff, Brian, Gregg W Snider, Nicholas Fredette, Jason Stumpff, Robert J Hondal, and Nicholas H Heintz. 2014. "Resolution of Oxidative Stress by Thioredoxin Reductase: Cysteine versus Selenocysteine." *Redox Biology* 2. Elsevier:475–84.

D'Arcy, Allan, Terese Bergfors, Sandra W Cowan-Jacob, and May Marsh. 2014. "Microseed Matrix Screening for Optimization in Protein Crystallization: What Have We Learned?" *Acta Crystallographica Section F: Structural Biology Communications* 70 (9). International Union of Crystallography:1117–26.

D'Arcy, Allan, Aengus Mac Sweeney, and Alexander Haber. 2003. "Using Natural Seeding Material to Generate Nucleation in Protein Crystallization Experiments." *Acta Crystallographica Section D: Biological Crystallography* 59 (7). International Union of Crystallography:1343–46.

Deniziak, Marzanna, Christine Thisse, Mathieu Rederstorff, Colette Hindelang, Bernard Thisse, and Alain Lescure. 2007. "Loss of Selenoprotein N Function Causes Disruption of Muscle Architecture in the Zebrafish Embryo." *Experimental Cell Research* 313 (1). Elsevier:156–67.

Dikiy, Alexander, Sergey V. Novoselov, Dmitri E. Fomenko, Aniruddha Sengupta, Bradley A. Carlson, Ronald L. Cerny, Krzysztof Ginalski, Nick V. Grishin, Dolph L. Hatfield, and Vadim N. Gladyshev. 2007. "SelT, SelW, SelH, and Rdx 12: Genomics and Molecular Insights into the Functions of Selenoproteins of a Novel Thioredoxin-like Family." *Biochemistry* 46 (23):6871–82. https://doi.org/10.1021/bi602462q.

Emsley, Paul, and Kevin Cowtan. 2004. "Coot: Model-Building Tools for Molecular Graphics."

Acta Crystallographica Section D: Biological Crystallography 60 (12). International Union of Crystallography:2126–32.

Evans, Phil. 2014. “CCP4 Tools for X-Ray Integration and Data Processing.” *Nihon Kessho Gakkaishi* 56 (Supplement). The Crystallographic Society of Japan:s24–s24.

Evans, Philip. 2006. “Scaling and Assessment of Data Quality.” *Acta Crystallographica Section D: Biological Crystallography* 62 (1). International Union of Crystallography:72–82.

Felgner, Philip L, and G M Ringold. 1989. “Cationic Liposome-Mediated Transfection.” *Nature* 337 (6205). Springer:387–88.

Ferguson, Andrew D., Vyacheslav M. Labunskyy, Dmitri E. Fomenko, Demet Araç, Yogarany Chelliah, Carlos A. Amezcua, Josep Rizo, Vadim N. Gladyshev, and Johann Deisenhofer. 2006. “NMR Structures of the Selenoproteins Sep15 and SelM Reveal Redox Activity of a New Thioredoxin-like Family.” *Journal of Biological Chemistry* 281 (6):3536–43. https://doi.org/10.1074/jbc.M511386200.

Flohe, L, W A Günzler, and H H Schock. 1973. “Glutathione Peroxidase: A Selenoenzyme.” *FEBS Letters* 32 (1). Elsevier:132–34.

Flot, David, Trevor Mairs, Thierry Giraud, Matias Guijarro, Marc Lesourd, Vicente Rey, Denis van Brussel, Christian Morawe, Christine Borel, and Olivier Hignette. 2010. “The ID23-2 Structural Biology Microfocus Beamline at the ESRF.” *Journal of Synchrotron Radiation* 17 (1). International Union of Crystallography:107–18.

Fomenko, Dmitri E., Sergey V. Novoselov, Sathish Kumar Natarajan, Byung Cheon Lee, Ahmet Koc, Bradley A. Carlson, Tae Hyung Lee, Hwa Young Kim, Dolph L. Hatfield, and Vadim N. Gladyshev. 2009. “MsrB1 (Methionine-R-Sulfoxide Reductase 1) Knock-out Mice: Roles of MsrB1 in Redox Regulation and Identification of a Novel Selenoprotein Form.” *Journal of Biological Chemistry* 284 (9):5986–93. https://doi.org/10.1074/jbc.M805770200.

Fomenko, Dmitri E, and Vadim N Gladyshev. 2003. “Identity and Functions of CxxC-Derived Motifs.” *Biochemistry* 42 (38). ACS Publications:11214–25.

Franke, Daniel, and Dmitri I Svergun. 2009. “DAMMIF, a Program for Rapid Ab-Initio Shape Determination in Small-Angle Scattering.” *Journal of Applied Crystallography* 42 (2). International Union of Crystallography:342–46.

Franke, D, M V Petoukhov, P V Konarev, and A Panjkovich. 2017. “Computer Programs ATSAS 2 . 8 : A Comprehensive Data Analysis Suite for Small-Angle Scattering from Macromolecular Solutions.” International Union of Crystallography, 1212–25. https://doi.org/10.1107/S1600576717007786.

Fritz-Wolf, Karin, Sebastian Kehr, Michaela Stumpf, Stefan Rahlfs, and Katja Becker. 2011. “Crystal Structure of the Human Thioredoxin Reductase-Thioredoxin Complex.” *Nature Communications* 2:383.

Fritz-Wolf, Karin, Sabine Urig, and Katja Becker. 2007. “The Structure of Human Thioredoxin Reductase 1 Provides Insights into C-Terminal Rearrangements during Catalysis.” *Journal of Molecular Biology* 370 (1). Elsevier:116–27.

Gabadinho, José, Antonia Beteva, Matias Guijarro, Vicente Rey-Bakaikoa, Darren Spruce, Matthew W Bowler, Sandor Brockhauser, David Flot, Elspeth J Gordon, and David R Hall. 2010. “MxCuBE: A Synchrotron Beamline Control Environment Customized for Macromolecular Crystallography Experiments.” *Journal of Synchrotron Radiation* 17 (5). International Union of Crystallography:700–707.

Gorman, Stephen O, DANIEL T Fox, and Geoffrey M Wahl. 1991. “Recombinase-Mediated Gene Activation and Site-Specific Integration in Mammalian Cells.” *Science* 251 (4999). The American Association for the Advancement of Science:1351.

Grumolato, Luca, Hafida Ghzili, Maité Montero-Hadjadje, Stéphane Gasman, Jean Lesage, Yannick Tanguy, Ludovic Galas, Djida Ait-Ali, Jérôme Leprince, and Nathalie C Guérineau. 2008. “Selenoprotein T Is a PACAP-Regulated Gene Involved in Intracellular Ca2+ Mobilization and Neuroendocrine Secretion.” *The FASEB Journal* 22 (6). FASEB:1756–68.

Guex, Nicolas, Manuel C Peitsch, and Torsten Schwede. 2009. “Automated Comparative Protein Structure Modeling with SWISS-MODEL and Swiss-PdbViewer: A Historical Perspective.” *Electrophoresis* 30 (S1). Wiley Online Library.

Guinier, A, and G Fournet. 1955. “Small Angle Scattering.” *Rays* 14.

Hamieh, Abdallah, Dorthe Cartier, Houssni Abid, André Calas, Carole Burel, Christine Bucharles, Cedric Jehan, Luca Grumolato, Marc Landry, and Patrice Lerouge. 2017. “Selenoprotein T Is a Novel OST Subunit That Regulates UPR Signaling and Hormone Secretion.” *EMBO Reports*. EMBO Press, e201643504.

Hawkes, W C, and L Hornbostel. 1996. “Effects of Dietary Selenium on Mood in Healthy Men Living in a Metabolic Research Unit.” *Biological Psychiatry* 39 (2):121–28. https://doi.org/10.1016/0006-3223(95)00085-2.

Hidiroglou, M. 1979. “Trace Element Deficiencies and Fertility in Ruminants: A Review.” *Journal of Dairy Science* 62 (8):1195–1206. https://doi.org/10.3168/jds.S0022-0302(79)83400-1.

Incardona, M-F, Gleb P Bourenkov, Karl Levik, Romeu A Pieritz, Alexander N Popov, and Olof Svensson. 2009. “EDNA: A Framework for Plugin-Based Applications Applied to X-Ray Experiment Online Data Analysis.” *Journal of Synchrotron Radiation* 16 (6). International Union of Crystallography:872–79.

Jerabek-Willemsen, Moran, Chistoph J Wienken, Dieter Braun, Philipp Baaske, and Stefan Duhr. 2011. “Molecular Interaction Studies Using Microscale Thermophoresis.” *Assay and Drug Development Technologies* 9 (4). Mary Ann Liebert, Inc. 140 Huguenot Street, 3rd Floor New Rochelle, NY 10801 USA:342–53.

Jurynec, Michael J, Ruohong Xia, John J Mackrill, Derrick Gunther, Thomas Crawford, Kevin M Flanigan, Jonathan J Abramson, Michael T Howard, and David Jonah Grunwald. 2008. “Selenoprotein N Is Required for Ryanodine Receptor Calcium Release Channel Activity in Human and Zebrafish Muscle.” *Proceedings of the National Academy of Sciences of the United States of America* 105 (34):12485–90. https://doi.org/10.1073/pnas.0806015105.

Kabsch, Wolfgang. 1988. “Evaluation of Single-Crystal X-Ray Diffraction Data from a Position-

Sensitive Detector." *Journal of Applied Crystallography* 21 (6). International Union of Crystallography:916–24.

Kalisz, Henryk M, Hans-jtirgen Hecht, Dietmar Schomburg, Rolf D Schmid, Gbf-gesellschafl Biotechnologische Forschung, Mascheroder Weg, and D- Braunschweig. 1990. "Crystallization and Preliminary X-Ray Diffraction Studies of a Deglycosylated Glucose Oxidase from Aspergillus Niger," 207–9.

Kelley, Lawrence A, Stefans Mezulis, Christopher M Yates, Mark N Wass, and Michael J E Sternberg. 2015. "The Phyre2 Web Portal for Protein Modeling, Prediction and Analysis." *Nature Protocols* 10 (6). Nature Research:845–58.

Khurshid, Sahir, Emmanuel Saridakis, Lata Govada, and Naomi E Chayen. 2014. "Porous Nucleating Agents for Protein Crystallization." *Nature Protocols* 9 (7). Nature Research:1621–33.

Kikhney, Alexey G, and Dmitri I Svergun. 2015a. "A Practical Guide to Small Angle X-Ray Scattering (SAXS) of Flexible and Intrinsically Disordered Proteins." *FEBS Letters* 589 (19). Federation of European Biochemical Societies:2570–77. https://doi.org/10.1016/j.febslet.2015.08.027.

Kikhney, Alexey G, and Dmitri I Svergun . 2015b. "A Practical Guide to Small Angle X-ray Scattering (SAXS) of Flexible and Intrinsically Disordered Proteins." *FEBS Letters* 589 (19PartA). Wiley Online Library:2570–77.

Kim, Hyeonwoo, Hong Zhang, David Meng, Geoffrey Russell, Joon No Lee, and Jin Ye. 2013. "UAS Domain of Ubxd8 and FAF1 Polymerizes upon Interaction with Long-Chain Unsaturated Fatty Acids." *Journal of Lipid Research* 54 (8). ASBMB:2144–52.

Kiremidjian-Schumacher, L, M Roy, H I Wishe, M W Cohen, and G Stotzky. n.d. "Supplementation with Selenium and Human Immune Cell Functions. II. Effect on Cytotoxic Lymphocytes and Natural Killer Cells." *Biological Trace Element Research* 41 (1–2):115–27. Accessed October 16, 2017. http://www.ncbi.nlm.nih.gov/pubmed/7946899.

Knäblein, Jörg, Torsten Neuefeind, Frank Schneider, Andreas Bergner, Albrecht Messerschmidt, Jan Löwe, Boris Steipe, and Robert Huber. 1997. "Ta 6 Br 12 2+, a Tool for Phase Determination of Large Biological Assemblies by X-Ray Crystallography." Elsevier.

Konarev, Petr V, and Dmitri I Svergun. 2015. "A Posteriori Determination of the Useful Data Range for Small-Angle Scattering Experiments on Dilute Monodisperse Systems." *IUCrJ* 2 (3). International Union of Crystallography:352–60.

Labunskyy, Vyacheslav M, Dolph L Hatfield, Vadim N Gladyshev, Labunskyy Vm, Hatfield Dl, Gladyshev Vn, and Selenoproteins Molecular. 2014. "SELENOPROTEINS : MOLECULAR PATHWAYS AND PHYSIOLOGICAL ROLES," 739–77. https://doi.org/10.1152/physrev.00039.2013.

Lacourciere, G M. 1999. "Biosynthesis of Selenophosphate." *BioFactors (Oxford, England)* 10:237–44. https://doi.org/10.1002/biof.5520100222.

Lees, Jonathan G, Andrew J Miles, Frank Wien, and B A Wallace. 2006. "A Reference Database

for Circular Dichroism Spectroscopy Covering Fold and Secondary Structure Space." *Bioinformatics* 22 (16). Oxford University Press:1955–62.

Lei, Xin Gen, Wen-Hsing Cheng, and James P McClung. 2007. "Metabolic Regulation and Function of Glutathione Peroxidase-1." *Annual Review of Nutrition* 27:41–61. https://doi.org/10.1146/annurev.nutr.27.061406.093716.

Leslie, Andrew G W, and Harold R Powell. 2007. "Processing Diffraction Data with MOSFLM." *Evolving Methods for Macromolecular Crystallography* 245. Springer:41–51.

Li, Shawn S-C. 2005. "Specificity and Versatility of SH3 and Other Proline-Recognition Domains: Structural Basis and Implications for Cellular Signal Transduction." *Biochemical Journal* 390 (3). Portland Press Limited:641–53.

Liu, Jun, Zhengqi Zhang, and Sharon Rozovsky. 2014. "Selenoprotein K Form an Intermolecular Diselenide Bond with Unusually High Redox Potential." *FEBS Letters* 588 (18). Wiley Online Library:3311–21.

Lobley, A, Lee Whitmore, and B A Wallace. 2002. "DICHROWEB: An Interactive Website for the Analysis of Protein Secondary Structure from Circular Dichroism Spectra." *Bioinformatics* 18 (1). Oxford University Press:211–12.

Loregger, A., Raaben, M., Tan, J., Scheij, S., Moeton, M., van den Berg, M., Zelcer, N. 2017. Haploid Mammalian Genetic Screen Identifies UBXD8 as a Key Determinant of HMGCR Degradation and Cholesterol Biosynthesis. *Arteriosclerosis, thrombosis, and vascular biology*, ATVBAHA-117.

Lu, Cailing, Feichan Qiu, Haijun Zhou, Yong Peng, Wei Hao, Jialin Xu, Jiangang Yuan, Shizhen Wang, Boqin Qiang, and Caimin Xu. 2006. "Identification and Characterization of Selenoprotein K: An Antioxidant in Cardiomyocytes." *FEBS Letters* 580 (22). Wiley Online Library:5189–97.

Lubos, Edith, Joseph Loscalzo, and Diane E. Handy. 2011. "Glutathione Peroxidase-1 in Health and Disease: From Molecular Mechanisms to Therapeutic Opportunities." *Antioxidants & Redox Signaling* 15 (7):1957–97. https://doi.org/10.1089/ars.2010.3586.

Manavalan, Parthasarathy, and W Curtis Johnson. 1987. "Variable Selection Method Improves the Prediction of Protein Secondary Structure from Circular Dichroism Spectra." *Analytical Biochemistry* 167 (1). Elsevier:76–85.

Matthews, Brian W. 1968. "Solvent Content of Protein Crystals." *Journal of Molecular Biology* 33 (2). Elsevier:491–97.

McClung, James P, Carol A Roneker, Weipeng Mu, Donald J Lisk, Paul Langlais, Feng Liu, and Xin Gen Lei. 2004. "Development of Insulin Resistance and Obesity in Mice Overexpressing Cellular Glutathione Peroxidase." *Proceedings of the National Academy of Sciences of the United States of America* 101 (24). National Acad Sciences:8852–57.

McCoy, Airlie J. 2007. "Solving Structures of Protein Complexes by Molecular Replacement with Phaser." *Acta Crystallographica Section D: Biological Crystallography* 63 (1). International Union of Crystallography:32–41.

Mesters, Jeroen R, and Rolf Hilgenfeld. 2007. “Protein Glycosylation , Sweet to Crystal Growth ? † & DESIGN 2007,” 18–20.

Moghadaszadeh, Behzad, Branden E Rider, Michael W Lawlor, Martin K Childers, Robert W Grange, Kushagra Gupta, Steve S Boukedes, Caroline A Owen, and Alan H Beggs. 2013. “Selenoprotein N Deficiency in Mice Is Associated with Abnormal Lung Development.” *The FASEB Journal* 27 (4). FASEB:1585–99.

Mueller-Dieckmann, Christoph, Matthew W Bowler, Philippe Carpentier, David Flot, Andrew A McCarthy, Max H Nanao, Didier Nurizzo, Petra Pernot, Alexander Popov, and Adam Round. 2015. “The Status of the Macromolecular Crystallography Beamlines at the European Synchrotron Radiation Facility.” *The European Physical Journal Plus* 130 (4). Springer:70.

Mullur, Rashmi, Yan-Yun Liu, and Gregory A Brent. 2014. “Thyroid Hormone Regulation of Metabolism.” *Physiological Reviews* 94 (2). Am Physiological Soc:355–82.

Murshudov, Garib N, Pavol Skubák, Andrey A Lebedev, Navraj S Pannu, Roberto A Steiner, Robert A Nicholls, Martyn D Winn, Fei Long, and Alexei A Vagin. 2011. “REFMAC5 for the Refinement of Macromolecular Crystal Structures.” *Acta Crystallographica Section D: Biological Crystallography* 67 (4). International Union of Crystallography:355–67.

Ness, Steven R, Rudolf A G de Graaff, Jan Pieter Abrahams, and Navraj S Pannu. 2004. “CRANK: New Methods for Automated Macromolecular Crystal Structure Solution.” *Structure* 12 (10). Elsevier:1753–61.

Newby, Zachary E R, Joseph D O’Connell, Franz Gruswitz, Franklin A Hays, William E C Harries, Ian M Harwood, Joseph D Ho, John K Lee, David F Savage, and Larry J W Miercke. 2009. “A General Protocol for the Crystallization of Membrane Proteins for X-Ray Structural Investigation.” *Nature Protocols* 4 (5). Nature Publishing Group:619–37.

Nishihara, Kazuyo, Masaaki Kanemori, Masanari Kitagawa, Hideki Yanagi, and Takashi Yura. 1998. “Chaperone Coexpression Plasmids: Differential and Synergistic Roles of DnaK-DnaJ-GrpE and GroEL-GroES in Assisting Folding of an Allergen of Japanese Cedar Pollen, Cryj2, inEscherichia Coli.” *Applied and Environmental Microbiology* 64 (5). Am Soc Microbiol:1694–99.

Nurizzo, Didier, Trevor Mairs, Matias Guijarro, Vicente Rey, Jens Meyer, Pablo Fajardo, Joel Chavanne, J-C Biasci, Sean McSweeney, and Edward Mitchell. 2006. “The ID23-1 Structural Biology Beamline at the ESRF.” *Journal of Synchrotron Radiation* 13 (3). International Union of Crystallography:227–38.

Pan, J. L., & Bardwell, J. C. 2006. The origami of thioredoxin-like folds. *Protein science*, *15*(10), 2217-2227.

Papers, J B C, R Michael Garavito, and Shelagh Ferguson-miller. 2001. “Detergents as Tools in Membrane Biochemistry *,” 32403–7. https://doi.org/10.1074/jbc.R100031200.

Park, Saebomi, Congmin Li, Françoise Haeseleer, Krzysztof Palczewski, and James B Ames. 2014. “Structural Insights into Activation of the Retinal L-Type Ca2+ Channel (CaV1. 4) by Ca2+-Binding Protein 4 (CaBP4).” *Journal of Biological Chemistry* 289 (45). ASBMB:31262–73.

Pernot, P, P Theveneau, T Giraud, R Nogueira Fernandes, D Nurizzo, D Spruce, J Surr, S McSweeney, A Round, and F Felisaz. 2010. “New Beamline Dedicated to Solution Scattering from Biological Macromolecules at the ESRF.” In *Journal of Physics: Conference Series*, 247:12009. IOP Publishing.

Petit, Nathalie, Alain Lescure, Mathieu Rederstorff, Alain Krol, Behzad Moghadaszadeh, Ulla M Wewer, and Pascale Guicheney. 2003. “Selenoprotein N: An Endoplasmic Reticulum Glycoprotein with an Early Developmental Expression Pattern.” *Human Molecular Genetics* 12 (9). Oxford University Press:1045–53.

Petoukhov, Maxim V, Peter V Konarev, Alexey G Kikhney, and Dmitri I Svergun. 2007. “ATSAS 2.1–towards Automated and Web-Supported Small-Angle Scattering Data Analysis.” *Applied Crystallography* 40 (s1). International Union of Crystallography:s223–28.

Pitts, Matthew W, and Peter R Hoffmann. 2017. “Endoplasmic Reticulum-Resident Selenoproteins as Regulators of Calcium Signaling and Homeostasis.” *Cell Calcium*. Elsevier Ltd, 1–11. https://doi.org/10.1016/j.ceca.2017.05.001.

Provencher, Stephen W, and Juergen Gloeckner. 1981. “Estimation of Globular Protein Secondary Structure from Circular Dichroism.” *Biochemistry* 20 (1):33–37.

Putnam, Christopher D, Michal Hammel, Greg L Hura, and John A Tainer. 2007. “X-Ray Solution Scattering (SAXS) Combined with Crystallography and Computation: Defining Accurate Macromolecular Structures, Conformations and Assemblies in Solution.” *Quarterly Reviews of Biophysics* 40 (3). Cambridge University Press:191–285.

Reeves, M A, and P R Hoffmann. 2009. “The Human Selenoproteome: Recent Insights into Functions and Regulation.” *Cellular and Molecular Life Sciences* 66 (15). Springer:2457–78.

Reich, Hans J, and Robert J Hondal. 2016. “Why Nature Chose Selenium.” *ACS Chemical Biology* 11 (4):821–41. https://doi.org/10.1021/acschembio.6b00031.

Sanctis, Daniele de, Antonia Beteva, Hugo Caserotto, Fabien Dobias, José Gabadinho, Thierry Giraud, Alexandre Gobbo, Matias Guijarro, Mario Lentini, and Bernard Lavault. 2012. “ID29: A High-Intensity Highly Automated ESRF Beamline for Macromolecular Crystallography Experiments Exploiting Anomalous Scattering.” *Journal of Synchrotron Radiation* 19 (3). International Union of Crystallography:455–61.

Schneider, Thomas R, and George M Sheldrick. 2002. “Substructure Solution with SHELXD.” *Acta Crystallographica Section D: Biological Crystallography* 58 (10). International Union of Crystallography:1772–79.

Schweizer, Ulrich, and Clemens Steegborn. 2015. “New Insights into the Structure and Mechanism of Iodothyronine Deiodinases.” https://doi.org/10.1530/JME-15-0156.

Shchedrina, Valentina A., Robert A. Everley, Yan Zhang, Steven P. Gygi, Dolph L. Hatfield, and Vadim N. Gladyshev. 2011a. “Selenoprotein K Binds Multiprotein Complexes and Is Involved in the Regulation of Endoplasmic Reticulum Homeostasis.” *Journal of Biological Chemistry* 286 (50):42937–48. https://doi.org/10.1074/jbc.M111.310920.

Shchedrina, Valentina A, Robert A Everley, Yan Zhang, Steven P Gygi, Dolph L Hatfield, and Vadim

N Gladyshev. 2011b. “Selenoprotein K Binds Multiprotein Complexes and Is Involved in the Regulation of Endoplasmic Reticulum Homeostasis.” *Journal of Biological Chemistry* 286 (50). ASBMB:42937–48.

Shchedrina, Valentina A, Yan Zhang, Vyacheslav M Labunskyy, Dolph L Hatfield, and Vadim N Gladyshev. 2010. “Structure–function Relations, Physiological Roles, and Evolution of Mammalian ER-Resident Selenoproteins.” *Antioxidants & Redox Signaling* 12 (7). Mary Ann Liebert, Inc. 140 Huguenot Street, 3rd Floor New Rochelle, NY 10801 USA:839–49.

Sheldrick, George M. 2008. “A Short History of SHELX.” *Acta Crystallographica Section A: Foundations of Crystallography* 64 (1). International Union of Crystallography:112–22.

Slotboom, Dirk Jan, Ria H Duurkens, Kees Olieman, and Guus B Erkens. 2008. “Static Light Scattering to Characterize Membrane Proteins in Detergent Solution.” *Methods* 46 (2). Elsevier:73–82.

Sreerama, Narasimha, Sergei Y U Venyaminov, and Robert W Woody. 1999. “Estimation of the Number of α-Helical and β-Strand Segments in Proteins Using Circular Dichroism Spectroscopy.” *Protein Science* 8 (2). Cambridge University Press:370–80.

Sreerama, Narasimha, Sergei Yu Venyaminov, and Robert W Woody. 2000. “Estimation of Protein Secondary Structure from Circular Dichroism Spectra: Inclusion of Denatured Proteins with Native Proteins in the Analysis.” *Analytical Biochemistry* 287 (2). Elsevier:243–51.

Sreerama, Narasimha, and Robert W Woody. 1993. “A Self-Consistent Method for the Analysis of Protein Secondary Structure from Circular Dichroism.” *Analytical Biochemistry* 209 (1). Elsevier:32–44.

Sreerama, Narasimha, and Robert W Woody . 2000. “Estimation of Protein Secondary Structure from Circular Dichroism Spectra: Comparison of CONTIN, SELCON, and CDSSTR Methods with an Expanded Reference Set.” *Analytical Biochemistry* 287 (2). Elsevier:252–60.

Stokkum, Ivo H M Van, Hans J W Spoelder, Michael Bloemendal, Rienk Van Grondelle, and Frans C A Groen. 1990. “Estimation of Protein Secondary Structure and Error Analysis from Circular Dichroism Spectra.” *Analytical Biochemistry* 191 (1). Elsevier:110–18.

Sun, Q A, L Kirnarsky, S Sherman, and V N Gladyshev. 2001. “Selenoprotein Oxidoreductase with Specificity for Thioredoxin and Glutathione Systems.” *Proceedings of the National Academy of Sciences of the United States of America* 98 (7):3673–78. https://doi.org/10.1073/pnas.051454398.

Svergun, D I. 1993. “A Direct Indirect Method of Small-Angle Scattering Data Treatment.” *Journal of Applied Crystallography* 26 (2). International Union of Crystallography:258–67.

Svergun, Dmitri I. 1999. “Restoring Low Resolution Structure of Biological Macromolecules from Solution Scattering Using Simulated Annealing.” *Biophysical Journal* 76 (6). Elsevier:2879–86.

Tang, Jie, Christine Luong Yu, Steven R Williams, Eric Springman, Douglas Jeffery, Paul A Sprengeler, Alberto Estevez, et al. 2005. “Expression , Crystallization , and Three-Dimensional Structure of the Catalytic Domain of Human Plasma Kallikrein *” 280

(49):41077–89. https://doi.org/10.1074/jbc.M506766200.

Tsai, Kuo-wang, Chung-man Leung, Yi-hao Lo, Ting-wen Chen, and Wen-ching Chan. 2016. “Arm Selection Preference of MicroRNA-193a Varies in Breast Cancer.” *Nature Publishing Group*, no. February. Nature Publishing Group:1–13. https://doi.org/10.1038/srep28176.

Turanov, Anton A., Dan Su, and Vadim N. Gladyshev. 2006. “Characterization of Alternative Cytosolic Forms and Cellular Targets of Mouse Mitochondrial Thioredoxin Reductase.” *Journal of Biological Chemistry* 281 (32):22953–63. https://doi.org/10.1074/jbc.M604326200.

Vagin, Alexei, and Alexei Teplyakov. 2010. “Molecular Replacement with MOLREP.” *Acta Crystallographica Section D: Biological Crystallography* 66 (1). International Union of Crystallography:22–25.

Volkov, Vladimir V, and Dmitri I Svergun. 2003. “Uniqueness of Ab Initio Shape Determination in Small-Angle Scattering.” *Journal of Applied Crystallography* 36 (3). International Union of Crystallography:860–64.

Weekley, Claire M, and Hugh H Harris. 2013. “Which Form Is That? The Importance of Selenium Speciation and Metabolism in the Prevention and Treatment of Disease.” *Chemical Society Reviews* 42 (23). Royal Society of Chemistry:8870–94.

Whitmore, Lee, and B A Wallace. 2004. “DICHROWEB, an Online Server for Protein Secondary Structure Analyses from Circular Dichroism Spectroscopic Data.” *Nucleic Acids Research* 32 (suppl_2). Oxford University Press:W668–73.

Whitmore, Lee, and Bonnie A Wallace. 2008. “Protein Secondary Structure Analyses from Circular Dichroism Spectroscopy: Methods and Reference Databases.” *Biopolymers* 89 (5). Wiley Online Library:392–400.

Wittig, Ilka, Hans-Peter Braun, and Hermann Schägger. 2006. “Blue Native PAGE.” *Nature Protocols* 1 (1). Nature Publishing Group:418.

Wittig, Ilka, and Hermann Schägger. 2005. “Advantages and Limitations of Clear-native PAGE.” *Proteomics* 5 (17). Wiley Online Library:4338–46.

Wittig, Ilka, and Hermann Schägger . 2008. “Features and Applications of Blue-native and Clear-native Electrophoresis.” *Proteomics* 8 (19). Wiley Online Library:3974–90.

Wittwer, A J, and W M Ching. 1989. “Selenium-Containing tRNA (Glu) and tRNA (Lys) from Escherichia Coli: Purification, Codon Specificity and Translational Activity.” *BioFactors (Oxford, England)* 2 (1):27–34.

Wittwer, Arthur J. 1983. “Specific Incorporation of Selenium into Lysine-and Glutamate-Accepting tRNAs from Escherichia Coli.” *Journal of Biological Chemistry* 258 (14). ASBMB:8637–41.

Wittwer, Arthur J, Lin Tsai, Wei Mei Ching, and Thressa C Stadtman. 1984. “Identification and Synthesis of a Naturally Occurring Selenonucleoside in Bacterial tRNAs: 5-[(Methylamino) Methyl]-2-Selenouridine.” *Biochemistry* 23 (20):4650–55.

Yamashita, Yumiko, Heidi Amlund, Tamami Suzuki, Tatsuro Hara, Mohammed Anwar Hossain, Takeshi Yabu, Ken Touhata, and Michiaki Yamashita. 2011. “Selenoneine, Total Selenium, and Total Mercury Content in the Muscle of Fishes.” *Fisheries Science* 77 (4). Springer:679–86.

Yamashita, Yumiko, and Michiaki Yamashita. 2010. “Identification of a Novel Selenium-Containing Compound, Selenoneine, as the Predominant Chemical Form of Organic Selenium in the Blood of Bluefin Tuna.” *Journal of Biological Chemistry* 285 (24):18134–38. https://doi.org/10.1074/jbc.C110.106377.

Ye, Yihong, Yoko Shibata, Chi Yun, David Ron, and Tom A Rapoport. 2004. “A Membrane Protein Complex Mediates Retro-Translocation from the ER Lumen into the Cytosol.” *Nature* 429 (6994). Nature Publishing Group:841–47.

Yu, S Y, Y J Zhu, and W G Li. 1997. “Protective Role of Selenium against Hepatitis B Virus and Primary Liver Cancer in Qidong.” *Biological Trace Element Research* 56 (1):117–24. http://www.ncbi.nlm.nih.gov/pubmed/9152515.

Zhang, Junmin, Xinming Li, Xiao Han, Ruijuan Liu, and Jianguo Fang. 2017. “Targeting the Thioredoxin System for Cancer Therapy.” *Trends in Pharmacological Sciences* 38 (9). Elsevier Ltd:794–808. https://doi.org/10.1016/j.tips.2017.06.001.

Zhang, Yan, You Zhou, Ulrich Schweizer, Nicolai E Savaskan, Deame Hua, Jonathan Kipnis, Dolph L Hatfield, and Vadim N Gladyshev. 2008. “Comparative Analysis of Selenocysteine Machinery and Selenoproteome Gene Expression in Mouse Brain Identifies Neurons as Key Functional Sites of Selenium in Mammals.” *Journal of Biological Chemistry* 283 (4). ASBMB:2427–38.